University of Alberta

Polymeric Optofluidic Biochips

by

Hooman Hosseinkhannazer Ⓒ

A thesis submitted to the Faculty of Graduate Studies and Research
in partial fulfillment of the requirements for the degree of

Master of Science

Department of Mechanical Engineering

Edmonton, Alberta
Spring 2008

Canada

ABSTRACT

Design and fabrication of analytical systems for bio-chemical detection have been an attractive topic in micro- and nanoscale research in the past few years. These devices have improved with the introduction of lab on a chip technology and the utilization of sensitive and non-destructive optical methods. It has been shown previously that using the laser induced fluorescence (LIF) detection methods along with the integration of the fluidic and optical devices into an all-in-one biochip, the light delivery to the microchannel can be accomplished. Although many research laboratories have introduced optics-integrated biochips, most of these devices were solely used as alpha-prototypes and were not commercializable since they were fabricated in fragile and expensive material such as glass and silicon.

In this work, the design and fabrication of four generations of optofluidic biochips are presented. The goal of this research was to improve the earlier glass/silicon designs. Starting from microreplication of the microfeatures from silicon v-grooves, it was shown that the hollow v-groove waveguides could be fabricated in a layer of heat or UV-curable polymethylmethacrylate and polyepoxyacrylate. The microfluidic layer was fabricated into polydimethylsoloxane and polysiliconeacrylate. The two layers were bonded together to create an all-polymeric biochip with in-plane and out-of-plane optical waveguides for detection. The innovative methods of integration of fluidic and

optical features into polymeric biochips, as well as the materials selected for this project, resulted in the creation of novel devices. A series of LIF experiments presented in this thesis have shown that an in-expensive single-layer biochip, resulted from this research, was capable of LIF detection of two different species of fluorophores.

AKNOWLEDGEMENTS

TABLE OF CONTENTS

LIST OF TABLES

LIST OF FIGURES

LIST OF SYMBOLS

Ag	silver
APD	avalanche photo diode
APFPE	acryloxy perfluoroepolyether
Au	gold
BOE	buffered oxide etch
BPO	dibenzoylperoxide
CE	capillary electrophoresis
Cr	chrome
DAQ	data acquisition card
dB	decibels
DFT	discrete Fourier transform
DI	deionized
DMA	N, N- dimethylaniline
DRIE	deep reactive ion etching
EDP	ethylenediamine pyrocatechol
EDW	ethylendiamine pyrocatechol with water
EO	electroosmotic flow
FACS	fluorescence-activated cell-sorting
GUI	graphical user interface
HF	hydrofluoric acid
Hz	hertz
HMDS	hexamethyldisilazane
IPA	isopropyl alcohol
KOH	potassium hydroxide
LCW	liquid core waiveguide
LOAC	lab on a chip
LIF	laser induced fluorescence
LPCVD	low pressure chemical vapor deposition
MEMS	microelectromechanical systems
MMA	methylmethacrylate
mTorr	millitorr
NOA	Norland optical adhesive
PDF	pressure driven flow
PDMS	polydimethylsiloxane
PEA	polyepocyacrylate
PFPE	perfluoroepolyether

PMMA	polymethylmethacrylate
PMT	photomultiplier tube
POC	point of care
PSiA	polysiliconeacrylate
Pt	platinum
PUA	polyurethaneacrylate
PVA	polyvinylalcohol
RIE	reactive ion etching
sccm	standard cubic centimetres per minute
SCW	solid core waiveguide
Si	silicon
SiN2	silicon nitride
SNR	signal to noise ratio
Ti	titanium
UV	ultraviolet
W	Watts
μm	micrometer
μTAS	micro-total-analysis systems

CHAPTER 1

INTRODUCTION

1.1. Background to BioChips

Miniaturized fluidic systems developed for diagnostics, usually referred to as lab-on-a-chip (LOAC) or micro-total-analysis systems (μTAS), are expected to be the main tools for tomorrow's biological analysis industry[1] [1, 2]. A wide spectrum of applications such as genomics and proteomics [3-5], blood cell analysis [6], cell sorting and biochemistry sensing [7, 8] benefit from many of these newly invented diagnosis methods. The first efforts towards miniaturized analysis systems were reported in the 1970s [9]. However, the creation of microfluidic detection biochips is nominally attributed to H. M. Widmer in 1983 [10] who suggested improvements in analytical tools and instrumentation. Many research groups commenced their efforts to bring this concept to reality. Based on Widmer's ideas, Manz et al. initially proposed the idea of μTAS in 1990 [11]. This report advocated the efficiency and optimum performance that can be achieved by scaling down the dimensions of the systems. Small scale fluidic elements, such as the channels and input/output ports, bring many advantages such as decreasing the sample and reagents volumes as well as high speed

---

[1] According to the Worldwide Biochips & Equipments Market, 2005, the total biochip market size in 2004 was approximately $2.0 billion and was projected to grow to about $5.1 billion in 2009. [1]
CMC Microsystems Annual report, 2006, predicts a 33% increase in LOAC sales growth from 2002 to 2008 in Canadian market. [2]

analysis and the feasibility of integration of such devices into portable handheld equipment. Hence, handheld diagnostic devices, also known as point-of-care (POC) systems in medical applications, were the objective of many research projects in recent years [10-14].

Employing knowledge based on the physics of microfluidics, and by integration of detection and analysis tools into biochips, recent developments in LOAC have lead our research group and many others around the globe towards integrating more features into their products [12, 14]. Applications such as pathogen detection[15], environmental testing [16], cell counting and sorting [17] and fuel cells [18, 19] have motivated more efforts towards creation of systems largely used for detection and sensing. Many of these detection systems are using integrated mechanical parts for flow control systems, e.g. valves and pumps [20-26], as well as the inclusion of optical devices for detection [13, 20-23]. Optical detection along with methods such as electrochemical [24], mass spectrometry [25] and temperature change measurement [26] can be used for discovery and analytical applications [2] [27] as well as detection in microfluidic biochips.

Since optical techniques are sensitive and non-destructive, They are usually favoured among all detection methods. While there have been many methods invented for optical detection in biochips, e.g. fluorescence detection [28], infrared detection [29], Raman scattering detection [30] and chemiluminiscence detection [31], laser induced fluorescence (LIF) detection remains the most popular. This technique has been used for fluorescence-activated cell-sorting (FACS) in flow cytometry for the past decade [10, 11]. A description of the mechanism of fluorescence detection from fluorophores is reviewed in [28, 32].

Many of the commercially available solutions for microarray and biochip diagnostics, marketed by companies such as Agilent, Caliper, Micralyne, Cepheid

---

[2] According to Investext Company and Industry Research, 2006, 57% of the biochip products and services related are demanded for drug discovery.

and Dolomite, utilize LIF or the other optical detections methods mentioned above. However, bulky instrumentation especially large optical devices, are still used in these systems. By integrating optics into LOAC microsystems, more cost efficient and portable devices can be manufactured [13, 33]. The recent literature on research and development reports an increasing number of innovations all with the incentive of integration of novel optical techniques [13, 21, 34, 35]. An important enabler of system integration was the knowledge and technology of micro-scale and nano-scale fabrication inherited from the microelectromechanical systems (MEMS) industry [36]. By micro-fabricating waveguides within the biochip for light distribution and collection, the LIF method can be miniaturized.

1.2. Problems with Existing BioChips

Primarily fabricated using chemical vapour deposition of dielectrics onto glass substrates, early integration of optical waveguides into biochips was complicated, time consuming and costly [37, 38]. Other fabrication methods for systems with integrated optics, such as laser-written UV-curable epoxy waveguides [39], silver ion-exchange waveguides in glass, [23, 40], SU-8 (a negative photoresist) devices [22, 41, 42] and liquid core waveguides [43, 44], are described in the literature. All of these waveguides require many steps in the fabrication process.

A majority of commercial LOAC devices are made using glass [45, 46] and silicon [47] which implies an inevitable high cost of production. These devices, due to contamination issues, should be single-use (disposable) tools with low-cost and high-volume production procedures. Plastic devices, contrary to the traditional biochips, can be fabricated with mass replication methods and are much less expensive.

A popular option in micro-replication processes for fabrication of biochips is polydimethylsiloxane (PDMS) replication or soft lithography [28, 48, 49]. Moreover, another process utilizing micro-replication into plastics and mainly

3

using polymethylmethacrylate (PMMA) has been developed recently and is known as "step and flash" [50]. Also, in the past few years, many replication methods in ultraviolet (UV) curable polymers have been introduced [51]. Some papers report fabrication processes using large molecular diacrylates [52] and others used more flexible material such as siliconized urethane acrylate [53]. Quake et al. pioneered the fabrication of microfluidic devices in polyurethaneacrylate (PUA) for solvent resistant applications [54] and a few other research groups furthered the development of such devices [55]. A more detailed work on a variety of UV-curable materials, such as polyepoxyacrylate(PEA) and PUA for micro-replication processes was reported by Zhou et al. [56] Shortly after, some new methods and material such as hard PDMS [57] perfluoroepolyether (PFPE) [58-60] and acrylated PFPE (APFPE) [61] were used for micro and nano-scale replication and device fabrication.

Further information on biochips fabrication can be found at [62]. For further reading on blood sampling, cellomics and a general description of biological applications of microfluidic biochips, the reader is encouraged to refer to [12, 63-66].

1.3. Thesis Objectives

The goal of the present work is the fabrication of high throughput microfluidic systems with integrated optical detection systems. As an important motivation for the development of commercializable biochips, the fabricated devices are all designed to decrease the cost of manufacture and increase the system reliability. Here, we propose a different approach compared to traditional microfluidics and microoptical devices fabrication methods, in that the devices are created using polymeric material.

Another advance in biochip technology that can result from this thesis is the design of multi-layer biochips. Having the optical system in one layer bonded to a

separate layer with the microfluidic system, the material and processes can be selected and optimized for each layer separately. This multi-level approach can result in more efficient performance of the final product as well as fewer issues with the layout and spacing. Combining the optics and fluidics in one layer can limit the options of device arrangement in the biochip design when a number of waveguide and microchannels are needed.

The biochips presented in this work were designed to form multilayer structures. Inspired by incentives such as increasing the number of biochip applications, incorporating parallel sensing processes and selecting the optimal materials for each layers individually, multilayer biochips were fabricated for this project. Multilayer systems such as multiple task chips [67, 68] and absorption measurements between two glass fluidic layers with an optical cuvette [7] have been previously introduced. In a different work, the system reported by Han *et al* [69] contained a complex multilayer system with integrated fluid control, electrical and optical devices, but yet called for an external optical system for characterization. To the writer's knowledge, the biochip introduced by Spicer [70] of our lab, was the first multilayer biochip with integrated optics. His work inspired a major part of the chapters presented in this thesis.

1.4. Prototypical Optofluidic Biochips

The biochips fabricated in this thesis have integrated functionality of optical and microfluidics components with the intended application in bio-detection. The prototypical task of the chip is to identify specific fluorescently tagged particles in a liquid sample. The reasons for particle identification are left undefined, but a typical application would be to sort particles based on their characteristics.

The optical systems highlighted in the following chapters are based on two basic designs of biochips; hollow V-groove waveguides [70, 71] and liquid core waveguides (LCW) [50, 51, 79, 80]. The multi-layer optofluidic biochips

discussed here are novel in both fabrication methods and design and are expected to be inexpensive and easy to fabricate, unlike many reported previously [7, 8]. Improvements in design and fabrication of the biochips, as well as the selection of novel materials selection make these new generations of biochips unique.

1.4.1. Biochips Generations

The motivation for the present work was to create an improved design of biochips. This thesis describes many improvements achieved over four generations of biochips. Every generation challenges the issues that were in the zeroth generation, the biochips presented by Spicer [71], and any problems that occurred in the previous generation. The first generation of biochips was produced by re-fabrication of the zeroth generation biochips using the same fabrication processes and materials with minor changes. The second generation of biochips were designed and fabricated by introducing a polymeric layer to replace the Pyrex glass material. In addition, the fluidics layer was inverted and a thin capping layer was placed between the fluidic and optical layers in the second generation. This change resulted in the fluidic microchannels and the optics waveguides being located closer together and improves the biochip detection performance. The third and fourth generations adopted the layered structure of the second generation and more effort was put into material selection and rapid prototyping of all-polymeric optofluidic biochips. In the fourth generation, the in-plane LCWs and SCWs were added to the fluidics layer, fabricated in PDMS or PSiA, enabling the option of using this layer as a single-layer biochip. Third and fourth generations use PMMA and PEA in the optical layer respectively. Table 1.1 presents a summary of the biochip generations, their key characteristics, issues and improvements over previous generations.

Generation	Key Features	Issues	Improvements over previous generation	Discussed in
0	1) Designed and fabricated by D. Spicer 2) Origin of the present work 3) Multilayer biochip 4) One fluidics layer (top) 5) One optics layer(bottom) 6) Fluidics in Pyrex glass 7) Optics in Silicon 8) Capping fluidics with PDMS 9) Metal- coated hollow v-groove waveguides 10) Design bottom to top: a) Optics groove on top b) Fluidics, groove on top c) Capping layer on top of optics layer	1) Bonding 2) High production cost 3) Alignment of the layers 4) Microchannels too deep 5) Refraction of reflected beam at air/glass interface not accounted for resulting in misalignment of beam and microchannel		Chapter 1
1	1) Refabrication of generation 0 with minor changes 2) Multilayer biochip 3) One fluidics layer (top) 4) One optics layer(bottom) 5) Fluidics in Pyrex glass 6) Optics in Silicon 7) Capping fluidics with PDMS 8) Metal- coated hollow v-groove waveguides 9) Design bottom to top: a) Optics groove on top b) Fluidics, groove on top c) Capping layer on top of optics layer	1) Bonding 2) High production cost	1) Depth of the microchannels was reduced to 50µm 2) Beam alignment issue temporarily solved by moving layers 5 microns relative to each other	Chapter 2
2	1) A new multi-layer structure 2) One fluidics layer (top) 3) One optics layer(bottom) 4) Fluidics in PDMS 5) Optics in Silicon 6) Intermediate 50µm think PMMA layer between the optics layer and fluidics 7) Metal- coated hollow v-groove waveguides 8) Design bottom to top: a) Optics groove on top b) Fluidics, groove on bottom c) Intermediate PMM layer caps both grooves on either side	1) Bonding 2) Medium to high production cost	1) PDMS polymeric fluidics 2) Flipped fluidics layer: micro channel only 50 microns away from optics layer 3) PMMA intermediate layer 4) Lower cost of production	Chapter 2

Table 1.1 A summary of optofluidic biochips generations, *Continued on page8*

7

Generation	Key Features		Issues	Improvements over previous generation	Discussed in

3	1) Double replication of optics and fluidics layer
	2) One fluidics layer (top)
	3) One optics layer(bottom)
	4) Fluidics in PDMS
	5) Optics in PMMA
	6) Intermediate 50μm think PMMA layer between the optics layer and fluidics
		7) PVA used as negative replica
		8) Metal- coated hollow v-groove waveguides
		9) Design bottom to top:
		  a) Optics groove on top
		  b) Fluidics, groove on bottom
		  c) Intermediate PMM layer caps both grooves on either side
			1) Bonding
			2) Costly dicing
			3) Time consuming monomer mixture preparation
				1) PDMS polymeric fluidics
				2) Flipped fluidics layer: micro channel only 50 micros away from optics layer
				3) PMMA intermediate layer
				4) PMMA optics layer
				5) Better bonding
				6) Less expensive material
					Chapters 2

4	1) Double replication of optics and fluidics layer
	2) One optofluidics layer (top)
	3) One optics layer(bottom)
	4) Optofluidics in PSiA or PDMS
	5) Optics in PEA
	6) Intermediate 50μm think PMMA layer between the optics layer and fluidics
	7) LCW and SCW integration into fluidics layer
		8) PSiA used as negative replica
		9) Metal- coated hollow v-groove waveguides
		10) Design bottom to top:
		  a) Optics groove on top
		  b) Fluidics, groove on bottom
		  c) Intermediate PMM layer caps both grooves on either side
		11) A new Y-channel design for the fluidics
		12) A new tear-shaped reservoir design
			1) Some bonding issues	1) PDMS or PSiA polymeric optofluidics
				2) LCW and SCW integration into fluidics layer
				3) **Optofluidic layer can be used as a single-layer biochip**
				4) Lower cost of production
				5) PEA optics layer
				6) Better bonding
				7) Less expensive material
				8) Fabricated in UV-curable material: much less fabrication time
					Chapters 2 & 3

Table 1.1 A summary of optofluidic biochips generations

8

1.4.2. Multi-layer Biochips

In Chapter 2 a brief analysis of the first generation of biochips fabricated in glass and silicon is presented. The glass/silicon first generation biochips were a re-fabrication of the zeroth generation biochip, introduced by Spicer [71] (Figure 1.1.a), with some improvements for the present project. The original design, shown schematically in Figure 1.2, was capable of detection and analysis of fluorescence (Figure 1.1.b).
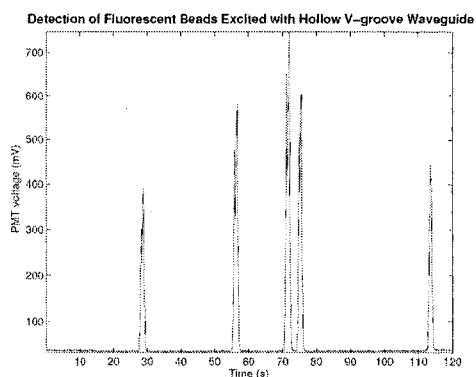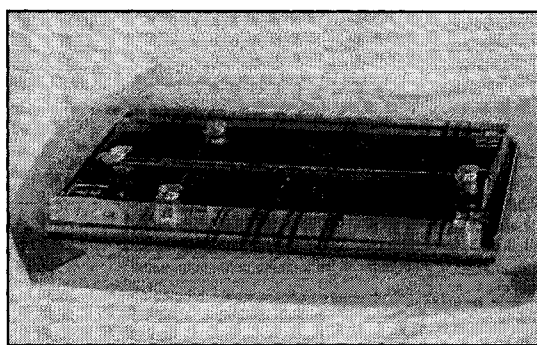
**Figure 1.1 Biochip fabricated by Spicer and the experimental results produced [71],
a. Biochip fabricated by D.Spicer, b. Electrical pulses from fluorescent particles passing trough laser beam**

The main idea in this 3D structure design is to have a fluidic layer sitting on top of an optical layer. The schematic drawing in Figures 1.2 illustrates the delivery of light reflected by the end facet (Figure 1.3) at 54° angle, after travelling through metallized hollow v-groove waveguides, and reaching the fluidics in the glass layer. The glass fluidics is capped with a layer of PDMS. The illumination of the fluidic channel causes fluorescence from the particles in the microchannel which is collected by an optical fiber sitting on top of the PDMS capping layer. The signal is then directed to a photomultiplier tube (PMT) which sends a voltage signal to a computer for signal processing (Figure 1.1.b).

9
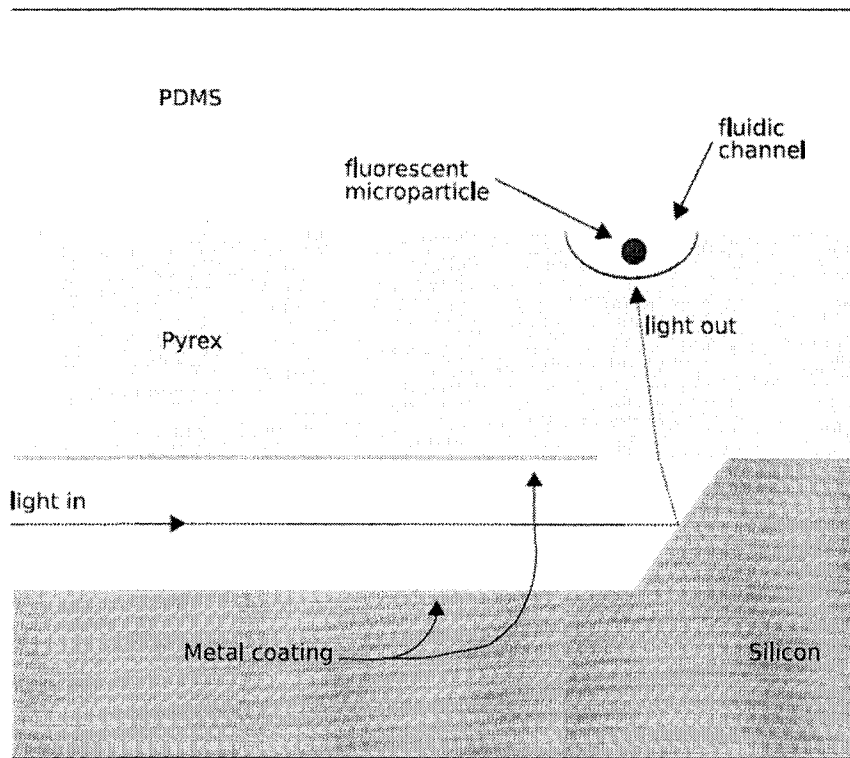
Figure 1.2 Schematic drawing of the zeroth generation biochip [71]
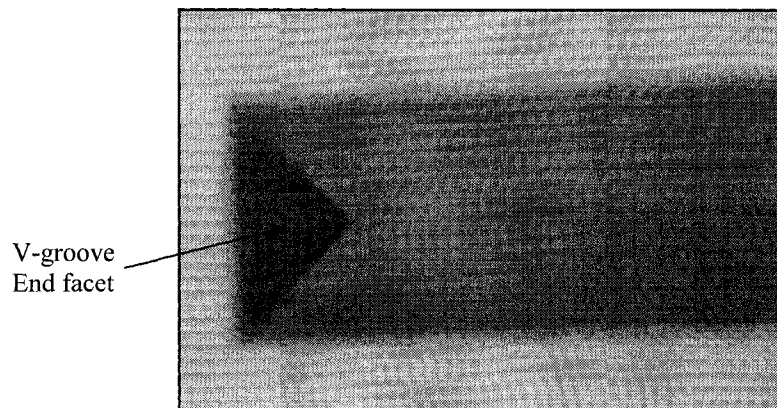
Figure 1.3 100 μm wide v-groove end facet

The v-grooves are formed when the silicon wafer with an etch mask layer, e.g.
silicon nitride, has rectangular openings in the masking layer and is exposed to an
etchant such as potassium hydroxide (KOH). The crystal planes in silicon etch at

10

different rates depending on their angle (Figure 1.4.a) [72]. Hence {100} or the Si wafer flat (horizontal) plane is etched faster than the {111} plane and once the etching volume is bounded by {111} planes the etching process is practically stopped. The v-groove is formed when the etchant creates two {111} planes that meet in the bottom of the v-shape. These two surfaces along with a third {111} plane meet in the end of the etched feature and create a v-groove end facet, at 54° (Figure 1.3). Frühauf in [73] describes the silicon crystal, the orientation of silicon planes and shape of the etched features in more detail. Figure 1.4 sections b and c. show the dimensions chosen in [71] by Spicer and were used for the present work as well (W/D=√2). The v-grooves were designed with different widths (depths) for different amounts of optical delivery and pickup. Hollow v-groove waveguides in the silicon and applications of the v-groove end facet are discussed more in [74-77].

v-groove width (μm)	v-groove depth (μm)
50	35
75	53
200	141
300	212
400	282

a. {111} plane in silicon crystal   b. v-groove side section   c. v-groove dimensions
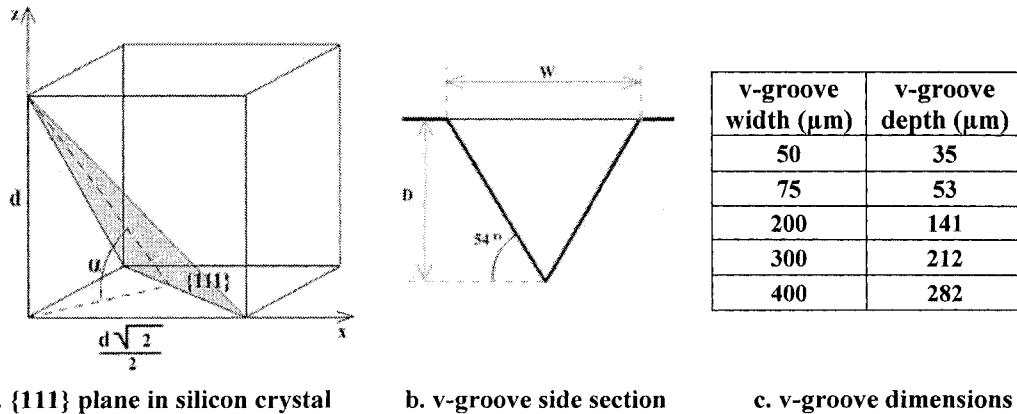
Figure 1.4 Silicon crystal plane and v-groove dimension

Design flaws were discovered in the device made by Spicer. [71]. Due to the refraction occurring when the light leaves the v-groove layer and enters the glass fluidic layer, the angle of the laser beam in the fluidic layer, was different from what was calculated for his biochip. This resulted in the reflected beam not reaching the fluidics which necessitated the re-fabrication of this design. Moreover, since the depth of the channels was designed to be 100 microns and the

size of microparticles or fluorescent beads used in the experiments are approximately 15µm in diameter, the depth of the channels in the first generation, re-fabricated in this project, were changed to 50 microns for more accurate optical pickup.

Second and third generations of this design with some improvements in the structure and material are discussed after the first generation. Second generation multilayer biochips employ plastics for fluidics layer and have a new structural orientation of layers. The third part of Chapter 2 discusses the third generation of the biochips that are created completely in plastics. The last part of Chapter 2 is a brief introduction to multilayer biochips fabricated in UV-curable plastics.

Appendix A describes the basic knowledge that can be used for better understanding of the polymers and their fabrication procedures presented in Chapter 2. In addition, the clamps and polymer punches used for the processes are elaborately described in Appendix B. Further information on the background and techniques used in Si crystal plane identification and deep reactive ion etching can be found in Appendix C.

1.4.3. Single-layer BioChips with Liquid-core and Solid-core waveguides

In Chapter 3 the design and fabrication of LCW and SCW integrated microfluidic biochips are discussed. These biochips can be used as a fluidics layer placed on top of the v-groove structure and present a fourth generation biochip or they can be used as standalone devices. In order to have a better understanding of the fabrication processes described in Chapter 3, basic information about the nitrogen purging system for fabrication and the soft polymer punches are necessary. More information on these topics can be found in the Appendices A and B.

The original approach to integration of optical waveguides was to have both optical and fluidics components in the same layer. This structure has been used in many designs and has more history than the multilayer biochips. Recently, these structures have been created using SU8 fluidics and waveguides [22, 42, 78, 79] or liquid core waveguides [80, 81]. The work presented in Chapter 4 was inspired after my colleague, C. Bliss, conducted his research on rapid prototyping of PDMS fluidic biochips with LCW network using SU8 masters. The biochips for this research were fabricated with LCWs in PDMS and polysiliconeacrylate (PSiA) biochip structures. The biochips were made in PDMS and PSiA were fabricated using microreplication from Deep Reactive Ion Etching (DRIE) machined Si masters. The characterization of these devices with regards to DRIE micromachining methods (Bosch and Cryo) in different polymers demonstrated the novelty and efficiency of the procedures used. Also, by injecting a novel polyepoxyacrylate (PEA) in the LCWs, solid core waveguides (SCW) were fabricated and tested on the same design. Moreover, the fabrication processes and DRIE methods employed for this type of biochips were a gradual effort to improve the techniques for better etched surfaces and especially sidewalls. The DRIE processes developed resulted in a series of novel etch mask fabrication and characterization techniques.

1.5. Thesis Structure

The following chapters review the motivation for this work, as well as the fabrication and experimental processes employed. Devoted to the fabrication of multilayer biochips and material selection for these products, Chapter 2 describes the author's efforts and the results. Chapter 3 is a more detailed discussion of the design and fabrication of the standalone single-layer opto-biochips with the capability of merging it into multilayer structures similar to the biochips explained in Chapter 2. Chapter 4 presents the experimental methods used to examine the fabricated biochips, the test setup utilized for this work and provides experimental

results. The biochips were tested using pressure-driven flow (PDF) and electroosmotic flow (EOF). More information on flows in microfluidics can be obtained from [66, 82].

Chapter 5 summarizes the conclusions to this work and highlights the opportunities for future work.

CHAPTER 2

MULTILAYER OPTOFLUIDIC BIOCHIPS

This chapter presents the evolution of four generations of multilayer optofluidic biochips. The biochips described here were designed and fabricated to optimize the final product costs and the optical detection quality in the system. The following section focuses on the first generation biochip through an overview of its basic design, and provides details on the fabrication of the optics layer, the fluidics layer and the capping layer, and concludes with a discussion of problems and issues relative to its performance and cost. The subsequent sections provide similar information on the second, third and fourth generations of biochips.

2.1. Si-Glass Optofluidic Biochips: First Generation

The biochips discussed in this section, similar to any other LOAC, may provide advantages, specific to their applications. One, for example, is low fluid volumes consumption that lowers the costs of expensive reagents. Also, the biochip has high analysis speed of the particle detection in the microchannels. This design, originally designed by Spicer [70, 71] and shown in Figure 2.1, was remade for the purpose of understanding the advantages and disatvantages of this multilayer structure. Some of the minor problems in the initial design were corrected, but the major parts and materials are the same. Figure 2.2 illustrates the L-Edit software sketch containing the first generation biochips features.
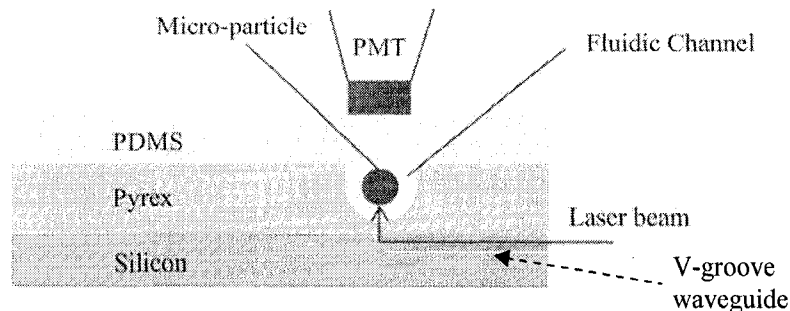
Figure 2.1 Schematic drawing of the zeroth generation biochip

2.1.1. Optics Layer

The silicon optical layer was fabricated from commercially-available silicon wafers 500 μm thick and coated each side with silicon nitride. Low-stress 1000 A^O thick silicon nitride was deposited on the Si wafers using low-pressure chemical vapor deposition (LPCVD) supplied by Norcada Inc.[83]

The first step is to determine the silicon wafer crystal plane orientation so that the etched v-grooves are smooth and the optical loss is small. This determination was accomplished by using reactive ion etching (RIE) on the nitride layer to expose a fan-shaped pattern of small lines on the silicon. The silicon was the anisotropically etched for 30 minute in a 30% KOH aqueous bath at 80^OC and the Si crystal planes were identified. More information on the crystal plane identification method can be found in Appendix C.1.

The waveguide mask was then aligned to the wafer and RIE and KOH etching were again used to etch the v-grooves. After evaluation of the formed v-grooves to ensure the etching process of v-grooves was completely finished, the remaining nitride was etched away in hydrofluoric acid (HF) bath.

Coating the hollow v-grooves waveguides with a thin layer of reflective metal enables the guiding of light through the feature as well as reflecting the light to the top layer from the end facets. While being concerned about the reflectance of the thin metal film, the stability of deposited thin film over time and oxidation

16

resistance was also considered in the choice of metal. Although silver is less expensive than gold and can reflect a wider spectrum of light, gold doesn't oxidize with time so it was decided to use gold as reflecting layer.

Using a Lesker two-target sputter system, 30 nm of chromium (for better adhesion to Si) and then 75 nm of gold were sputtered on the surface of the Si wafer followed by optical lithography and wet etch processes to remove the Cr/Au thin film from any part away from the v-grooves. The optical layer with metallized v-grooves was then diced into single chips each with several sizes of parallel v-grooves of different width and depth ranging from 50 m by 35 μm to 400 μm by 278 μm. These dimentions were originally designed and described in [71].
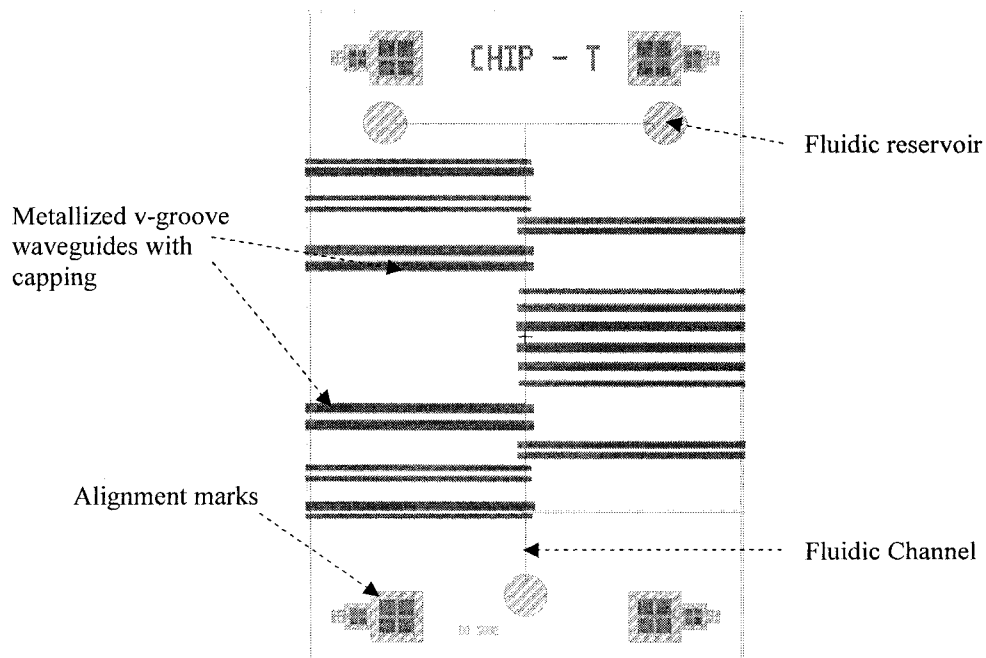
Figure 2.2 First generation biochips: A T-channel fluidics design with v-grooves in the bottom

2.1.2. Fluidics Layer

Commercially-available Pyrex glass with a low-stress sputtered Cr/Au film was used to make the fluidic layer. Lithography and wet etching of gold and chromium, sequentially, were used to create openings in the Cr/Au film corresponding to the microchannel patterns. The channels were wet-etched using a HF isotropic etch bath up to the depths of 50 and 100μm and then the remaining Cr/Au was etched away. The reason for trying two different depths was to find the optical resolution and efficiency between the original 100μ-deep design and 50μ depth. The fluidic layer was topped with fresh PDMS layer to seal the channels. (Figure 2.3)
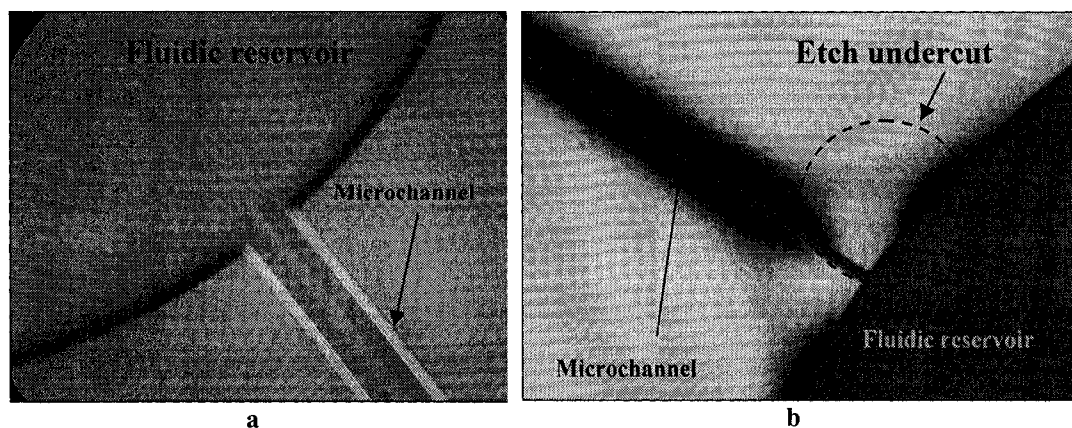
Figure 2.3 Glass microfluidic features, a. Isotropically etched 50μ deep fluidic channel/reservoir in Pyrex glass, b. The edge effects in the isotropic etching

2.1.3. PDMS Capping Layer

The fluidic layer was topped with a fresh PDMS layer to seal the channels. The thickness of this layer is not a critical parameter. For the re-fabrication of the biochips, first generation, the thickness of 0.5mm was chosen. The PDMS was made from a 10:1 ratio prepolymer/hardener mixture and was cured on top of a polished Si wafer in vacuum oven at $80^{\circ}C$.

2.1.4. First Generation Issues

In the first generation, since the fluidic channel was etched on the top face of the glass layer and the optical layer was shining the laser beam from the bottom, the beam was traveling through the 400μ glass layer before entering the fluidic medium, which resulted in laser beam missing the fluidic channel. Subsequently good experimental results were obtained after a temporary solution, changing the alignment of the layers.

Two problems were encountered in bonding the layers in the original design reported in [71]. Bonding between the Si and glass layers was done using UV-curable Norland Optical Adhesive (NOA) [84] and caused misalignment and occasionally filling of the v-grooves with the adhesive resulting in blocking the waveguide. Moreover, the PDMS capping layer was put on the glass layer without using any adhesive or treatment for bonding resulting in a weak seal.

Using Pyrex glass and HF wet etching is a time-consuming and expensive method to fabricate microfluidic channels. While many other ways are presently used to reduce the cost of fabrication and material, it was decided that replacing this layer in the second generation can benefit the biochip project in many aspects.

2.2. Polymeric Biochips: Second and Third Generations

Using {100} silicon and fabrication of v-grooves on its surface was noted to be the simplest way to make a reflective surface at the end of the waveguide at an angle close to 54° and making such a design work. A different more cost efficient approach, is to replicate the v-groove structure into some cheaper material. The latter was the initiative for the third generation.

This phase of the project was carried out to improve the multilayer Si-Glass biochips design and materials in two approaches:

19

The first improvement in the design towards the fabrication of improved second generation of biochips is that the fluidic layer has been inverted so that the channels are much closer to the waveguides as shown schematically in Figure 2.4.b. This required the addition of a thin (50 μm) layer of polymethylmethacrylate (PMMA) layer between the optical and fluidic layers that serves to cap both the waveguides and microchannels.
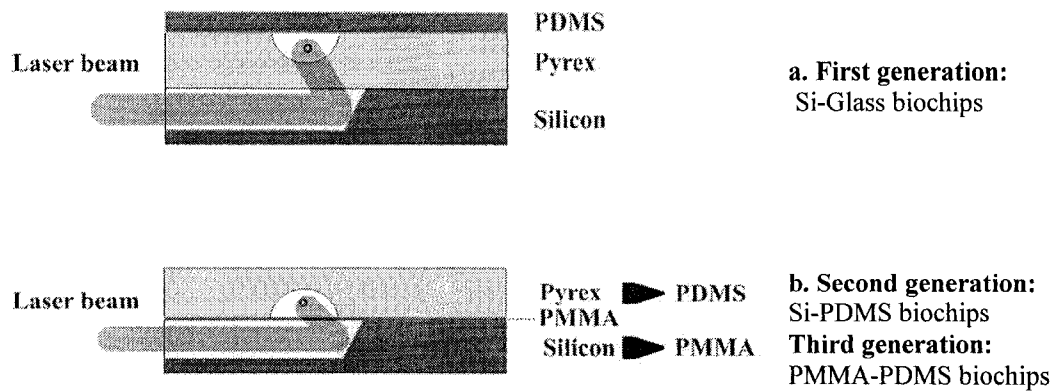
Figure 2.4 Conceptual design of three generation of optics integrated biochips.
a. initial design b. all plastic/low loss

PMMA thin films were chosen as the separating (intermediate) layer because, amongst all commercially available thin transparent films the 50-μm, Goodfellow® [85] PMMA films were proven to have enough strength under fluidic pressures, could pass most of the light and were easy to metallize. Both titanium/silver and chromium/gold thin films were sputtered on the thin PMMA films and the products were smooth, low stress and good-reflecting surfaces. The average roughness of the chromium/gold (30/75 nm) was measured to be less than the 10 nm along 100 microns. This measurement was performed using Zygo optical profilometer [86] and Alpha step profilometer.

The sputtered gold/chrome film on PMMA was compared to the same thickness of the film on glass, the original design of the first generation capping

(fluidic) layer, and the results were depicted in Figure 2.5. This diagram shows that though the loss in the thin PMMA reflecting layer is 10% more than the glass sample, it can still serve as a good capping layer for the hollow v-grooves waveguides.

Loss-Angle
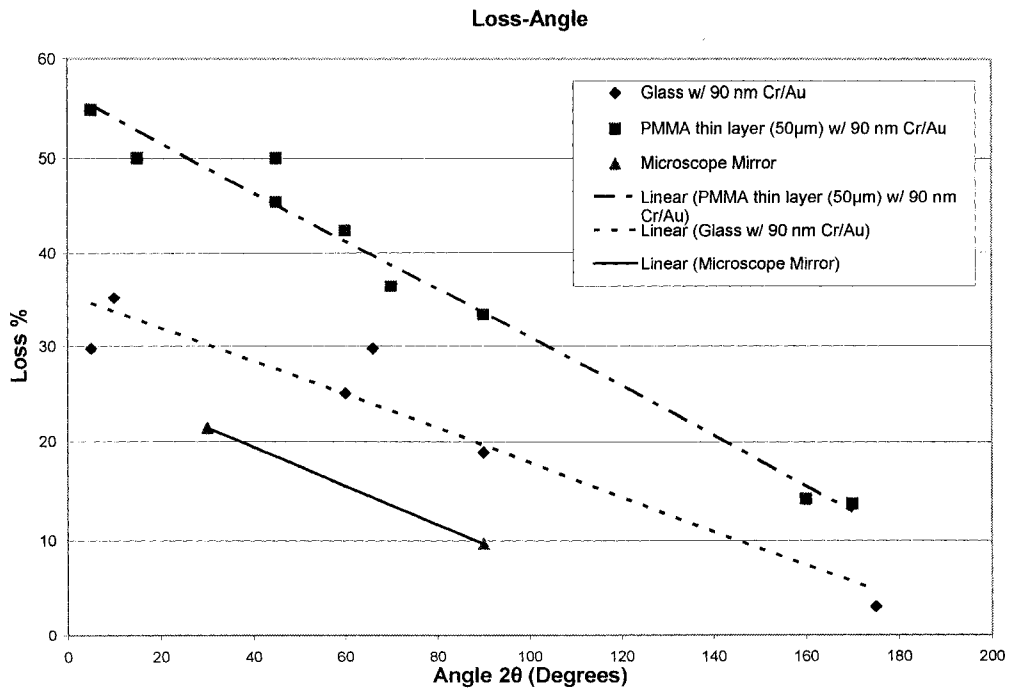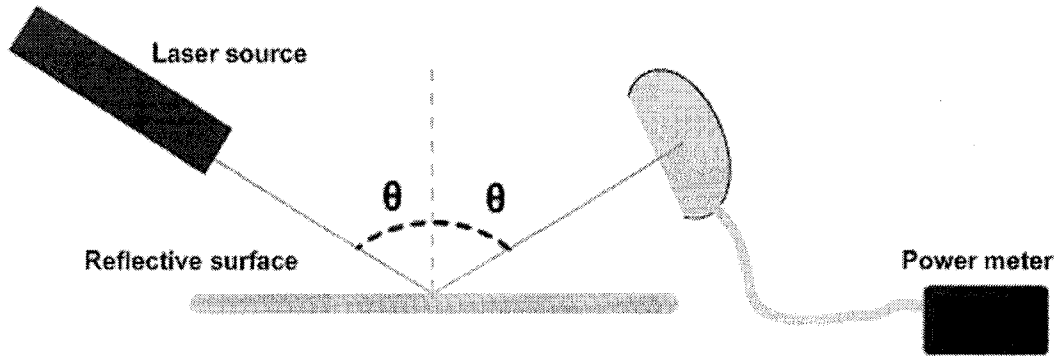
Figure 2.5 Optical loss calculated at different angles of illumination
(@ 532 nm) for thin metal layers on different material
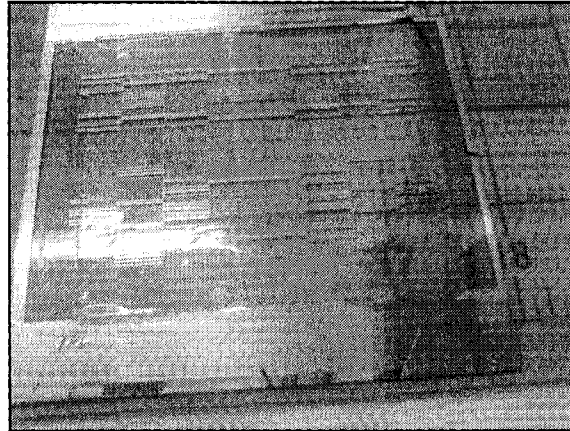
Figure 2.6 Metallized PMMA intermediate layer. Used for the second, third and fourth generation biochips

Using common lithography processes with HPR504 photresist, the sputtered metal film was removed using lift-off process and the capping stripes for the v-grooves were fabricated. PMMA thin film was then tested for different bonding methods, from which, UV-adhesives such as NOA and O_2 plasma bonding [87] with PDMS were successful. A film containing PMMA intermediate layer with metallic strips before dicing is illustrated in Figure 2.6.

Secondly, to address the cost issue in the future generations of biochips, inexpensive polymers can be used to make all of the layers. While polymeric microfluidic biochips have been subject of recent research [55, 88, 89], to the author's knowledge none have reported a multilayer polymeric biochip with integrated optics. The expensive microfabrication steps are still used to make silicon and glass replication masters from which the multiple chip layers may be copied. We have chosen polymethylmethacrylate (PMMA) for the optical layer in the third generation of biochips, since it is rigid and allows metallization, and polydimethylsiloxane (PDMS) was chosen for the fluidic layer since it may be used with both pressure-driven and electro-kinetic flows.

2.2.1.PMMA Intermediate Layer

Essential to both second and third generation biochips is the PMMA intermediate layer that caps both the v-groove waveguides and the microchannels in the PDMS layer. The bonding method used for the PDMS/PMMA interface is RIE in an O_2 plasma treatment [97]. Before bonding the thin PMMA layer to the Si and PDMS, a 95-nm film of Cr/Au was deposited on one side of the PMMA using the Lesker sputter system. Lithography and wet etching were used to define the metal stripes that cap the waveguides and the thin metallized PMMA layer was bonded to the optical layer using droplets of UV-curable NOA60 [84] and the AB-M UV-aligner lithography system.

The 50μ thick PMMA intermediate was proven to solve the accurate delivery of laser beam to the fluidics layer. By reducing the distance between the launching point, reflecting end facet, and the target point in the fluidics the problems due to diffraction and loss in the laser beam were corrected. Also, since the PMMA thin films can be easily treated in RIE chamber with O_2 plasma for 30 seconds and bonded to the PDMS fluidics layer, the bonding issues resulted in the first generation were partly solved.

2.3. Second generation biochips: Silicon-PDMS

The second generation optical masters were fabricated with the same procedure mentioned above; fabrication of Si optical layer for the first generation. After KOH etch process the Si wafers were metallized to be used with the second generation PDMS fluid layer chips.[3] (Figure 2.7)

With the same procedure used to make the glass fluidics, masters for the new PDMS fluidic layers were fabricated using HF wet etch bath with 50μ deep channels. These glass masters were used to make copies in PDMS by a double

---

[3] Some of the Si wafers with developed hollow v-grooves were put aside to be used as replication masters for the third generation biochips with polymer optical layers.

replication process. Before making the first negative PDMS replica, a two-hour silanization of the Glass surface was performed to neutralize surface charges and assist in the removal of the cured PDMS. The negative replica was similarly silanized and used as a master for the final PDMS fluidic layer. Each silanization involves placing the master and a small amount of 1,1,2,2-tetrahydrooctyl-1-trichloro-silane in a desiccator under vacuum for two hours. After silanization, the master is removed, PDMS is cast on it and cured for two hours at 80° C under vacuum in an oven. To make the reservoir inlet/outlets a metallic punch is used before bonding the fluidic layer to the other layers. (Appendix B.2)

Figure 2.8.a shows an intermediate layer and Figure 2.8.b shows the completed second generation biochip with the intermediate layer. Since the optical layer fabricated for the second generation of biochips was KOH etched silicon wafers, bonding defects occurred when using the NOA and consequently motivated the fabrication of the third generation of optofluidic biochips. Figure 2.9 illustrates the PMMA intermediate layer used for the second generation biochips and the final product.

a   b
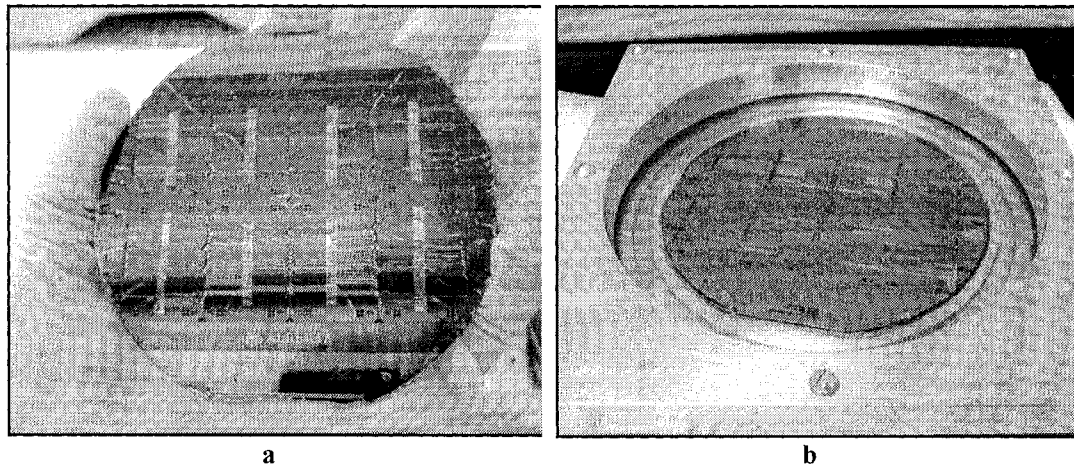
Figure 2.7 Si wafers with v-grooves, a. Si optical layer for first and second generation before dicing: metallized, thick resist spun, b. The Si layer with v-grooves sitting in the clamp for negative replica casting

24

Si V-grooves bonded to PMMA thin layer

PMMA thin layer

a   b
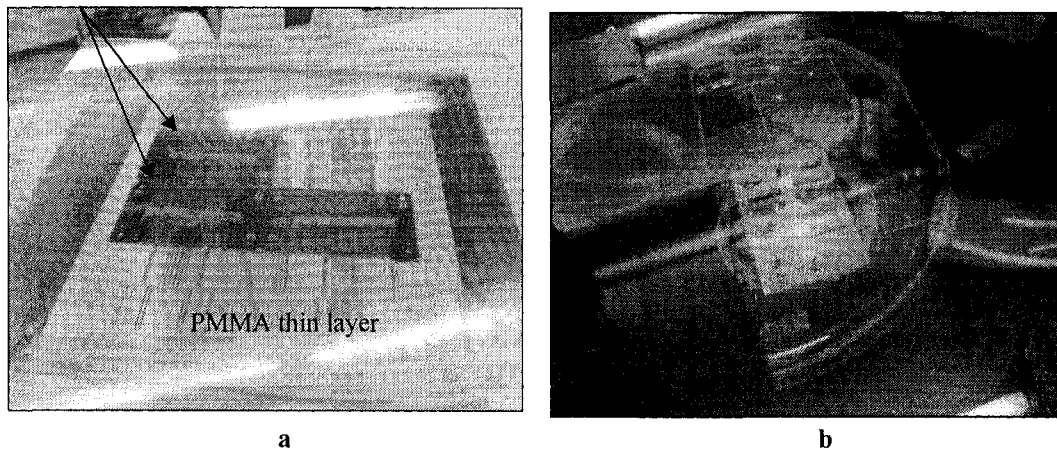
Figure 2.8 Bonding of Second generation biochips, a. Si layer bonded to PMMA layer,
b. bonding the PDMS layer on top of PMMA/Si layer

a.   b.
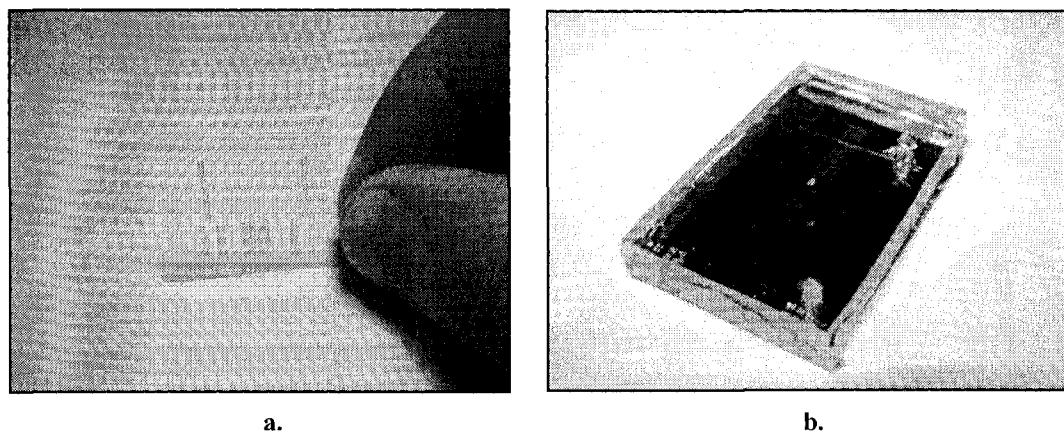
Figure 2.9 Second generation biochip and the PMMA intermediate layer, a. Intermediate
layer (50 μm PMMA film) with metal stripes that cap v-groove waveguides, b. Second
generation biochip with Si optical layer and PDMS fluidics layer

2.4. Third generation biochips: PMMA-PDMS

The third generation of biochips was fabricated with the motivation of having
an all-plastic biochip as the end product. It was determined as a double replication
in PMMA from the original v-groove etched Si masters. Although many double
replication methods were introduced in nanofabrication industry, most of the
common double replication processes are based on the usage of heat/UV-curable

25

PMMA or PDMS replicas using polyvinyl alcohol (PVA) or PDMS as negative replica material. [90-93]

In order to avoid cumbersome chemical compound preparation and fabrication methods for replication, h-PDMS [94] and hot embossing (nanoimprinting) [95] methods were not chosen over PDMS double replication. Moreover, after referring to the literature on PVA casting and microreplication characteristics [100, 101, 103], the double replication using either PDMS or PVA as negative intermediate process replica was chosen for the third generation of biochips.

The final product designed for the optical (bottom) layer is the positive replica fabricated in a way to carry the same topology of v-grooves replicated from Si master into negative replicas. Two materials were chosen for this layer; PMMA and PDMS.

Many advantages made PDMS a good option. Such attractive characteristics of PDMS for our project were flexible PDMS fabrication processes and excellent replication of micro and nanoscale features [49, 57, 62] as well as ease of bonding to the top PDMS layer (oxygen plasma treatment) [87] and cheap manufacturing costs. Also, since PDMS is transparent to a wide spectrum of light, it was obviously a good choice to bring the ability to have access to the biochip for video and signal capturing applications from underneath. PMMA, being inexpensive, transparent and rigid (when cured) alternatively was determined as another option for the double replicated layer containing v-grooves.

Previously, research on step and flash lithography fabrication methods [50] and the project conducted by Pérennès et al. [90] have both shown promising results regarding microreplication and fabrication in PMMA. This fabrication process can be simply described as compounding a mixture of monomer, polymerization initiator and some additives, to fill in the gaps and enhance the plasticity and

shrinkage characteristics, and curing it on a semi-rigid negative replica of the desired micro-components.

2.4.1. Negative Replica

The double replication of silicon v-grooves was considered to be achieved using two different polymers. In order to have an easy master/replica separation, the negative replica should contain a flexible polymer or preferably be an elastomer. Among options such as PDMS, PVA and RTV silicone, due to cheap procedure and material and availability PDMS was chosen as the first choice. The fabrication of the negative replicas and double replication on them were carried out using an aluminum clamp. (Appendix B.1.1)

<div align="center">a.   b.</div>
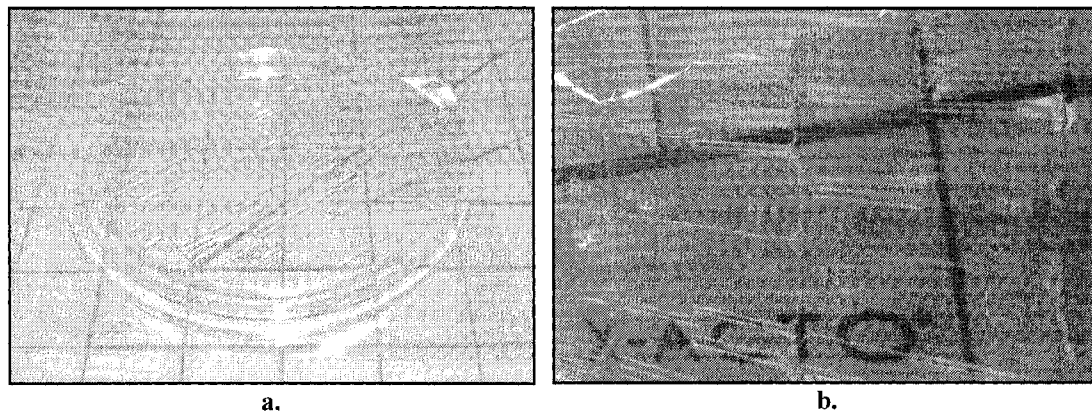
Figure 2.10 v-grooves negative replicas (a) PDMS (b) PVA

The first replication results with PDMS showed very good replicating capabilities. PDMS is elastomeric and transparent and that helps with casting and curing of another material. Figures 2.10.a and 2.11 show the results of fabrication of v-groove negative replicas in PDMS. The PDMS specimens were compared to the original Si samples and the shrinkage of features was not significant. Since the PDMS compound was degassed before casting and cured gradually over 2 hours, all the features were completely replicated into the PDMS structure.
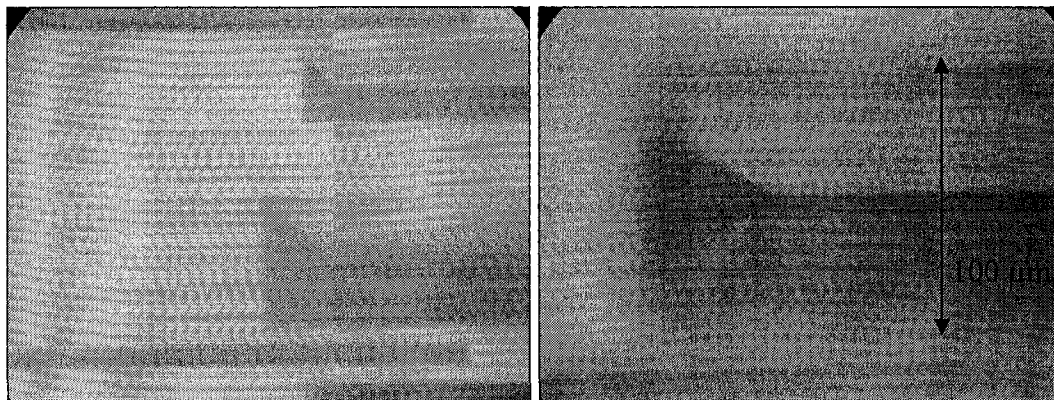
Figure 2.11 V-grooves' negative in PDMS replica

PDMS negative replicas are not the most durable, but based on the literature were expected to be used for more than one replication into positive replicas [96]. Using the same fabrication process used to make the negative replicas, as well as what we used for the fluidics layer in the second generation biochips, the double replicas in PDMS were fabricated. The positive replicas showed very promising compatibility with the original Si layer when the topologies of surface features were compared, but unfortunately, when these PDMS negative replicas were used for PMMA casting, they didn't last due to chemical incompatibility of methylmethacrylate (MMA) and PDMS. (Figure 2.12)

PVA, as the second choice, was then tested for negative replica fabrication (Figure 2.10.b). The PVA negative replicas were fabricated using a commercially available PVA solution PARTALL® coverall (Rexco Co.,USA) [97]. The solution was outgassed and boiled for reducing the water content. The PVA solutions with water contents reduced to 10,15, 25 and 30 percent[4] were tested and among all the compound with 25% less water content than the original

---

[4] The water content can be calculated using the densities of PVA and water and by knowing the initial PARTALL PVA concentration. The container is weighed before and after evaporation of the water from solution to determine the final concentration.

28

product returned the best results; no shrinkage, easy to pour and not very viscous, easy to cast and degas, good covering and no edge effects.
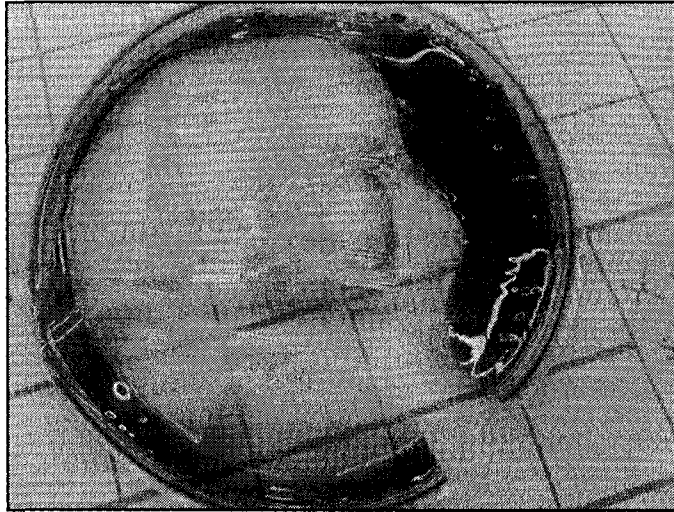
Figure 2.12   PDMS negative replica after curing PMMA on top

PVA has good chemical compatibility with PMMA and PDMS and is easier to remove from the double casts since it is water soluble ($40^{O}C$ water bath for 2 hours). Also the features replicated in PVA show no shrinkage or defect in the structure. The PVA compound entered all of the v-grooves and cured over a period of 12 hour at $55^{O}C$. (Figure 2.13)
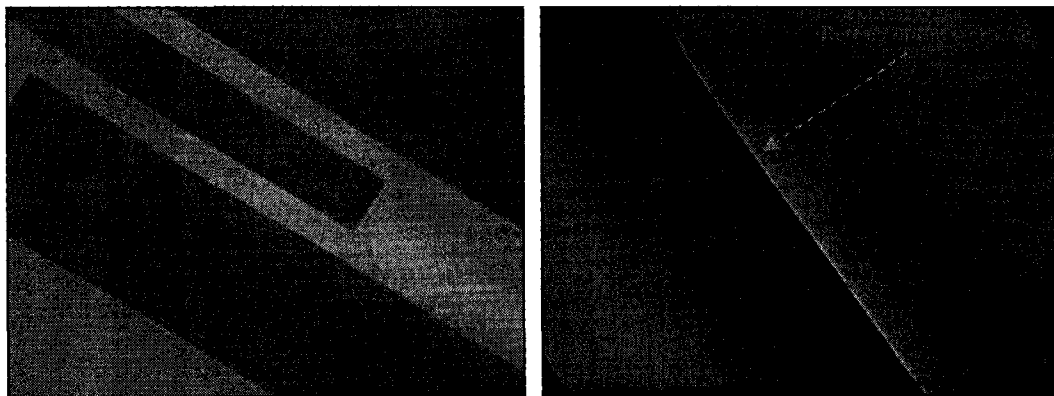
Figure 2.13 V-grooves' negative in PVA replica

Rexco PARTALL® PVA, which was chosen as the negative replica material, is transparent when cured enabling the cured features to be seen when the specimen is taken out of the oven. In addition, this product can be purchased in purple which distinctively assists separation of the negative replica from the positive replica, PMMA or PDMS, when PVA is dissolved in water.

2.4.2. Positive Replica

In this part the effort was to produce positive replicas that are fabricated to perform as fit as the original Si optical layers. The hollow waveguides fabricated in the Si layer are double replicated resulting in PDMS or PMMA replicas. The first and most important feature being sought is the replication quality. Both PMMA and PDMS specimens were tested for shrinkage after cure, covering and replication of features and defects in the surface as a cause of a bubble or discontinuity in the texture.

The v-grooves in the double replicated optical layers, as designed and fabricated in the first and second generations, were metallized by sputtering. Since the biochips in the first generation were designed to be used with a red laser, gold covered side walls were the most appropriate option. Due to the change in the optical layer material and in order to have better and maybe cheaper v-groove metal coatings, in addition to having the ability to guide green laser through the plastic v-grooves, both silver and gold were selected to be sputtered on PDMS and PMMA replicas. Chromium and titanium thin layers were sputtered to serve as gold and silver adhesion layers respectively. Other metals such as platinum, copper and aluminum, theoretically should be reflective to red light (Figure 2.14), they were found to be not suitable since the samples of these films on Si didn't demonstrate reflection and smoothness. Also, because silver tarnishes over time, silver coated samples were only stable when kept under vacuum conditions.
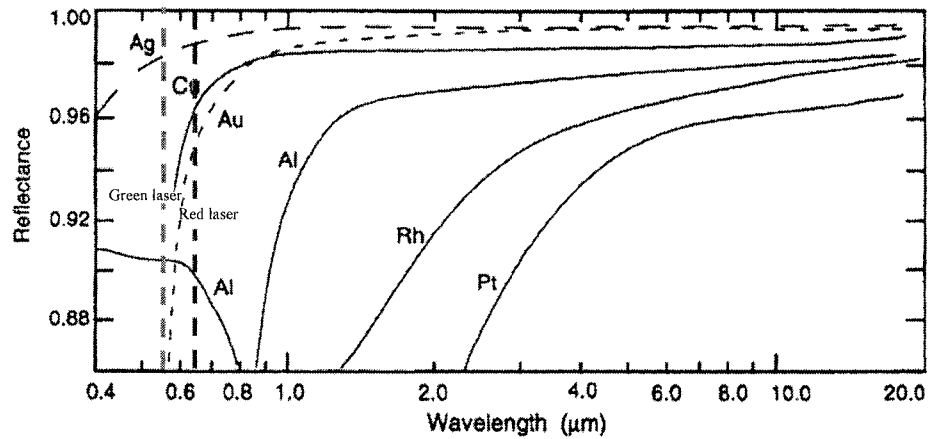
Figure 2.14 Reflectivity of 100nm thick films of metals [98]

When sputtered with metal, PDMS is subject to stress when the thin film is deposited on its surface [109]. Hence positive replicas in PDMS wrinkled and deformed after sputtering and the surface was nor reflecting any light (Figure 2.15.a). Conversely, the PMMA v-grooves, sputtered with metal showed good reflectivity (Figure 2.15.b).
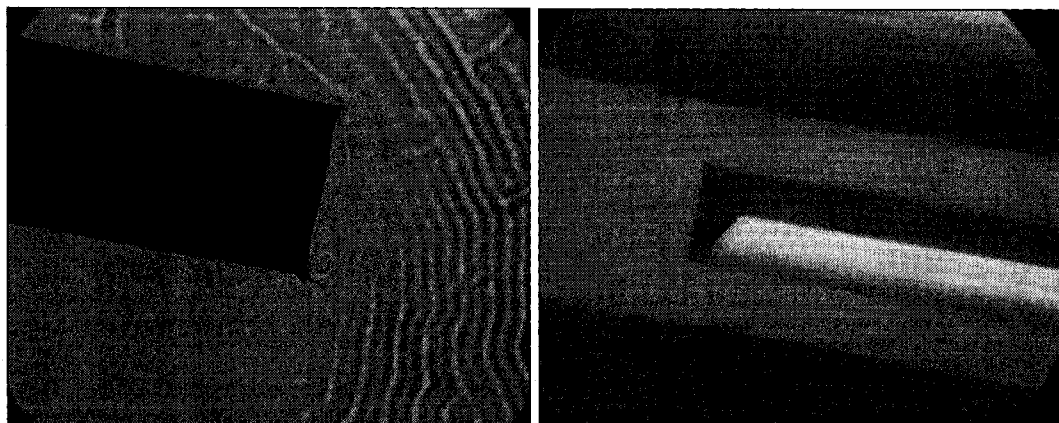
Figure 2.15 Metallized PDMS vs. metallized PMMA: a. Cr/Au metallized PDMS v-groove, b. Cr/Au sputtered PMMA v-groove

Different thicknesses of metal films were sputtered on commercial PMMA sheets to decide the balanced thickness for the reflective thin film. The metal coating should be both cost/time efficient in fabrication process and sufficiently

reflective. Table 2.1 shows the different thicknesses of thin films sputtered from which 30/75 nm Cr/Au and 30/60 nm Ti/Ag films were selected.

	I	II	III	IV
Silver	30 nm	40 nm	60 nm	90 nm
Titanium	10 nm	20 nm	30 nm	30 nm
Total thickness	40 nm	60 nm	90 nm	120 nm
Reflection	Poor	Fair	Good	Good
Surface quality	Smooth	Smooth	Smooth	Not Smooth
Durability (tape test)	Weak	Good	Good	

	I	II	III	IV
Gold	30 nm	40 nm	60 nm	75 nm
Chrome	10 nm	20 nm	30 nm	30 nm
Total thickness	40 nm	60 nm	90 nm	105 nm
Reflection	Poor	Fair	Fair	Good
Surface quality	Smooth	Smooth	Smooth	Smooth
Durability (tape test)	Weak	Weak	Good	Good

Table 2.1 results of sputtering various thicknesses of metal thin films on PMMA

2.4.3. The PMMA compounds

PMMA was decided to be the most suitable material for the fabrication of third generation optical layer. PMMA is widely used for bone replacements and bone adhesive applications from which much advancement in formulation of compounds based on MMA molecular backbone has arisen [99]. In this project, PMMA compounds used in different applications were synthesized and analyzed. Also, based on a few research papers, recently published on micro feature replication into PMMA casted compounds such as step and flash method [50] and the work done by Pérennès [90], a number of heat-initiator curable and UV-initiator curable compounds were used for replication.

PMMA beads are usually added to MMA and dissolved before curing MMA. Having PMMA molecules in the compound can accelerate the polymerization and reduces the shrinkage due to network formation. Since the optical layer has to have smooth surfaces and good optical clarity, PMMA beads that are commercially available for optical parts manufacturing were used in the

polymerization compounds. Different amounts of PMMA were dissolved in MMA. Among these, a 6:4 ratio was found the most efficient. More shrinkage was observed when the ratio was less than this amount. Dissolving more PMMA than this amount, although it will theoretically reduce shrinkage, results in lengthy (inefficient) polymerization and time consuming dissolution process.

Since the MMA is stored in containers with inhibitors and the process of washing the inhibitor, due to University of Alberta Nanofab regulations, was not possible, instead of removing the inhibitor hydroquinone, stronger initiator and accelerator concentrations were used to compensate and overcome the inhibitor.

The room temperature curing of PMMA compounds was carried out using dibenzoylperoxide (BPO) which was purchased with 1% water content and refrigerated, and only before mixing the compound, was finely ground and dehumidified. BPO concentrations of 1, 1.5, 2, 2.5, 3, 5 and 7 were added to different samples. Then, plasticizer dibutyl-phthalate was added to the MMA-PMMA-BPO mixture by 5% of total weight. In order to initiate the polymerization at room temperature, 1% w N, N- dimethylaniline (DMA) was added to the mixture and left to cure for 2 to 12 hours. BPO of 1.5 % was determined to be the best fit in the compound.
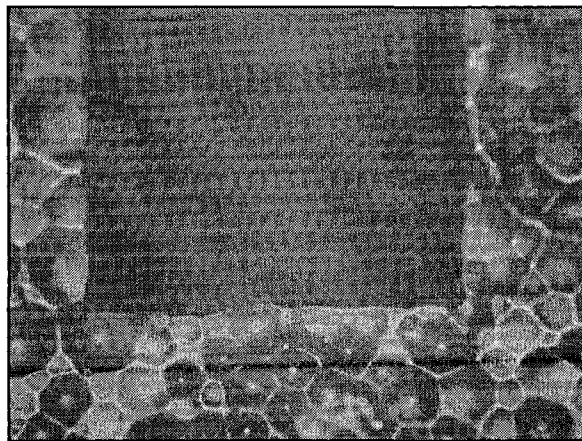
Figure 2.16 end facet of a BPO cured PMMA v-groove: bubbling issues
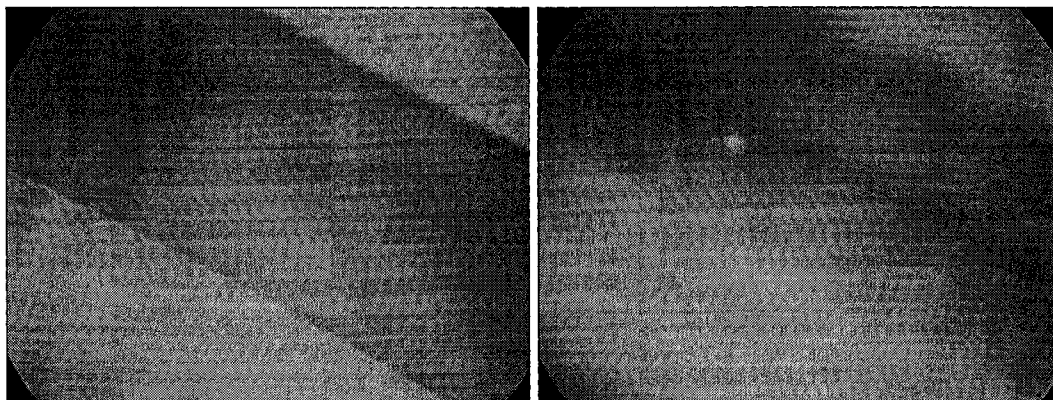
Figure 2.17 PMMA v-grooves: BPO cured

The first attempts at curing PMMA solution on PVA replicas using BPO and DMA resulted in rough surfaces and bubble production. (Figure 2.16) In order to solve this issue, the solutions were degassed in a 3 step degassing process in a desiccator chamber and while curing, the PVA replica covered by MMA-PMMA mixture was kept under vacuum. Low-shrink smooth PMMA features resulted from this procedure (Figure 2.17). For more information about PMMA, MMA and polymerization of MMA as well as inhibitors please refer to Appendix A.6.

2.4.4. Third generation fabrication processes

As mentioned above, in order to reduce the cost of the multiplayer biochips, methods were developed for replicating the optical layer in PMMA. PMMA was chosen due to its clarity after polymerization, its hardness and scratch resistance and the quality of the reflective surface after metallization. As with the fluidic layer, a double replication technique was used but in this case, polyvinyl-alcohol (PVA) was used for the first negative replica. PVA was chosen because it is water-soluble and thus is easily removed from the rigid, polymerized PMMA monomer in a $40^{O}C$ water bath [100]. Both PVA and PMMA have good capabilities for replicating features and with the fabrication methods employed, the shrinkage is negligible in both polymers.

In the first replication step, the silicon wafers with v-grooves were cleaned in a piranha solution and placed in a custom clamp system where a water mixture of PARTALL® coverall polyvinyl-alcohol (PVA) (Rexco Co.,USA) [29], was poured on top and cured in an oven at 55° C for 12 hours. The water content of the PVA solution was reduced by 25 % prior to casting. When the PVA replica was peeled away from the Si masters, it was placed in another vessel custom-designed for casting methylmethacrylate (MMA) mixtures. (Figure 2.18)

Both peroxide-activated and ultraviolet-initiated polymerizations were used to fabricate PMMA replicas. The base polymer mixture was DEGACRYL® PMMA (Degussa Corp., USA [30]) granules dissolved in MMA by 6:4 weight ratio. The reason PMMA was dissolved in the mixture in this ratio was to reduce the shrinkage of the polymer replica while speeding the polymerization due to presence of polymerized DEGACRYL powder. The mixture was degassed using a desiccator. An addition of 1.5% wt of a peroxide such as dibenzoylperoxide (BPO) along with 1% wt N, N- dimethylaniline and 3% wt dibutyl-phthalate as the plasticizer will initiate the polymerization of the mixture cast on the PVA negative replica at room temperature. After 4 hours of polymerization, the PMMA replica was placed in the water bath to wash the PVA away. After initial evaluations, the shrinkage of PMMA replica was found to be less than 3%. Figure 2.19.a shows a piece of peroxide polymerized PMMA with a Cr/Au reflective film. (Figure 2.20)
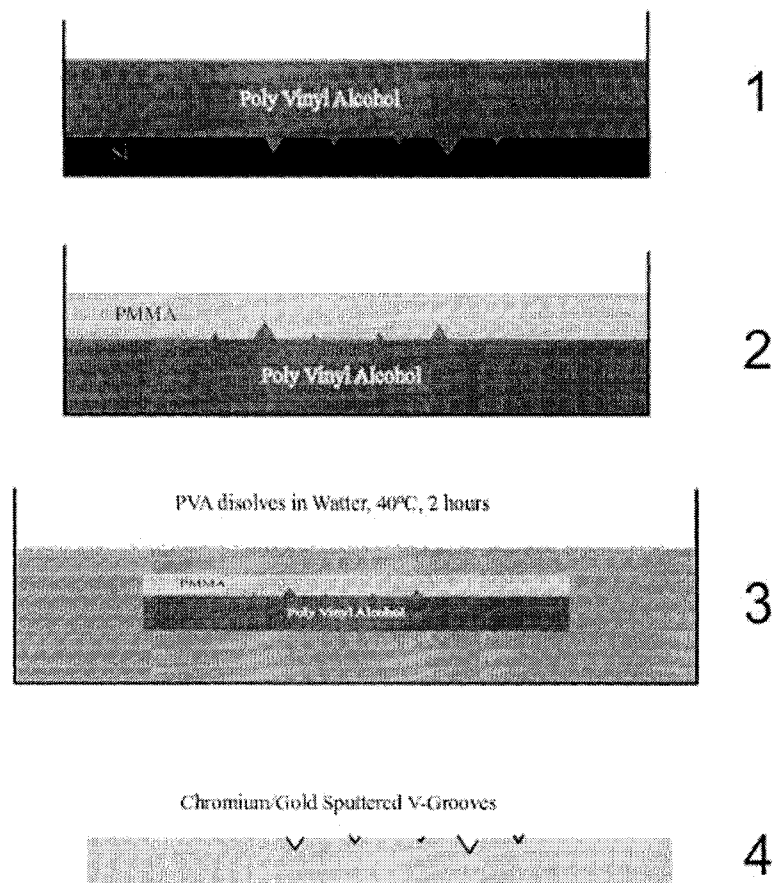
Figure 2.18 Double replication of v-grooves using PVA and PMMA

For the UV-initiated polymerization, the same 6:4 weight ratio was used for dissolving PMMA into MMA. Taking into account the mixture properties and the UV source used for curing, 1.5% wt of two different UV-initiators, IRGACURE 819, (bis(2,4,6-trimethylbenzoyl)phenylphosphine oxide) and IRGACURE 184 (1-Hydroxy-cyclohexyl-phenyl-ketone), Ciba Specialty Chemicals [101], were added to the mixture and then out-gassed under a slight vacuum. Pouring the UV-curable PMMA mixture onto the PVA sitting in a clamp, the PMMA replica was cured under a 360-nm UV light for 5 minutes. As before, the PVA was dissolved from the PMMA and initial evaluations show the shrinkage in the UV-cured

PMMA was less than 2%. Figure 2.19.b shows a piece of UV-cured PMMA with replicated features from a silicon master while the magnified view in Figure 2.21 shows the quality of the replicated v-grooves.
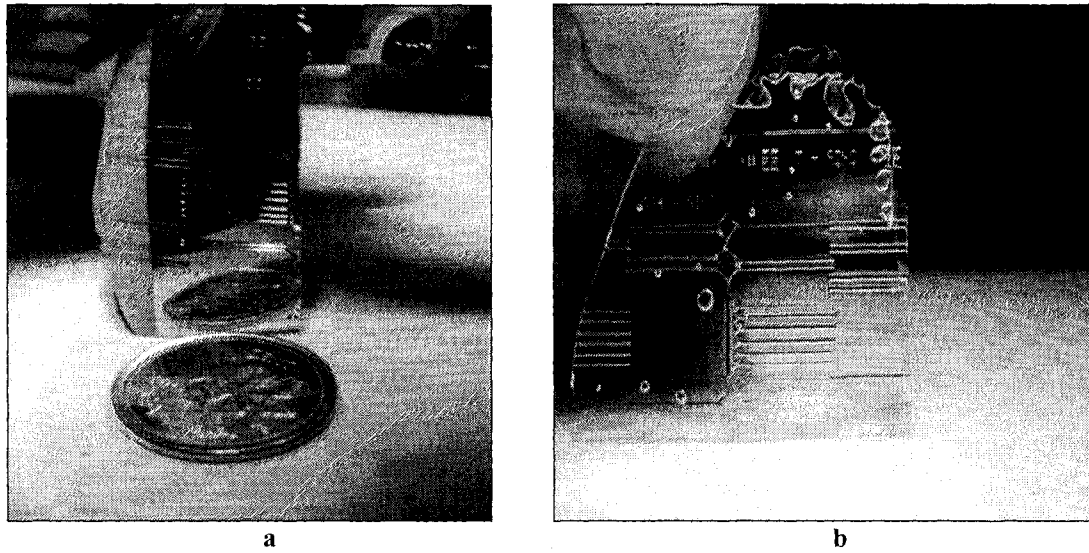
Figure 2.19 PMMA v-groove replica layer, a. Cr/Au reflective film deposited on peroxide polymerized PMMA, b. UV-cured PMMA optical layer before metallization
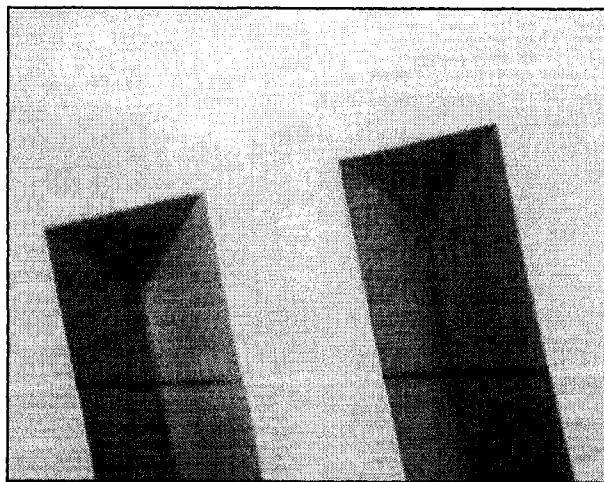
Figure 2.20 End facets of 200 microns wide V-grooves replicated in PMMA (BPO cured)

The PMMA replicas of V-groove optical layer made using these two different fabrication methods are optically transparent and rigid. These polymeric substrates were sputtered with titanium and silver as well as chromium and gold followed by lithography and wet etch processes to remove the excess metal from flat surfaces, leaving the v-grooves as the only metallized surfaces on PMMA. As with the second generation biochips, the optical layers were bonded to the thin-PMMA/PDMS fluidic layer using NOA UV-curable epoxy. The fluidic layer reservoirs were punched for inlet/outlet ports using punches. (Appendix B.2)
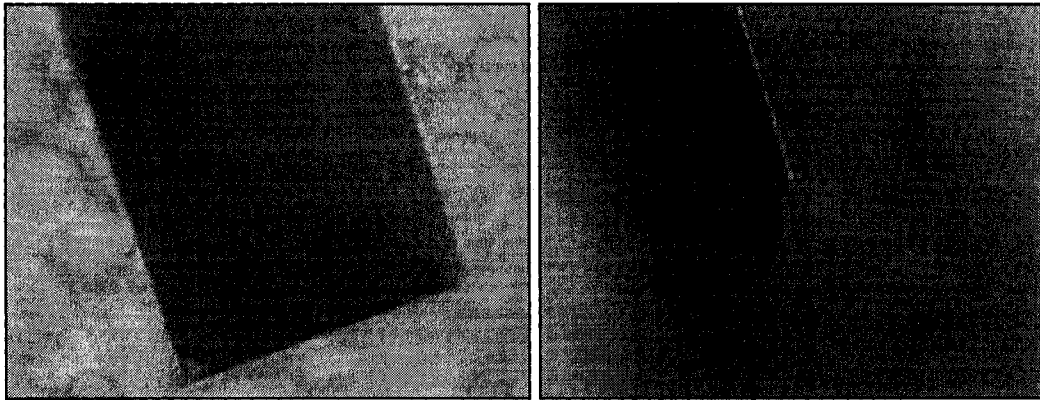
Figure 2.21 UV-cured PMMA v-grooves

2.4.5. Third generation issues

Third generation biochip's fabrication processes, compared to other fabrication processes reported in the literature [62, 98], are easy to use and the results were satisfactory, but some issues with dicing and bonding occurred. Dicing PMMA samples is costly since the dicing saws have very high maintenances costs after a few dicing passes of PMMA or other epoxy material.

PMMA shows good bonding results with PDMS when both are treated with O_2 plasma, but the same procedure cannot be used for PMMA-PMMA bonding. The only satisfactory solution was optical adhesives. Bonding the PMMA optical layer to the thin PMMA film with metallic stripes on its surface was carried out using

38

NOA UV-curing, however the use of NOA caused misalignment of the different layers bonded as well as extra gaps between the layers.

In addition, it was concluded that UV-cured PMMA mixture, though being fast and efficient curing and showing low shrinkage, it can be replaced by monomers and oligomers used in UV curing processes such as polyepoxyacrylate, and obtain the same results without lengthy preparation processes.

PMMA-MMA mixtures are hard to cast on any other material than PVA. Also, PVA, though it's cheap and water soluble, needs time for preparation, water reduction and curing stages. Furthermore, PVA negative replicas are used as single-time negative masters resulting in more time and cost inefficiency.

2.5. Fourth generation biochips

A fourth generation of biochips were designed and fabricated to solve the issues that occurred during the fabrication of third generation of biochips. The goal was to solve problems with time-consuming processes and master fabrication for replication. The biochip consists of three polymeric layers and contains a network of two different kinds of waveguides that can distribute light to the fluidic system and collect fluorescence from particles in the microchannels. Keeping the v-grooves optical layer design, the design of the fluidics layer was changed. Instead of simple PCR, T-channel or cross-channel fluidics that was replicated from glass masters in the first generation, the fourth generation fluidic layer was designed such that it carries one input and three outputs. This alignment marks on this layer were designed using the measurements and alignment marks of the original design of v-grooves mask. This allows the two layers to be bonded to each other.

Moreover, the fluidics in this generation were designed to carry a group of three liquid core waveguides converging at a point of the fluidic microchannel. This allows the user to illuminate this specific location of the fluidics using the v-

39

groove aligned underneath and pick up the fluorescence response of the samples using the LCWs. Another application can be illumination of the microchannel with two or three different wavelengths using the LCWs and picking up of the response through the v-groove beneath. Figure 2.22 summarizes the ideas and designed features for the fourth generation biochips.

UV-curable polysiliconeacrylate (PSiA) was synthesized to be used for the fluidics layer. PSiA monomeric solution is a mixture of siliconized acrylate monomers and UV sensitive ketone peroxide solution that serves as UV initiator. This novel polymeric material is more flexible and more durable than PDMS and, unlike oven-cured PDMS, cures within seconds under a UV lamp. One other advantage of PSiA, compared to PDMS, is that it can be silanized and used for double replication because it will not stick to the cured films of the positive replica.

BioChip layers

A: Polysiliconeacrylate
Opto-fluidic Layer

B: Polymethylmethacrylate
50 micron thickness
Intermediate Layer

C: Polyepoxyacrylate
Optics Layer

LEGEND:

Biochip side section view

1, 2, 3: Liquid core waveguides
4 - Output fluidic reservoirs
5 - Input fluidic reservoir
6 - Metallic strip to cap ...
7 - ... metallized hollow waveguide
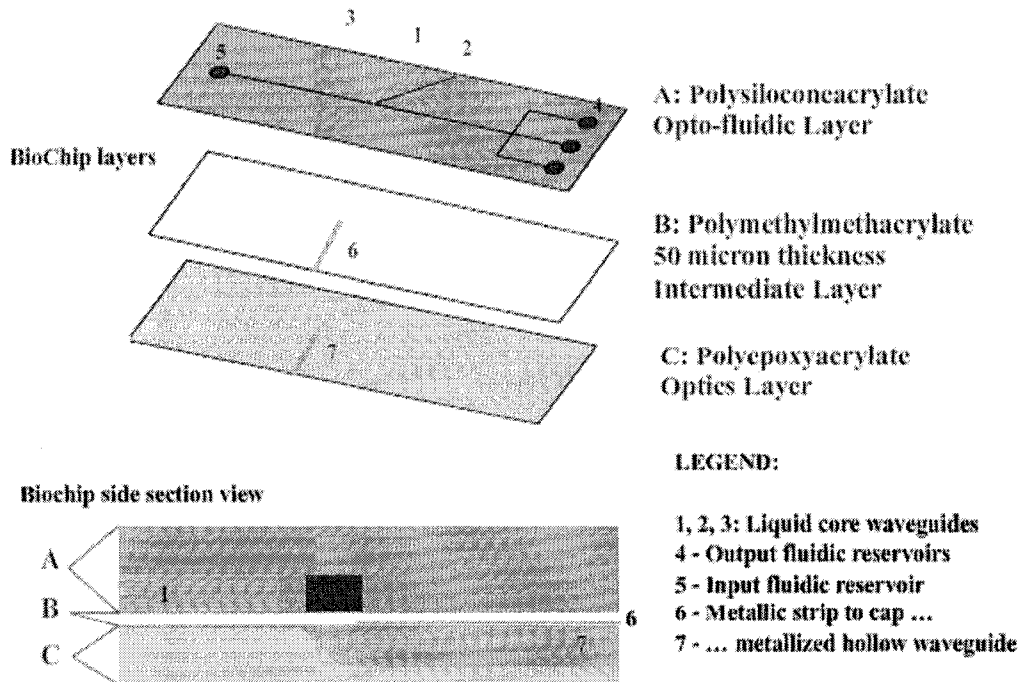
Figure 2.22 Fourth generation biochips, schematic design

40

The fluidics layer is fabricated using a double replication in PSiA from a Si master with micrchannels fabricated using deep reactive ion etching. The silicon master for the microchannel and LCW features was etched down to 50 μm. More details on fabrication of LCW biochips using silicon masters can be found in Chapter 3. (Figure 2.23)

Similar to the past generations, the optical (lower) level consists of a network of parallel chromium/gold sputtered hollow v-grooves with angled end facets which would serve as reflecting surfaces to illuminate the fluidic channel on the upper level. This layer was designed to be double replicated using PSiA as the negative replica and polyepoxyacrylate (PEA) as the final product material. The silicon master containing v-grooves was silanized and a negative master of PSiA was casted on the surface and then a PEA mixture was cured on top of the negative replica. The PEA monomeric solution contains a UV curing agent with a methyloxy chain and can be cured in a few seconds.
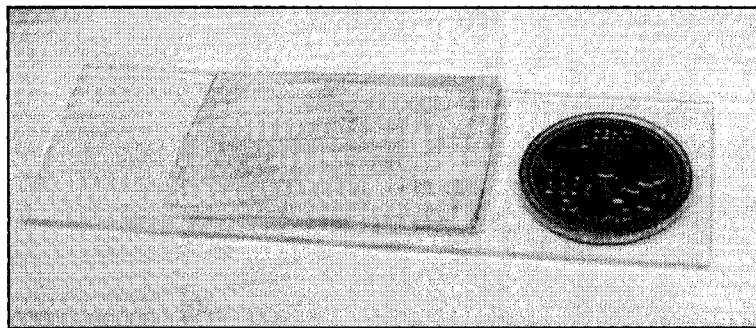
Figure 2.23 The Fourth generation fluidics layer in PSiA on a glass slide

The lower level is made of a hard epoxyacrylic material to assure the firmness of the structure. Following the etching of v-grooves in the Si, the wafer was silanized using a drop of trichloro(1,1,2,2-perfluoocytl)silane vaporized and spread into a single monolayer on top of the Si wafer under vacuum in a desiccator. A 95-2.5-2.5% mixture of a difunctional silicone acrylate (CN9800, Sartomer, USA [102]), 1-Hydroxy-cyclohexyl-phenyl-ketone and

Benzophenoneon (Irgacure 500, Ciba Special Chem., USA) was poured on the Si wafer with v-grooves. After exposing the mixture on top of the wafer to UV for 120 seconds and peeling off the silicone-acrylate with negative features (Figure 2.24.a), the replica is placed in the desiccator for a 2 hour silanization process. In order to prepare the photocurable epoxyacrylic mixture for the positive replica a 50-45-5% compound of Ethoxylated (3) Bisphenol A Diacrylate (SR349, Sartomer, USA), Ethoxylated (4) Bisphenol A Diacrylate (SR601, Sartomer, USA) and 2,2-Dimethoxy-1,2-diphenylethan-1-one (Irgacure 651, Ciba Special Chem., USA) was stirred mechanically and degassed under -28 inHg and stored at 15° C. The blend is then poured on the hydrophobized surface of the negative replica and was supported using a 500µm thick borosilicate glass substrate followed by a 10 second UV exposion. Stripping the PSiA negative replica, the PEA sample was sputtered with 30 nm of chromium and 75 nm of gold and then using traditional micro-optical lithography the metal was etched off anywhere outside of the v-grooves. Figure 2.24.b illustrates a v-groove replication into the surface of PEA.
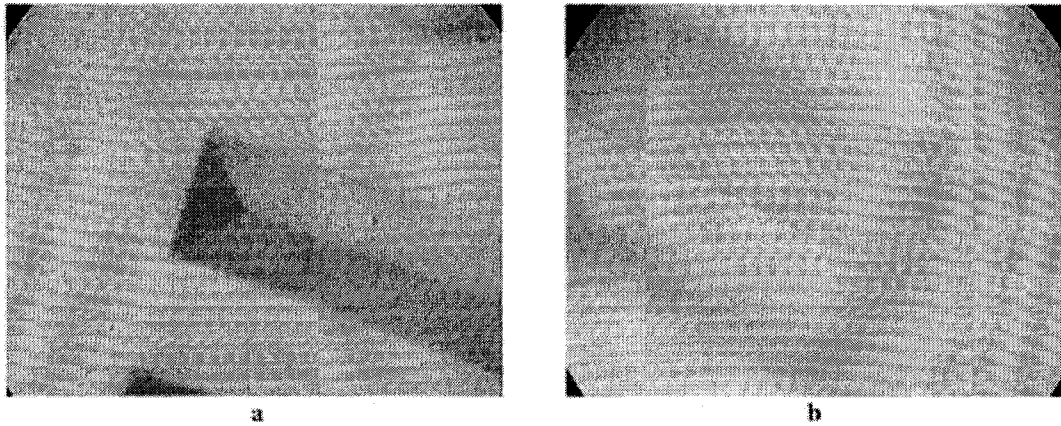
Figure 2.24 . a. Negative replicas of v-grooves in PSiA b.and Positive replicas in PEA

The advantage of using the PEA for the bottom part is that this hard polymer would make the composite biochip more rigid and the replication process would be a simple pour and cure process. A major part of UV-curable epoxy-acrylate

mixtures is Ethoxylated (3) Bisphenol A Diacrylate (Figure 2.25) which is a difunctional monomer for which, due to the large volume of the molecule, the shrinkage of the cured product is negligible. This molecule was compared to other multi-functional molecules such as Ebecryl 150 [103] (bis-phenol A ethoxy diacrylate) in experiments and showed less yellowing, more rigidity and faster polymerization results.
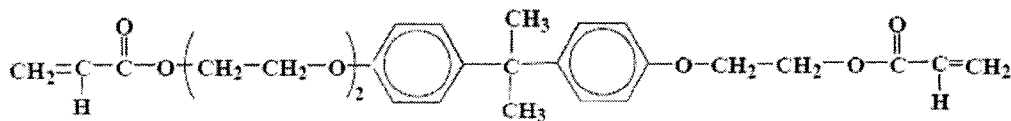
Figure 2.25 Ethoxylated (3) Bisphenol A Diacrylate (SR349, Sartomer, USA)

To complete the fabrication process, O_2 plasma treatment of the silicone-acrylate and thin PMMA capping layer for 35 seconds is utilized to seal-bond the two layers while the bottom side of the thin PMMA layer with the metallic stripes was bonded to the PEA optical layer using fast spun(5000 RPM for 4 minutes) NOA. This approach to NOA bonding reduced the issues due to misalignment. The NOA film thickness was estimated to be less than 10 microns.

The next chapter describes the procedure for the design and fabrication of the LCW biochips.

CHAPTER 3

SINGLE-LAYER BIOCHIPS

The single-layer biochips discussed here are the LCW embedded fluidics layers that were initially designed and fabricated for the fourth generation of multilayer biochips. The purpose of this part of the project was not only to make a new design of biochips with integrated of LCWs, but to compare the results with another research project. While C. Bliss [80, 89] was fabricating the LCWs using SU-8 masters in PDMS, it was decided to find another fabrication processes to make smoother sidewalls and higher quality waveguides. Moreover, by selecting a group of different plastics, mostly UV-curable, such as PSiA, PUA, PDMS and APFPE to fabricate this design of optofluidic biochips, a variety of fluids can be analyzed. PSiA and PUA are more corrosion resistant and APFPE can be used for high pressure flows or corrosive solutions [63, 67].

Over time, it was proven that these devices can be easily used as standalone single-layer biochips and still have the capability to be aligned on top of the v-grooves for more elaborate experiments. The fabrication method chosen for these biochips was to make Si masters using highly anisotropic etching methods such as deep reactive-ion etching (DRIE). One Si master can be fabricated, silanized and used for replication of micro-features into any of the above mentioned material and the end product would be a disposable specimen for lab-on-a-chip applications. In addition, the walls fabricated with DRIE have none of the problems associated with SU-8 fabrication such as t-toping [104], residual

photoresist, cracks and negatively sloped walls instead of vertical features [105]. For more information on DRIE process please refer to Appendix C.2.

3.1. The Evolution of biochips

In the process of fabricating optofluidic biochips with liquid waveguides, the focus was to make fluidic channels with at least 3 LCWs, hollow channels to be filled with a liquid e.g. glycerol, pointing at the microchannel detection spot. Since the main goal of this project was to improve the fabrication processes and material selection, four iterations of biochips were designed and fabricated in order to achieve the final design for LCW biochip. These biochips were progressively improved by making changes to the placement or shape of the component or fabrication processes involved.
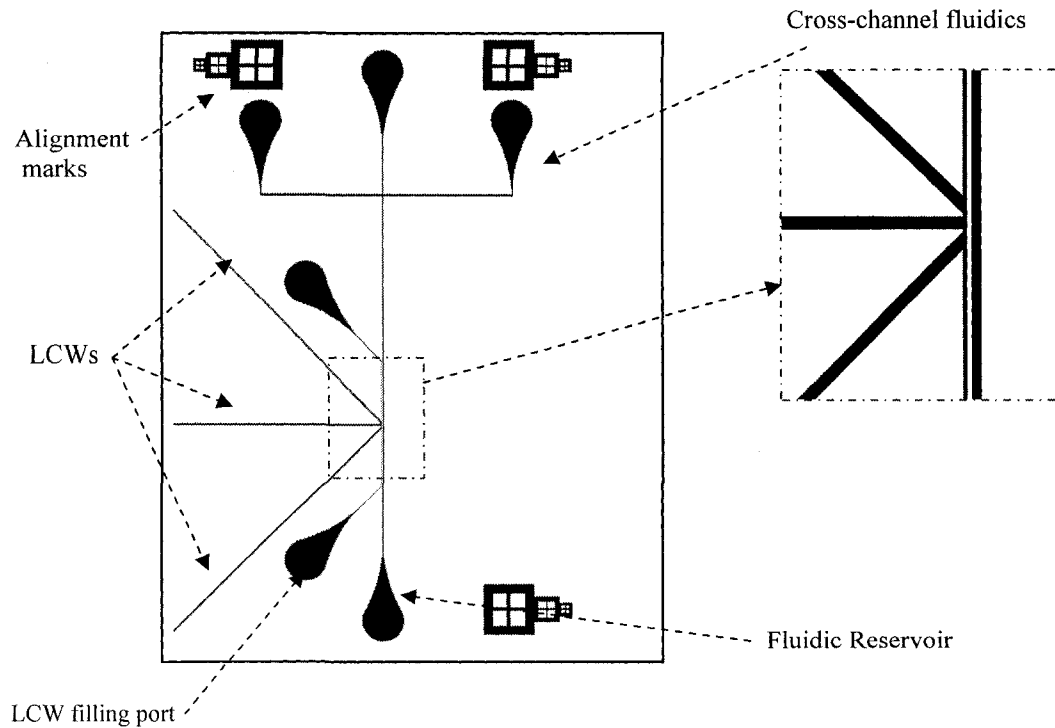
Figure 3.1 Initial Design of LCW biochips

45

3.1.1.Initial Design

The initial design, as depicted in Figure 3.1, has one input and three output 50μ wide and 50μ deep fluidic channels. Also, in this design, the tear drop shape of the reservoirs helps the particles in the fluid exit easily. The LCWs are all three connected to each other and to two side fluidic channels that serve as filling ports. The end or the adjacent wall of the LCW structure to the fluidics is placed 25μ from the fluidics wall. In addition, for better particle movements and in order to avoid clogs of particles in the microchannel entrance, the circle-shaped reservoirs, used in the other biochips, were substituted with tear-shaped reservoirs.

After designing the photolithography mask, both PDMS and PSiA were chosen to fabricate the LCW-integrated biochip. The Bosch DRIE process was utilized to fabricate the master in Si and using double replication the plastic replicas were fabricated. The piranha cleaned {100} silicon wafer was first sputtered with 150nm of chromium and using a chrome/glass mask and optical lithography followed by chrome wet etch the openings were made in the chromium mask. After removing silicon oxide (pre-cleaning step) with a 2 minute buffered oxide etch, a mixture of NH_4F and HF (B.O.E.) dip, Oxford ICP Deep Reactive Ion Etching (DRIE) was employed to etch the silicon wafer on the openings as deep as 50 microns. Bosch process DRIE would etch the silicon leaving low roughness, close to vertical walls.

After DRIE and removal of the rest of the chromium from the surface using a wet etch, the silicon wafer was silanized using the same procedure mentioned before for 2 hours. PDMS or PSiA mixtures were poured on top of the Si master in a stainless steel clamp (Appendix B.1.2) and cured. PSiA blend is a mixture of Sartomer CN9800 oligomer [102] with 5% wt IRGACURE 500 photoinitiator (Ciba specialty chemicals [101]) and degassed in a desiccator for 8 hours. The cure process is generally more efficient in the absence of oxygen, so a greater amount of photoinitiator is generally required in the presence of oxygen. The

46

negative replicas were then silanized and put in the clamped and covered with more of the curable polymer compounds. The PSiA UV-curable blend was cured under UV irradiation for 60 seconds and PDMS was cured for 2 hours in the oven ($80^{\circ}C$).

Alignment marks that fit the v-groove layer

LCW filling fluidic reservoir
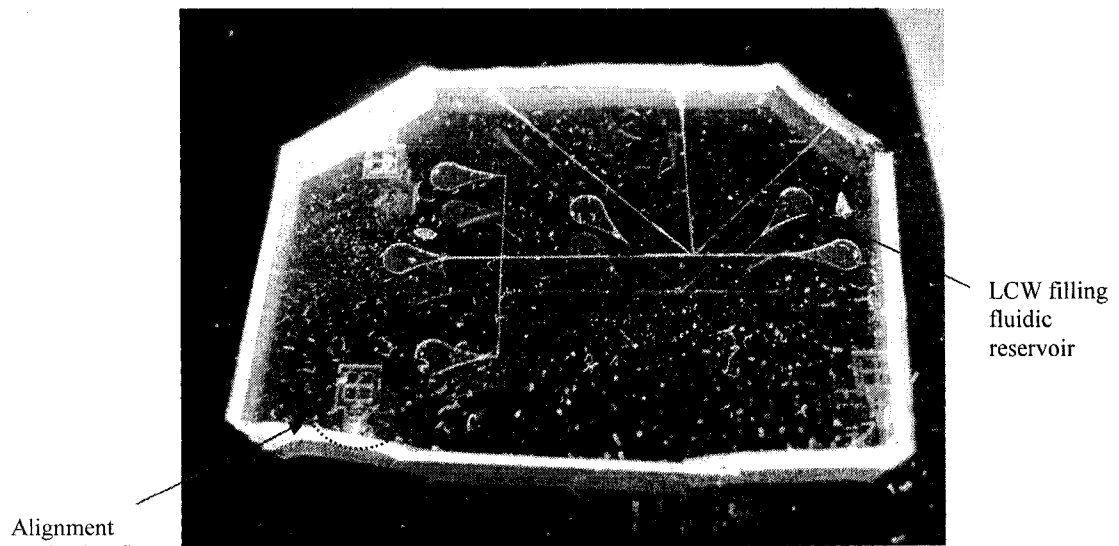
Figure 3.2 PDMS biochip with LCWs

Biochip fluidic reservoir

LCW negative feature

The wide input port (coupling) for the LCW

The broken part of LCW negative replica
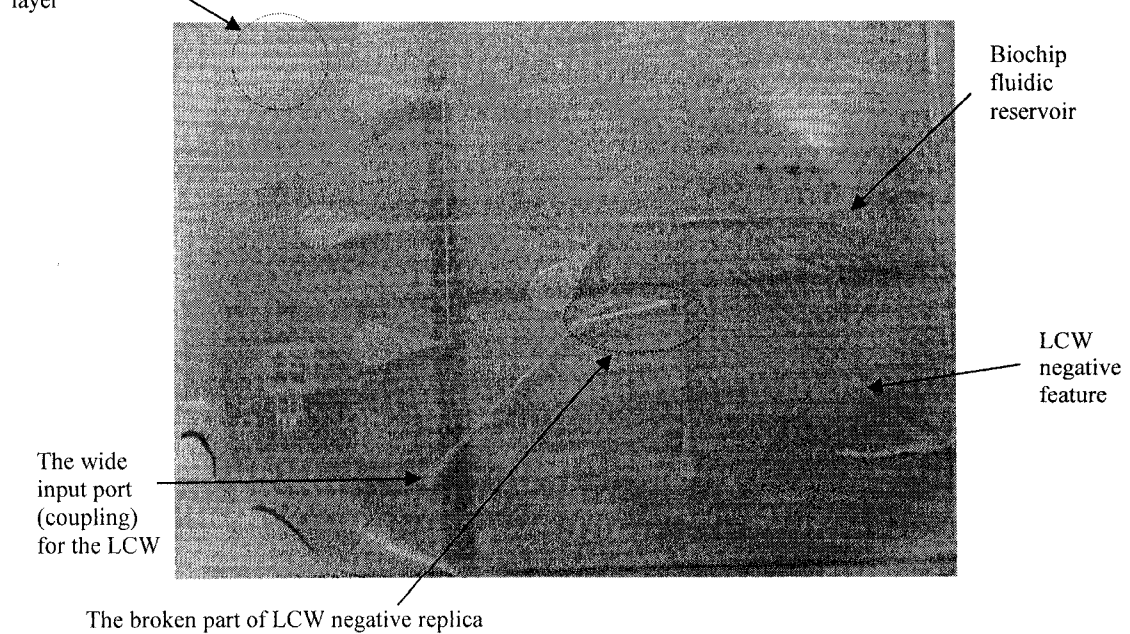
Figure 3.3   PSiA negative replica

The results with the PDMS biochips were satisfactory to some extent; the surface topology was replicated well and there were no sign of shrinkage. However, the 25μm thick wall between the microfluidic channel and the LCWS was not replicated completely and one of the waveguides was not formed completely to the desired depth. After more investigation, it was discovered that due to double replication and the use of Bosch etched features, some of the features were not replicated into the negative replica. Moreover, it was shown that having features such as narrow lines of fluidics caused problems while testing the PDMS-capped PDMS specimens. (Figures 3.2 & 3.5.a)

While suffering from the same problems just described for PDMS biochips, the PSiA biochips also showed some adhesion to the masters that resulted in the damage of some of the replicated negative features. (Figure 3.3)

3.1.2. Intermediate Design with Single Replication Process

It was observed that the Bosch DRIE process did not fabricate smooth walls. Moreover, double replication from a positive replica, can only one extra replication process that can be avoided by using a negative replica. In an attempt to overcome this problem, it was decided that the fabrication of the master with a negative mask and using the Cryo process might be a better approach. Also, since using chromium thin film as etch mask resulted in the growth of the silicon grass [106], silicon nitride and aluminum thin films were chosen to fabricate the biochips. Silicon nitride mask was low-stress LPCVD nitride with 1000 A^O thickness on silicon wafer (purchased from Norcada Inc [83]) and the Aluminum mask was a 100nm low stress sputtered film. It was observed that it is very crucial in the fabrication process to use low stress mask films as the film can delaminate in low temperatures Cryo process.

48

The DRIE results with nitride mask weren't very satisfactory, since the etch depths were 50, 75 and 100 micrometers and the nitride mask was etched away before thes DRIE process was finalized.

Deposition pressure - Film stress

Deposition pressure	Film stress
2mTorr	-10 MPa
3mTorr	-3 MPa
4mTorr	+5 MPa
7mTorr	+15 MPa
9mTorr	+17 MPa

Deposition pressure (mTorr)
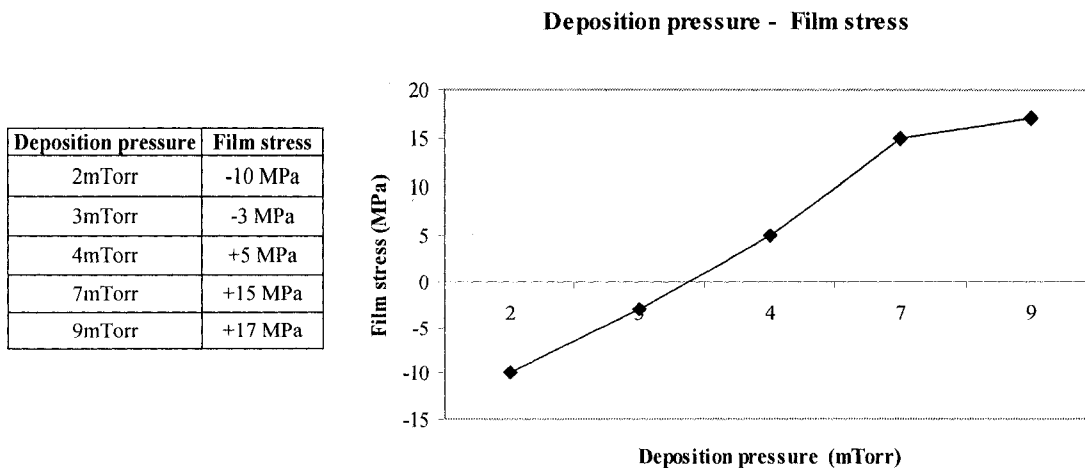
Figure 3.4 Film stress, DC sputtering deposition of aluminum on silicon

In order to produce low stress, and preferably zero stress, films of aluminum on the silicon wafer, some of the key factors in sputtering of metals were examined. Deposition pressure, deposition power, pre-deposition burning time and sample rotation speed were controlled in a series of experiment. Among all, choosing rotation speed of 2.5 rpm, it was decided that by keeping all but one factor, deposition pressure, and using the regular DC sputtering procedure, low stress films could be obtained. A number of experiments with deposition power of 300 watts and burning time of 3 minutes before deposition resulted in the data depicted in Figure 3.4.

Based on the diagram in Figure 3.4, deposition pressure of 3.4 mTorr was chosen for achieving the lowest stress in Al film. The base pressure was 1.5×10^{-6} Torr and the deposition rate was calculated as 30nm/min and Argon flow rate was 30 sccm.

<div align="center">a   b</div>
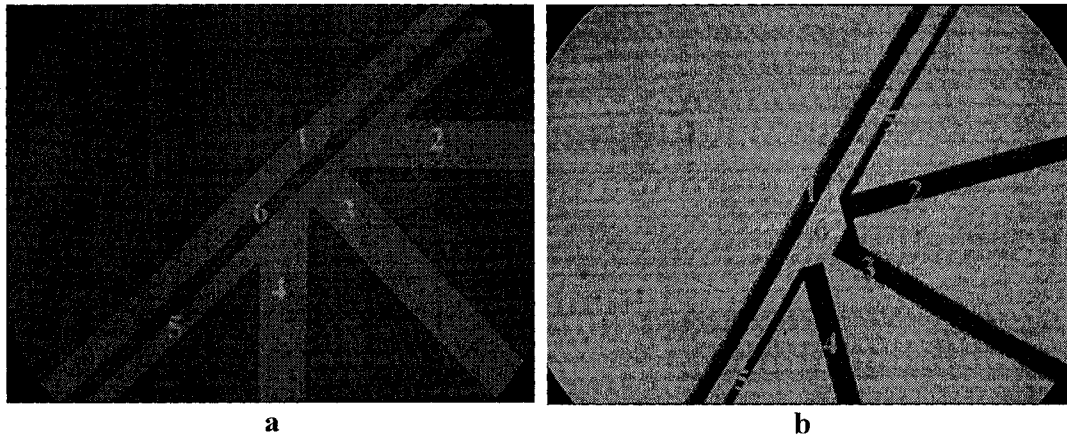
Legend:

1-Microfluidics channel	5-LCW filling channel
2,3,4- LCWs	6-separating wall between LCWs and the Microfluidic channel

Figure 3.5 LCW biochip first and second design iterations, a. The detection point on the biochip, Si master for first design, b. The detection point on the biochip in PDMS replica of the second design

Since the motivation for having LCWs was to have the ability of changing the medium in the LCW channels in order to obtain various filtering or different pickup capabilities. While designing the masks for the second prototype of the biochips, the futures placement were arranged so that two of the LCWs share one filling port while the third has a separate reservoir which leaves the option of filling the waveguides with different material. After simulating the focus point of the LCWs in the mask designing program, it was also decided that the arrangement of ends of the LCWs should be such that none is shadowing other LCWs (Figure 3.6). The depth and the width of the fluidic channels was decided to be 50µm and the LCW filling channels were 25 µm wide.
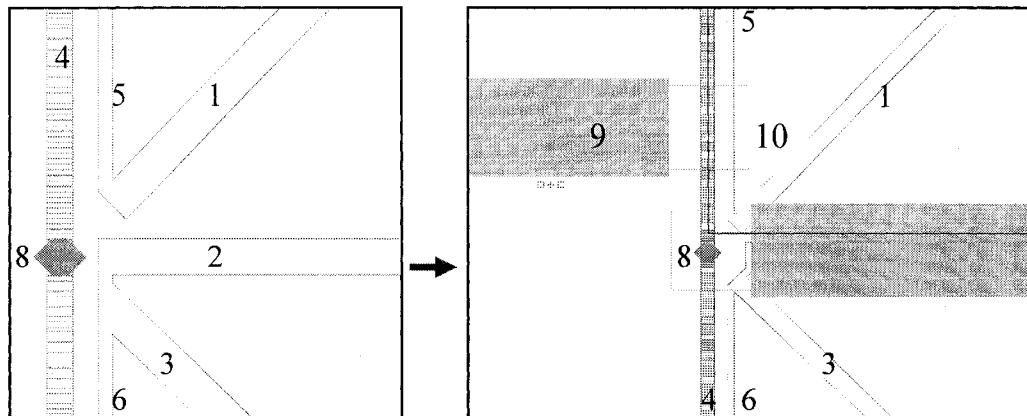
Figure 3.6 The mask design: improvement through simulating the focus point of the LCWs.

Cryo DRIE etched silicon was pre-cleaned and developed less silicon grass in the bottom of the features. After removing the aluminum mask from the surface, the silicon wafer was silanized for 2 hours. Both PDMS (Figure 3.5.b) and PSiA compounds were cured on top of the features and the cured specimens were bonded to the same material (PDMS or PSiA) using the oxygen plasma treatment.

3.1.3. Final Design

Although the second design of LCW biochips demonstrated good bonding results in particle sorting and waveguiding, it was decided that the design should be improved for better efficiency. Experiments showed that the biochips should be made using much more reliable process and with smoother walls. It was also determined that the design can be improved by having separate LCW filling channels with the same width as LCWs. This change will give more versatility to the LCW features when it comes to filling liquids and by having the width of 70μm, better illumination and pickup by LCWs can be achieved.

Moreover, the T-channel fluidics in the original design was replaced by Y-channel. The Y-channel microfluidics allows the option of having 3 input/output

reservoirs while it reduces the sharp corner effects that result in particle settling in the middle of the microchannel.
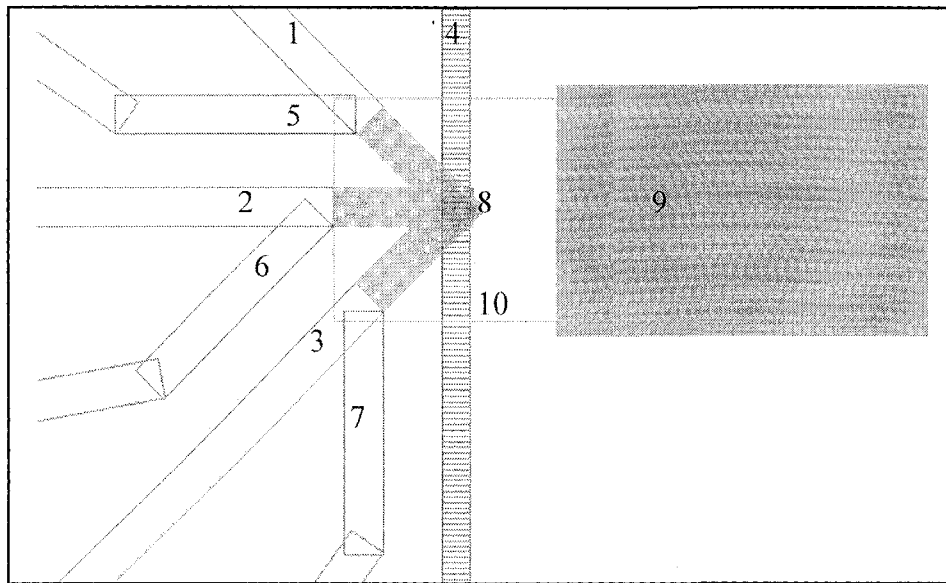
Figure 3.7 LCW biochips final design, mask layers and their features

In order to fit the final design to previously designed masks for v-grooves, a simulation of the geometrical orientation of the features in all of the three layers was performed in L-Edit software. As illustrated in Figure 3.7, the detection spot on the fluidic feature, called the LCWs focal point (8), can be simulated as the overlapping area of all three "laser beams" (blue) directed from the end point of LCWs. The result, fabricated features on silicon surface using Cryo DRIE, is depicted in Figure 3.8.

In order to have a better coupling of the tip of the fibers guiding the laser light to the LCWs and the waveguides on the biochips, a stopper edge inside the LCWs was fabricated. By sliding the optical fiber in the LCW, the tip would reach the

stopper edge and couple with the LCW. Figure 3.9 illustrates the fabricated stopper edge in silicon master.
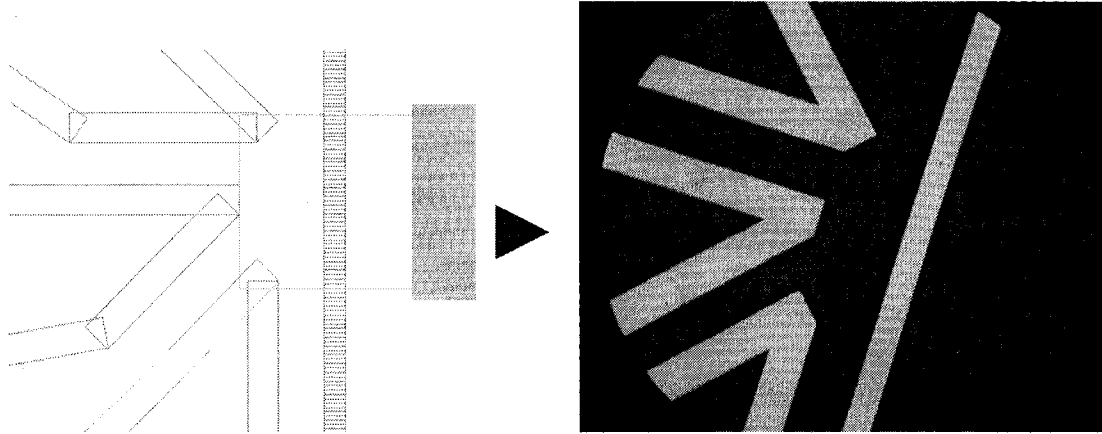
Figure 3.8 Fabricated LCW masters in Si (right) the features designed in L-Edit (left)
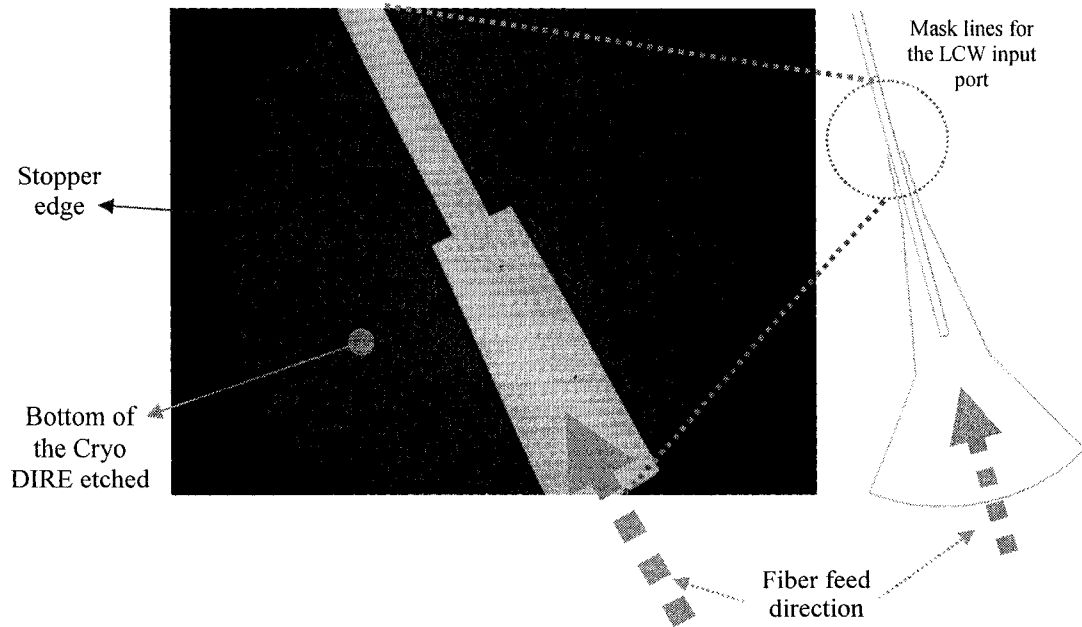
Right: DRIE fabricated feature   Left: mask designed feture

Figure 3.9   Fiber feeding port and fiber stopper

In addition, it was observed that even with a low-stress aluminum mask, some silicon grass will develop on the surface. Si grass, even in the scale of nanometer, will cause surface roughness, premature delamination of material being cured on the surface and "not fully cured areas" in the polymer replicas. In order to eliminate the silicon grass and fabricate even smoother surfaces and etch walls, aluminum oxide (Al_2O_3) was chosen as etch mask for this design. Aluminum oxide can be deposited on the surface of Si wafers using reactive sputtering or evaporation. These two processes and the perfection of the deposition methods are discussed below.

3.1.3.1. Aluminum oxide etch mask fabrication

In order to find an easy and reliable process, aluminum oxide etch mask was fabricated using both reactive sputtering and evaporation.

Pulsed dc magnetron reactive sputtering is a deposition process that opposed to dc power will prevent the formation of arcs [107]. This process, if carried out using carefully controlled parameters, can produce smooth and highly adhesive metal oxide thin films. Sputter deposition of dielectrics, such as oxides and nitrides, on the inside surfaces of a sputtering chamber causes the accumulation of electric charges from the plasma which can create arcs. The deposition process is usually carried out with pulsing frequencies in the range 10-350 kHz and duty cycles in the range 50-90%. [107-110]

The electrical cycle of a pulsed DC reactive sputtering with a single magnetron is illustrated in Figure 3.10. The power is applied to the aluminum target for the period of time titled as T_{on} which is a negative voltage pulse of 300 to 400 volts. At the end of T_{on}, the power is either switched off for a period of time, or more commonly, switched to a small positive voltage (20 V); reverse time, T_{rev}, 1/10 of T_{on}. Also, the duration of the T_{on} and T_{rev} verifies the lowest pulsing (critical) frequency, $f_c = 1/\tau_{cycle}$.
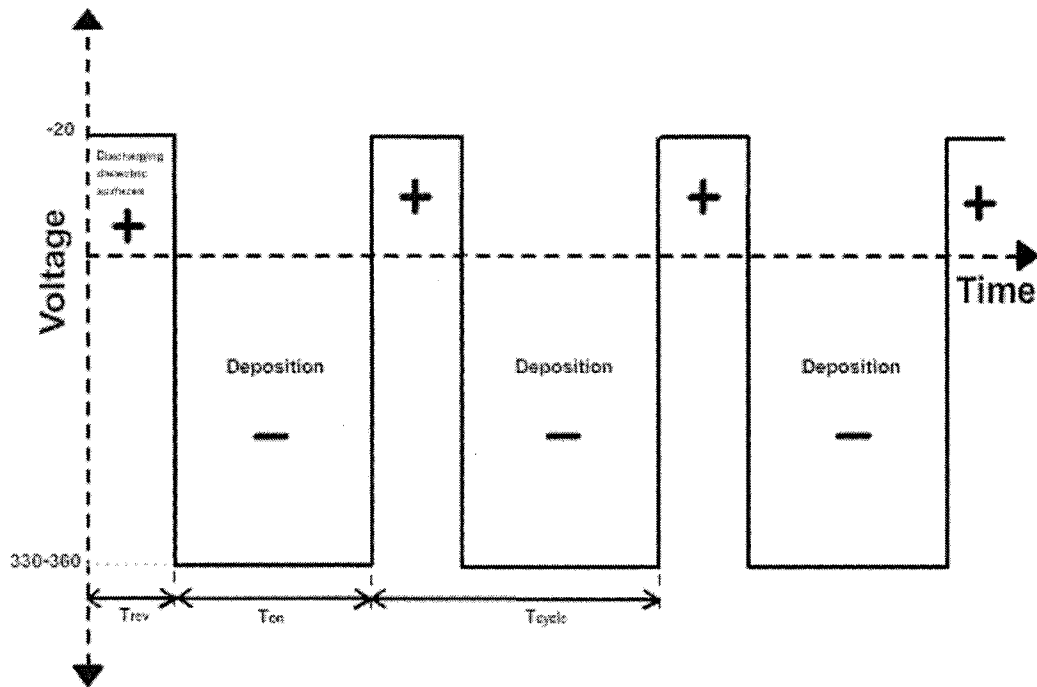
Figure 3.10 electrical cycle of a pulsed DC reactive sputtering

Reactive sputtering can grow a compound layer using a metallic target, a reactive gas (e.g. oxygen or nitrogen) in plasma. The reaction between the reactive gas and sputtered metal atoms on the substrate results in the formation of the compound oxide or nitride layer. Ideally, the reactive gas would react only with the growing film on the substrate to make a thin film of the required compound, but unfortunately the reactions occur with the sputter target surface as well. This phenomenon is usually known as target poisoning and is a source of poor thin film quality. Figure 3.11 illustrates a schematic of reactive sputtering process and apparatus.

A good thin film of aluminum oxide for etch mask should have low stress, low porosity and good adhesion to silicon. In this research, through a number of experiments using a pulsed magnetron source, reactive sputtering of aluminum oxide was examined. Care was taken when choosing the gas flow parameters as

the sputtering rates drop when a layer of compound film is grown on the surface and there is less demand for reactive gas molecule in the chamber. The results, as most of the parameters except gas flows were set constant, determined the best film quality results using the parameters listed below. The flow rates of 1.3, 1.5, 1.8, 2.1, 2.8 and 2.9 sccm for oxygen along with 50 sccm for argon were experienced and the most promising results were obtained using 1.5 sccm of oxygen which resulted in the deposition rate of 16nm/min. Table 3.1

Aluminum oxide pulsed reactive sputtering	
Voltage on target =334 V Burn-in time= 1 min Argon pressure =7 mTorr without O_2 Argon flow=50 sccm Oxygen flow =1.5 sccm ramped from zero	f_c=150 Khz pulse, T_{on}=0.5 µsec Power=300 W, 10 second ramp for power Rotation speed=3.5rpm Deposition pressure= 7.4 mTorr

Table 3.1 Aluminum oxide pulsed reactive sputtering parameters

An aluminum oxide layer was also deposited on the Si wafers using evaporation. Evaporation process involved positioning 99% pure aluminum oxide bits in a super-heated surface in a vacuum chamber and deposition of the Al_2O_3 thin film on the Si wafer surface. In order to achieve low stress and a well-adhered thin film, a number of parameters were controlled as variables to optimize the process. Although the evaporation control system reported the deposition of 6.7 A^0/sec, the rate for the optimized process was determined to be 0.8 A^0/sec. Table 3.2 shows the results for three best results in different deposition pressures. The conditions for the optimum process can be found in column three of this table.

Pump down time	60 min	75 min	64 min
Base Pressure	1.8×10^{-6}	1.2×10^{-6}	1.8×10^{-6}
Z factor	1	1	1
Density	2.73	2.73	2.73
Current	60 mA	40 mA	40 mA
Deposition Pressure	6×10^{-7}	2×10^{-6}	3×10^{-6}
Thickness	15 nm	200 nm	300 nm

Table 3.2 Aluminum oxide evaporation parameters in three different conditions
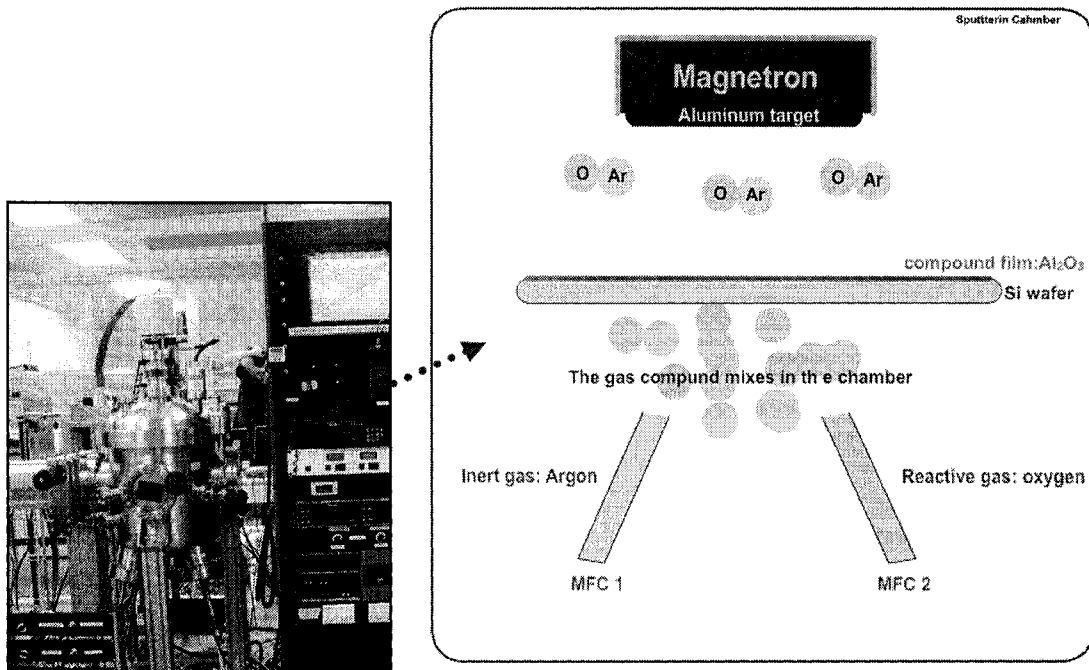
Figure 3.11 picture and schematic of reactive sputtering process and apparatus

Using standard Cryo DRIE process, the Si wafers with 100 nm of sputtered or evaporated aluminum oxide films were etched to the depth of 50μm. In order to compare the results of the aluminum oxide etch masks with aluminum etch masks, a silicon wafer with 100nm of aluminum film on the surface was etched using the same process. Although both evaporated and pulsed reactive sputtered films showed promising results, the aluminum mask, once again resulted in the growth of black silicon grass. (Figure 3.12)

Figure 3.13 illustrates the satisfactory results of a DRIE etched Si master using pulsed reactive sputtered etch mask. The process of fabrication, similar to the other designs, involved deposition of the etch mask, photolithography using HPR504 photoresist for fabrication of the openings defining negative of the features. The next step was the etching of the aluminum oxide mask in the aluminum etchant for 15 minutes and DRIE etch. Following the DRIE, the rest of

the etch mask was removed using the aluminum oxide. Then the Si wafer with negative features, for four biochips projecting outward from the surfaces, was silanized for replication (Figure 3.13)

Silicon/Silcon Grass
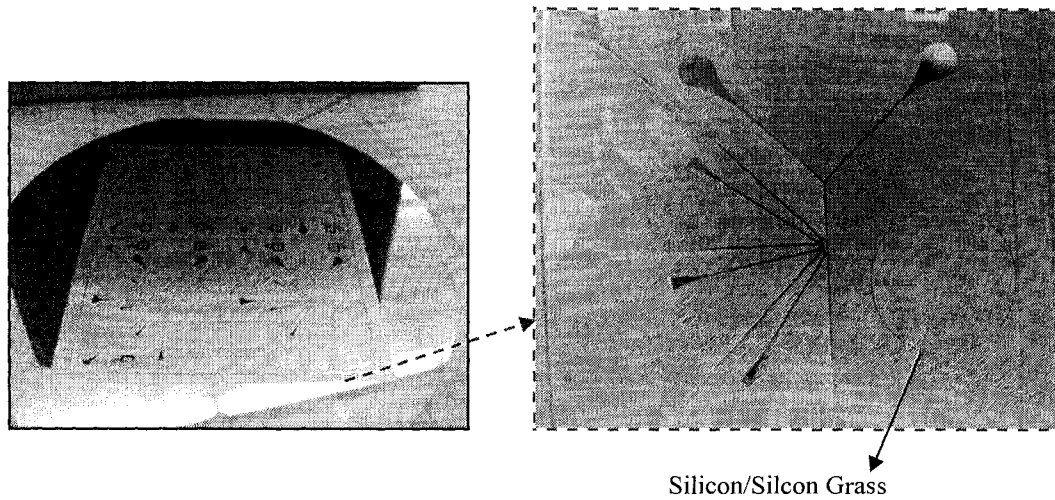
Figure 3.12 Si master for 3-LCW biochips fabricated evaporated Al₂O₃ etch mask

Alignment marks matching v-groove layer
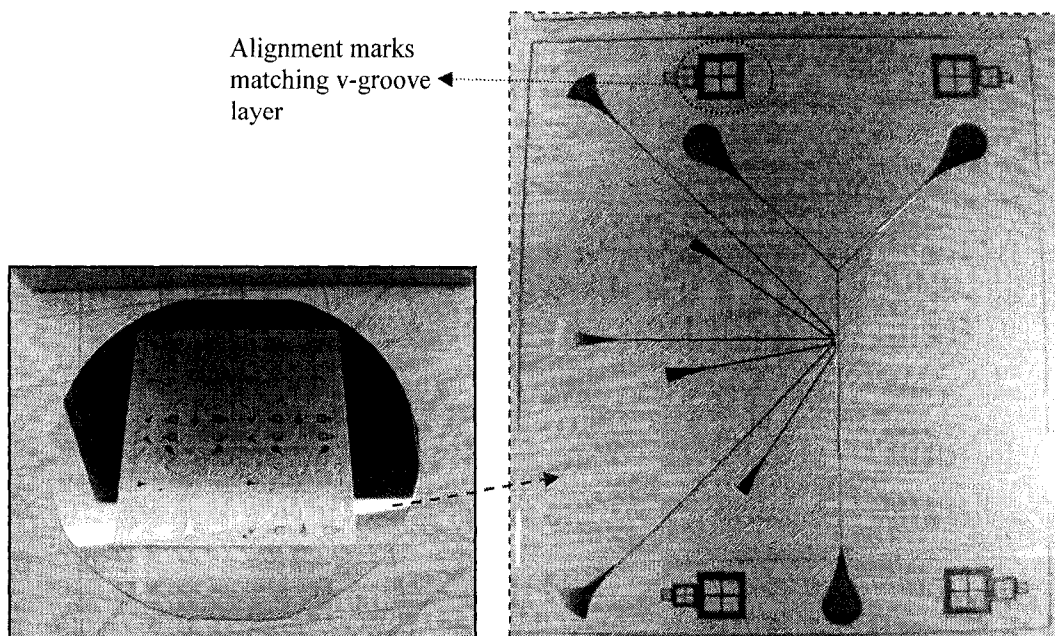
Figure 3.13 Si master for 3-LCW biochips fabricated using sputtered Al₂O₃ etch mask
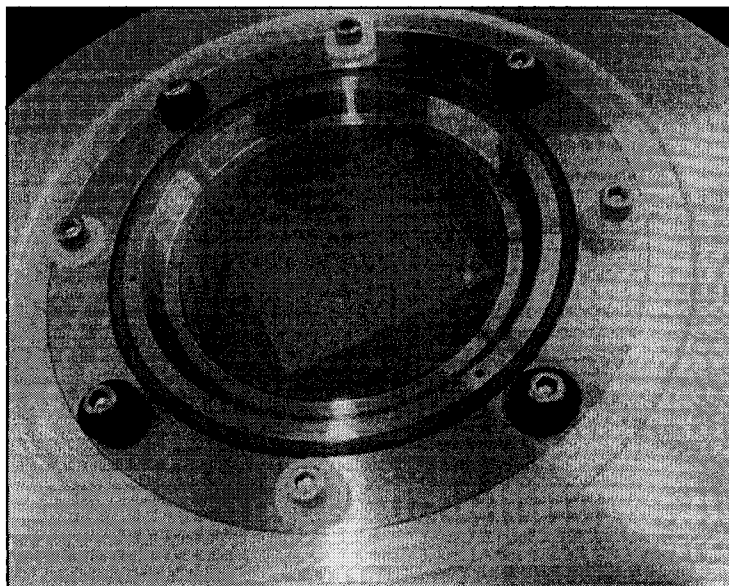
Figure 3.14 Si master in nitrogen purge apparatus before polymer molding

3.2. LCW biochips

PDMS and PSiA biochips were replicated using the silanized Si master depicted in Figures 3.13. PDMS was cured in a vacuum oven for 2 hours at 80 ^{O}C and PSiA was cured in a nitrogen purge. Nitrogen purge, Figure 3.14, was used due to the deteriorating effect of oxygen presence around the curing PSiA under UV light. A complete section on the design and fabrication of the nitrogen purge curing chamber can be found in Appendix B.4.

The PSiA compound was prepared using the same procedure described in the previous chapter. Then a 0.5% wt of fluorinated compound, Rad 2200N (TEGO Chemie Service), was added to the compound for easier substrate separation and degassed. The delaminated PSiA biochips, Figure 3.15, were then bonded to a 0.5mm layer of cured PSiA using oxygen plasma.

The PDMS replica, depicted in Figure 3.16, was capped using a commercially available 254μm PDMS layer. Oxygen plasma was utilized for bonding.
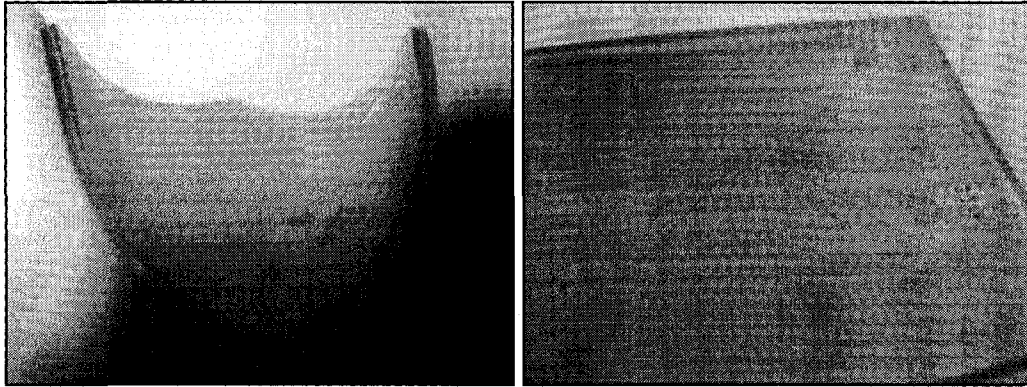
Figure 3.15 PSiA replicas of the final design of LCW biochips
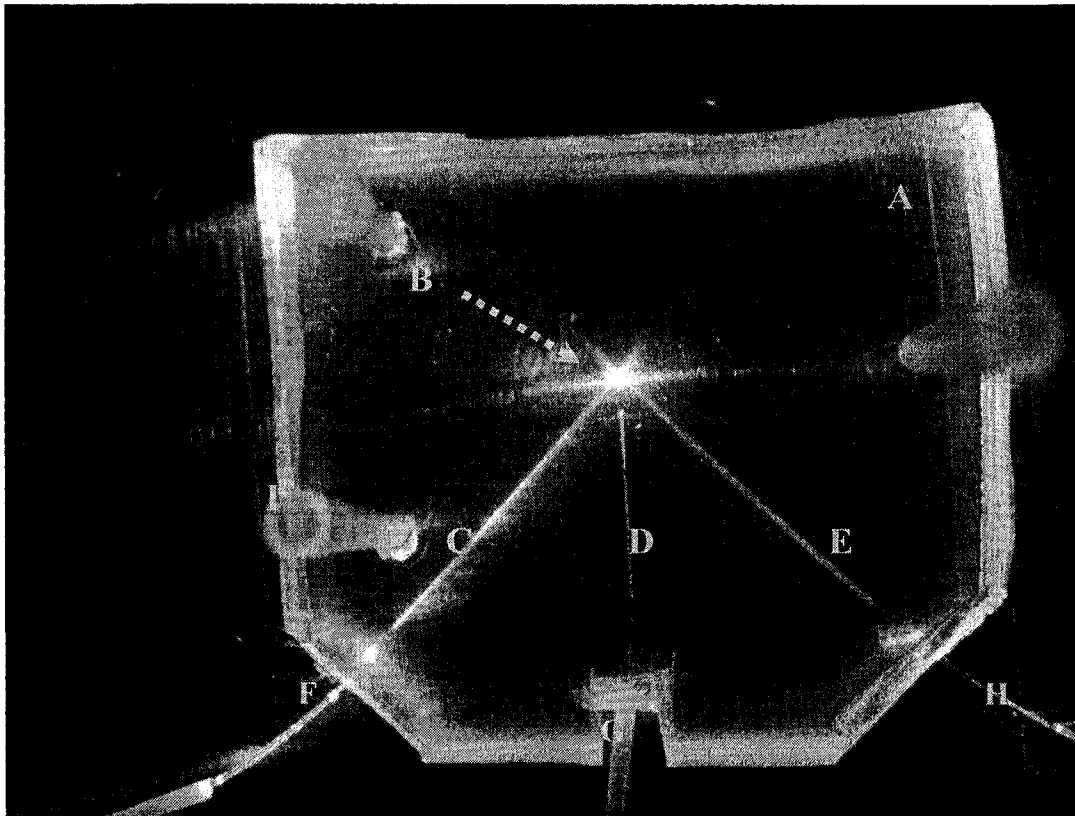
Legend:
A-Alignment mark
B-detection point, three LCWs focus point
C-Green laser LCW
D-Pickup LCW

E-Red laser LCW
F-Green laser fiber
G-Pickup fiber
H-Red laser fiber
I-Fluidics reservoir connector, PET

Figure 3.16 PDMS LCW biochip connected to laser sources and detection system

60

3.3. SCW biochips

Although the fabricated LCW biochips were successful specimens in experiment (refer to next chapter), it was determined that filling the waveguide channels with UV-curable polymers with index of refraction higher than the biochip material can ease the utilization of the biochip. According to total internal reflection theory, the waveguides should be filled using material with index of refraction higher than the biochip material refractive index[111]. LCWs, though efficient in fluorescence detection, can be modified by filling the channels using UV-curable PEA. The compound used for the solid core waveguides was a 50-45-4% compound of Ethoxylated (3) Bisphenol A Diacrylate (SR349, Sartomer, USA), Ethoxylated (4) Bisphenol A Diacrylate (SR601, Sartomer, USA) and 2,2-Dimethoxy-1,2-diphenylethan-1-one (Irgacure 651, Ciba Special Chem) with Rad 2200N (TEGO Chemie Service) at a loading level of 1 wt %. This compound can flow easily through the LCWs and fill the features due to the presence of fluorine-additive Rad 2200N. Moreover, using high-degree ethoxylated diacrylates both higher degree of cross-link and very low shrinkage are guaranteed [112].

In order to fill and cure the waveguides without having any cured polymer in the fiber feeding (coupling) port and create a vertical surface at the entrance of the waveguide, a novel curing process was utilized: The cured PDMS biochips were first capped with PDMS layers as mentioned above. Then 4x7 mm parts of a cutting knife blade, which is a low carbon stainless steel, were inserted into the biochip body vertically. These metallic blades are placed in approximately 100 microns away from the fiber stopper edge along the waveguide and vertical to the waveguide axis (Figure 3.17). When filling the waveguide channels, the PEA will reach the point where these metallic blades are inserted in and stop. After curing the PEA under UV illumination for 60 seconds, the blades were removed and the rest of the waveguide and the coupling port were filled with glycerol. The indices

of refraction for the main components of the filling PEA are 1.534 for SR601 and 1.543 for SR349 in visible light. The cured compound theoretically has an index of refraction close to 1.54 which is comfortably higher than the oven-cured Sylgard 184 PDMS, 1.41 or 1.469 for CN9800 which is the base for PSiA. A biochip with cured PEA waveguides and coupled to a red laser at one of the coupling ports is illustrated in Figure 3.18. Figure 3.19 depicts a biochip with both LCW and SCW.
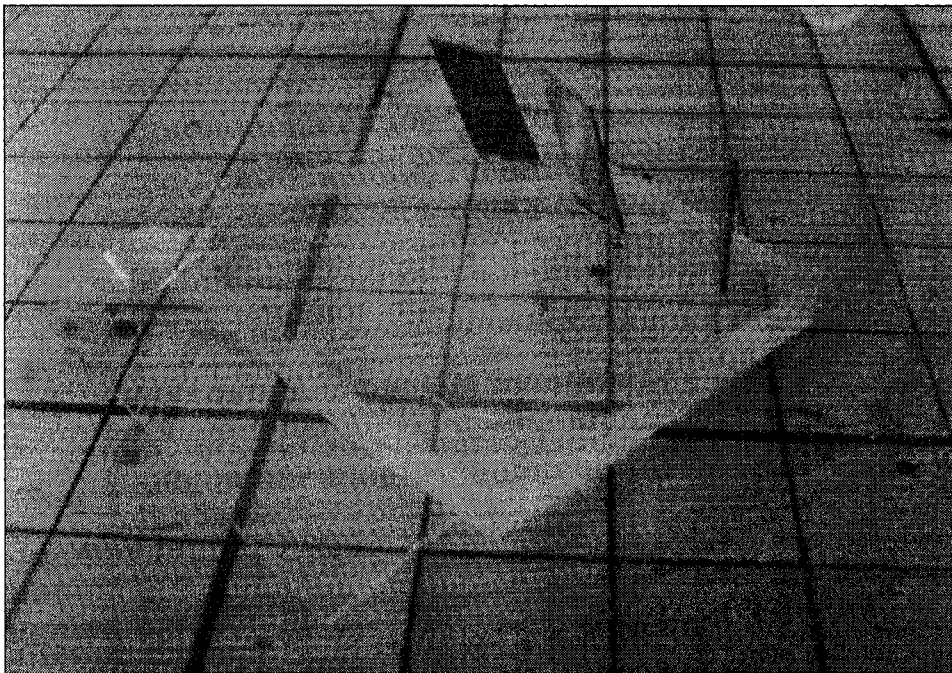
Figure 3.17 fabrication of SCW waveguides, curing the PEA using metallic blades

In order to determine the optical efficiency in the SCW and LCWs, biochips containing these waveguides were tested for loss in the waveguides. The method used was collecting the escaping light from the top surface of the waveguide by a fiber attached to a PMT and moving along the axis of the waveguide. When moving away from the coupling port towards the middle part of the biochip, the loss causes less light scattered to the top surface and less light being sensed by the

PMT that will cause lower levels of voltage. The values recorded for the poswer of light in milivolts are only for relative comparison. (Figure 3.20)
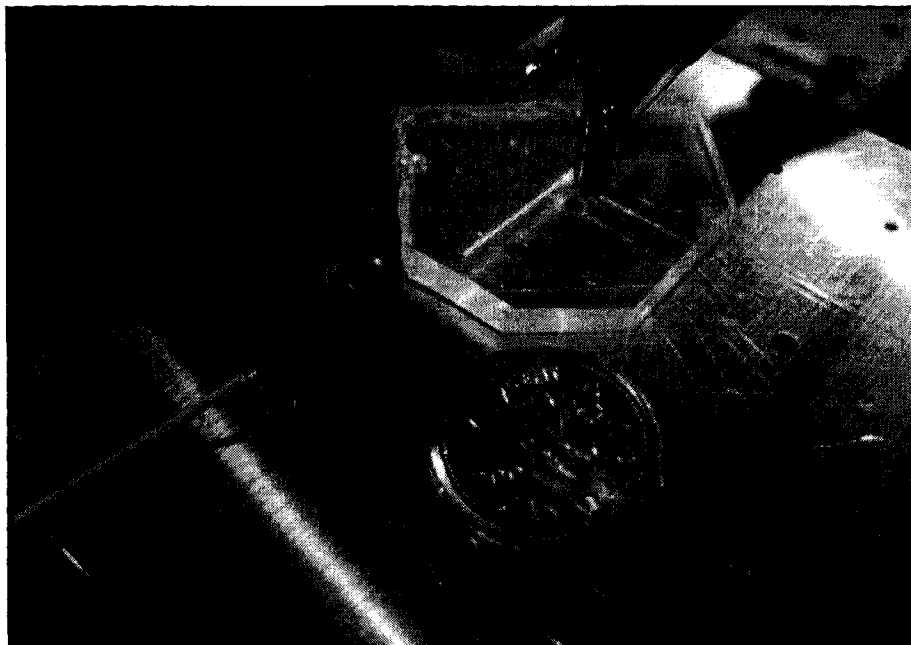
Figure 3.18 3-SCW biochip
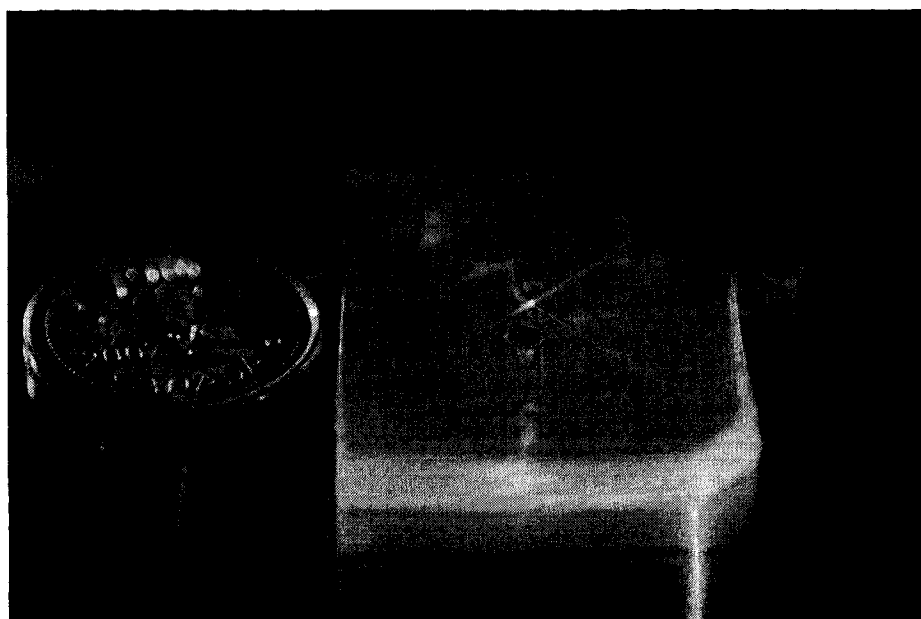
Figure 3.19 Biochip with one SCW and one LCW coupled to green and red lasers respectively
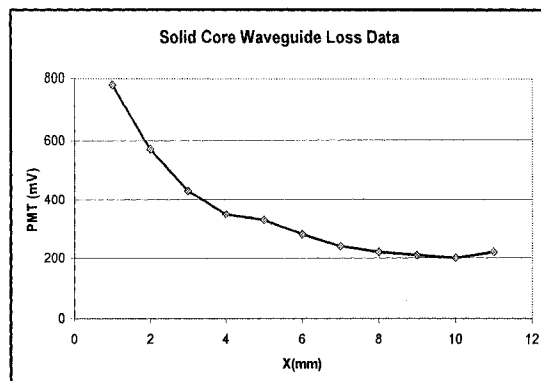
Figure 3.3.20 SCW loss calculation, a. Loss calculation
experiment setup b. PMT relative signal in mV vs.
distance along the SCW

The formula $P_{dB}=10 \times \log(PMT_{mV})$ is used to convert the PMT voltage to decibels (dB). The results of converting the PMT voltage for both LCWs and SCWs, are shown in Figure 3.21. The glycerol-filled LCWs showed an approximate loss of 1.3 dB along a centimeter distance of the waveguide while the loss for cured PEA SCWs was estimated to be 6.3 dB cm^{-1}. Both of the waveguides were tested using a 632nm red laser.

When comparing these results to the LCW biochips fabricated using SU-8 masters with losses of 2.2 dB cm^{-1} in red laser and 2.9 dB cm^{-1} in green laser (532nm wavelength), it was shown that Cryo DRIE fabricated masters can reduce the loss by 40% comparatively. [80, 89]

Moreover, although SCWs are not as efficient as LCWs, the SCWs in the biochips show enough efficiency for fluorescence detection. The experimental results will appear in the next chapter. The author will again emphasize that using SCWs, the experimental phase can be achieved in shorter time and less untidiness comparing to LCWs.
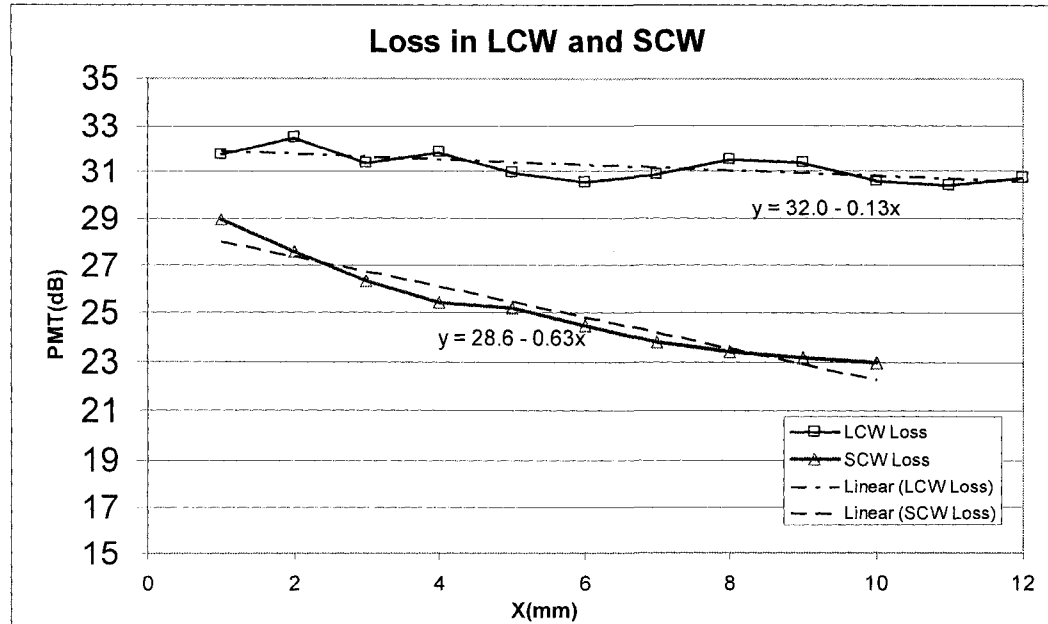
Figure 3.21 LCW and SCW relative loss along the waveguide

According to C. Bliss, the biochips reported in [80], were produced using Su-8 masters which were not durable enough to be used for more than ten replication cycles. The Si master fabricated for this work was inspected after more than 30 replications. The surface topography and microfeatures were in similar conditions as recorded before the replication cycles. More over, the fabrication processes involved in SU-8 procedure are time consuming comparing (6 hours) to the four-hour process employed for this project. Having more durability for higher number of replication cycles and shorter processing time, the biochip Si master fabrication process introduced here, can lower production costs especially in mass production.

CHAPTER 4

EXPERIMENTAL TESTING OF BIOCHIPS

Most of the biochips fabricated for this project were contained a single microfluidic channel and an optical layer for detection. Detection, means the process of shining a laser beam into the waveguides on the biochip, illuminating a specific location in the fluidic system, capturing the emission from fluorescent particles (cells) in the channel with another waveguide and delivering the light to the photomultiplier tube (PMT). The light collected is carried via a multimode optical fiber to the PMT. The PMT, interfaced to a data acquisition card (DAQ) in a computer, produces a signal measured in electrical potential (milivolts).

In this chapter, a brief introduction to fluorescence detection method is first described followed by the experimental setup, the components and the analyzing method. The third section is dedicated to the experiments and the results. The biochips tested in this chapter are the final design of the fourth generation fluidics layer with three LCWs or SCWs.

4.1. Experimental setup

The experimental setup consists of a red laser (632 nm), a green laser (532 nm), an experimental stand (Appendix B.3), a photomultiplier tube (PMT) and a computer with data acquisition card controlled with a LabVIEW program. The LabVIEW program was created prior to this project. The experimental setup is

66

similar to the work reported in [30, 48, 78, 124]. Figure 4.1 depicts the experimental setup.

Using two rotary choppers, the laser beams were chopped at two different frequencies and carried to the biochip via 50 μm core fibers. The fibers, carrying light from two semiconductor lasers, were inserted into the chip waveguide couplers 2 and 4 in Figure 4.2. Red and green laser beams can be modulated at the frequency range of 100 Hz to 130 Hz and 230 Hz to 260 Hz respectively. The optical power of the red laser was of the order of 1 mW and the green laser had the output of 5 mW.
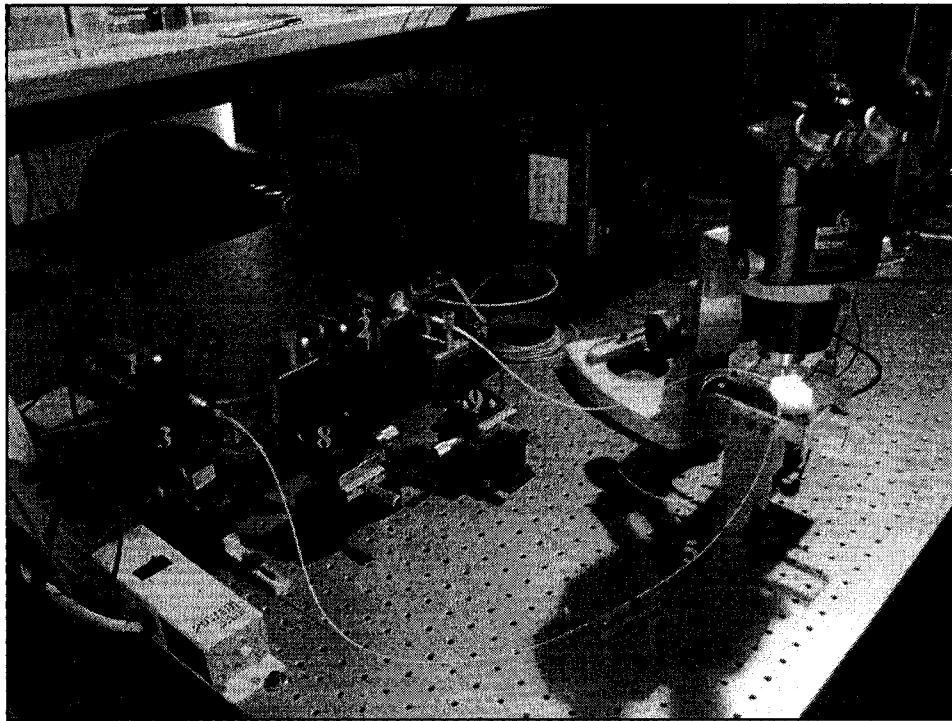
Legend:
1-Red laser
2- Green laser and chopper
3-Red laser chopper
4- Fiber from green laser to the biochip

5-- Fiber from red laser to the biochip
6- Microscope for visual inspection
7- Experimental stand with biochip on top
8&9- Three axis micrometer locators for fiber/laser coupling

Figure 4.1 Experimental setup

A third multimode fiber was inserted into waveguide 3 to collect the fluorescence and scattered light and deliver it to a Hamamatsu R2949 PMT

mounted on a Hamamatsu C6271 socket. In order to control the gain of the PMT, the output voltage is within the range of 0-10 V input coming from the computer DAQ analog output. The National Instruments PCI-MIO-16E-4 data acquisition card will also record the PMT output, sample signal, at 10 kHz. The light picked up from the biochip, passes a ball lends and a filter assembly before reaching PMT.
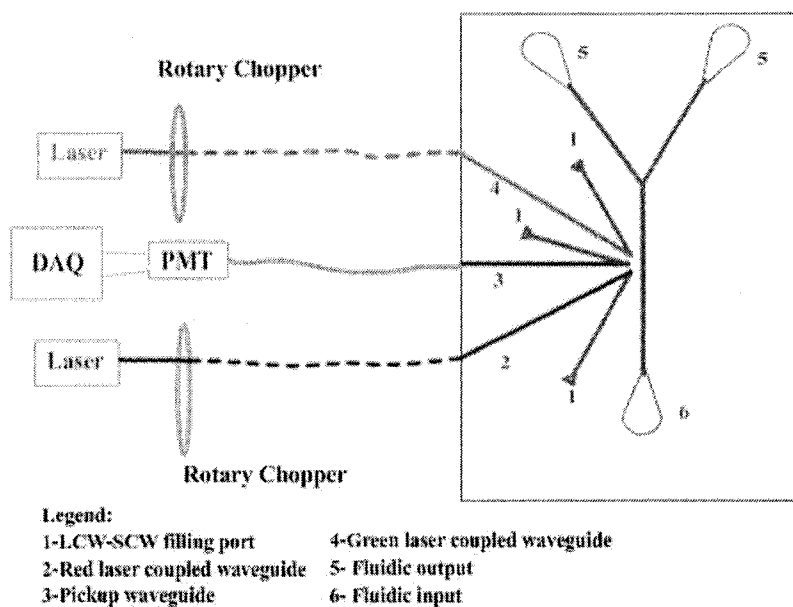
Figure 4.2 Biochip experimental setup

The filter assembly built into the PMT box has one high-pass filter to cut off any scattered 532 nm (green) laser light while passing both fluorescence bands. This filter is a Schott glass long pass filter with a cutoff at 540 nm. Another filter, a 10-nm bandwidth Rugate notch filter, is present that blocks 10 nm of the spectrum around the 632 nm to reduce background noise from the red laser. The filter assembly filtered and passed wavelengths are illustrated in Figure 4.3.

With a 10K samples per second rate, the DAQ records the PMT output. The LabVIEW® program that controls the PMT via DAQ records the signal with 100 consecutive samples averaged into one data point. The process of averaging the

68

data reduces the noise. The LabVIEW® program, compiles a text file in ASCII format containing the recorded samples. Figure 4.4 illustrates and example of raw sample, recorded into a text file, collected from a microparticle moving in the microchannel.
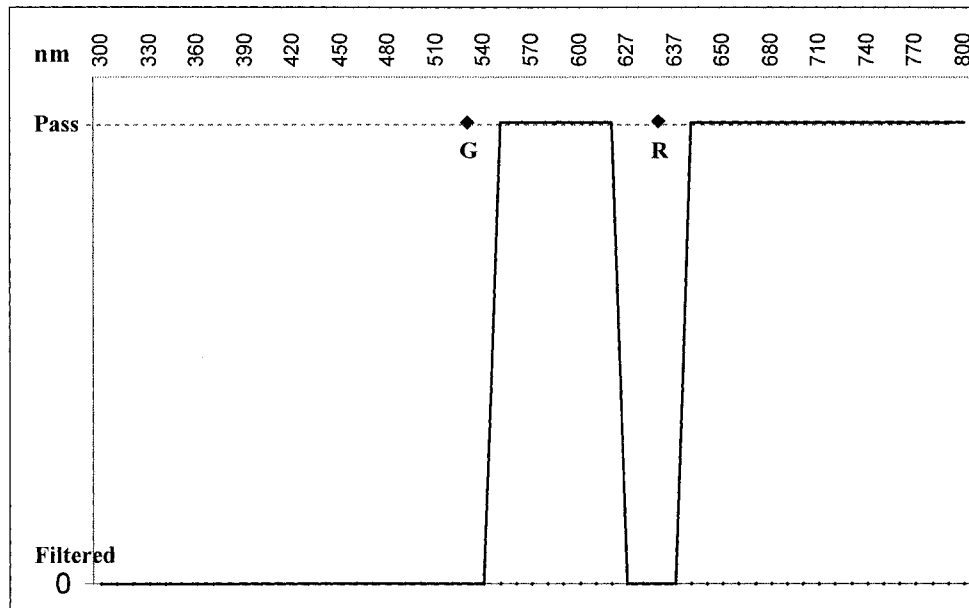
R: Red laser wavelength G: Green laser wavelength

Figure 4.3 Schematic drawing of the filtered and passed wavelengths in filter assembly (-)

By importing the text file into a Matlab® program that uses discrete Fourier transform (DFT) in a sliding time window, the samples were analyzed. This program was developed by Dr. J.N McMullin and is described in [89]. When the laser beam modulated with a specific frequency excites a fluorescent bead, an emission with same modulation frequency will shine back into the pickup waveguide. By having two lasers modulated at two different frequencies, the orange and scarlet beads can be identified using only one PMT. The Matlab® program analyzes the sample by using parameter N, input in the beginning of the code. When performing N-point FFT on the first N samples to find the first two non-zero frequencies, the program will plot the two signal frequencies, red and green. The sliding window analysis of the rest of the sample will result in the

69

diagrams plotting the red and green laser responses. Every peak in these two diagrams shows one or few of the species sensitive to red or green passed the detection point on a timeline. Figure 4.5 depicts fluorescence detection parts and processes.

In the experiments reported here, the Matlab program reported the red and green lasers modulation frequency at 109 Hz and 250 Hz respectively. The parameter N, number of FFT points, was set at 64.

A mixture of 15 μm orange and scarlet Fluospheres^{TM} [113] in a 10^{-4} molar NaCl solution was injected into the input reservoir. The orange and scarlet particles have maximum absorption/emission peaks in water at 540/560 nm and 645/680 nm respectively. NaCl solution was used to allow the option of electroosmotic (EO) flow in addition to pressure driven flow (PDF).

Figure 4.6 illustrates the PDMS LCW biochip on the experimental stand. Two platinum electrodes, where used to initiate and conduct the electroosmotic flow experiments. The punched reservoir openings in PDMS biochips were fitted with small conical plastic syringe tips to inject fluids and microparticles into the microchannel.

Figure 4.7 depicts the biochip from top view with two of the waveguides guiding red and green laser light to the detection point. Glycerol with refractive index of 1.47 is used to fill the LCWs. Figures 4.8 and 4.9 illustrate the fabricated LCW and SCW integrated biochips.
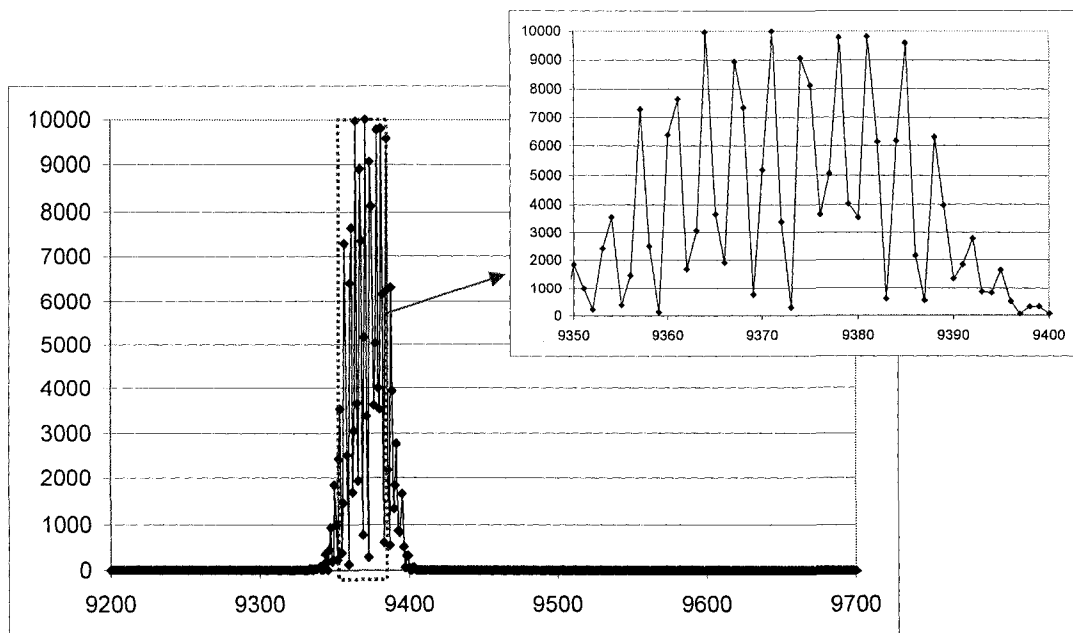
Figure 4.4 Raw sample from PMT: milivolts vs. sample number
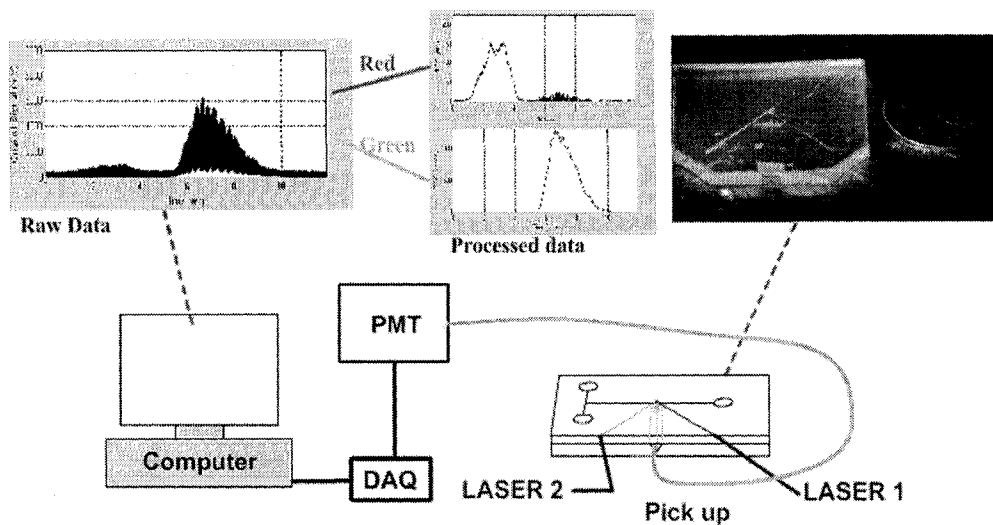
Figure 4.5 Fluorescence detection system with modulated laser beams

71
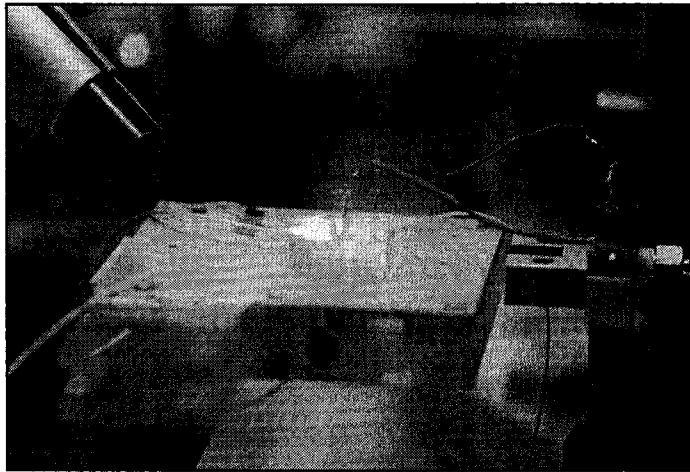
Figure 4.6 PDMS LCW biochip on the experimental stand
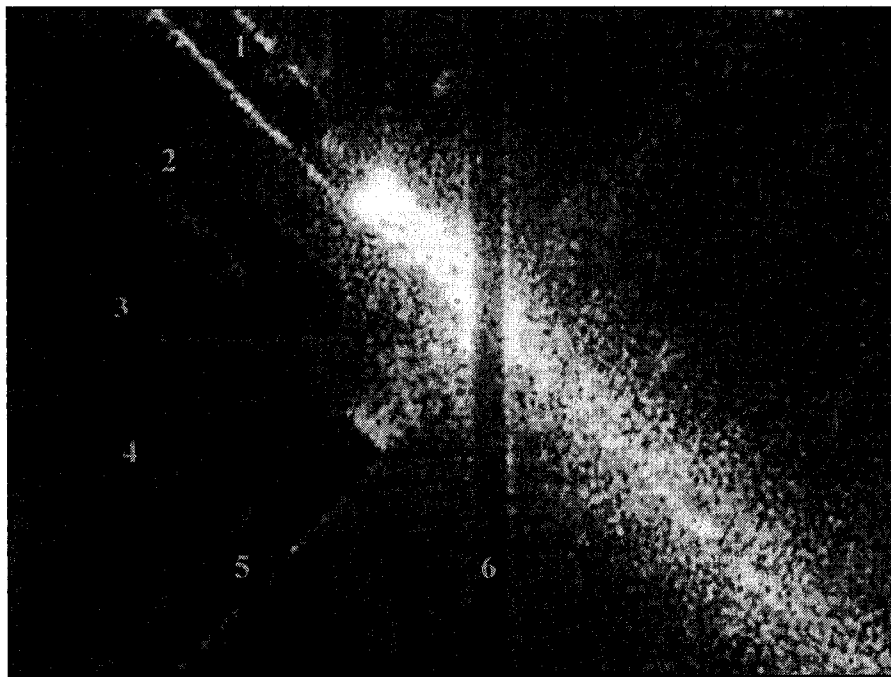
Legend:
1-Green laser waveguide
2 & 4- waveguide filling channels

3- Light collection (pickup) waveguide
5-Red Laser waveguide
6-Microchannel

Figure 4.7 Red and green lasers directed to the detection point

72
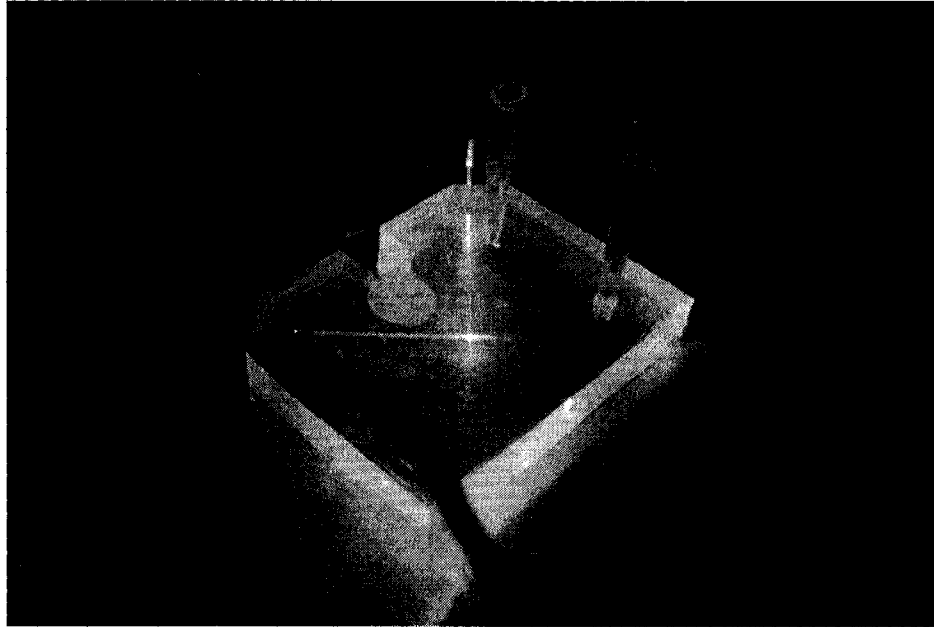
Figure 4.8 Red and green laser in Glycerol-filled LCWs
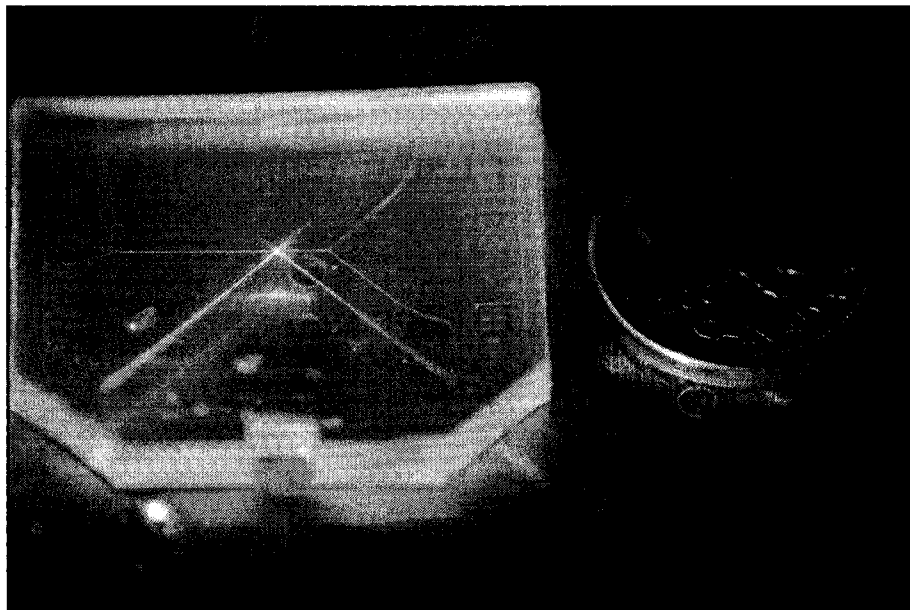
Figure 4.9 PEA filled SCW biochip coupled with w carrying red and green lasers

The signal collected from the experiments, including the results discussed above, had variable signal to noise ratios. The lowest signal to noise ratio measured in the experiments was 5 which resulted in a clear processed signal and detection of all fluorescent beads moving along the fluidic channel.

4.2. Experimental results: LCW biochips

Figure 4.10 illustrates a 12 second sample result of pressure driven flow passing the detection point on a LCW system. Figure 10.a depicts dominant frequencies of the signal which are the laser beam modulation frequencies. In part b, the original modulated signal, picked up by PMT is plotted. Figure 4.10 parts c and d illustrate the processed signals showing that in the collected signal, between time 1 sec and 5 sec a scarlet microparticle and in the period of 5 sec and 9 sec an orange bead passed the detection point. This result shows the accuracy of Matlab program in converting raw data (4.10.a) to interpreted red and green laser responses (4.10.c and 4.10.d).

Comparing the original signal, Figure 4.10 part b, with the two diagrams drawn for the red and green laser responses, it clearly concludes that the magnitude (peak max) of the red laser response is less than the green response. This occurred since different light wavelengths being filtered differently before reaching the PMT. The filter assembly is designed such that it passes lower wavelengths more than higher wavelengths. Moreover, the green laser beam has 5 times more power.

Figure 4.11 depicts another result of PDF in LCW biochip which is captured over 15 seconds. In the first two seconds of the original sample (4.11.b), two peaks are noticeable. The Matlab DFT program plotted the processed signal for the red (4.11.c) and green (4.11.d) sensitive spectrums. The results in the figure show that the first peak in the original signal is due to a group of beads of both

74

species passing the detection point simultaneously. The video captured while sampling shows that three orange and two scarlet beads pass and cause the superimposed signal.

By capturing a video file while storing the signal samples in the computer, the speed of the particles in fluidic channel was calculated. Using the video file and by calculating the number of frames of the video while the particle travels between the edges of the first and the third LCW tip (two horizontal lines in Figure 4.12.b) the time of the event was measured. This region was selected due to easy visual measurement of the particle location in the video with the reference to the features on the biochip, e.g. the edges of LCW tips. For the sample illustrated in Figure 12, the particle travels along the fluidic channel and passes the detection region in 0.775 sec (Figure 4.12.a). The distance between the two horizontal lines illustrated in part b, the detection length, is 350 µ. Therefore, the average speed of the particle is calculated 0.45 mm/sec.
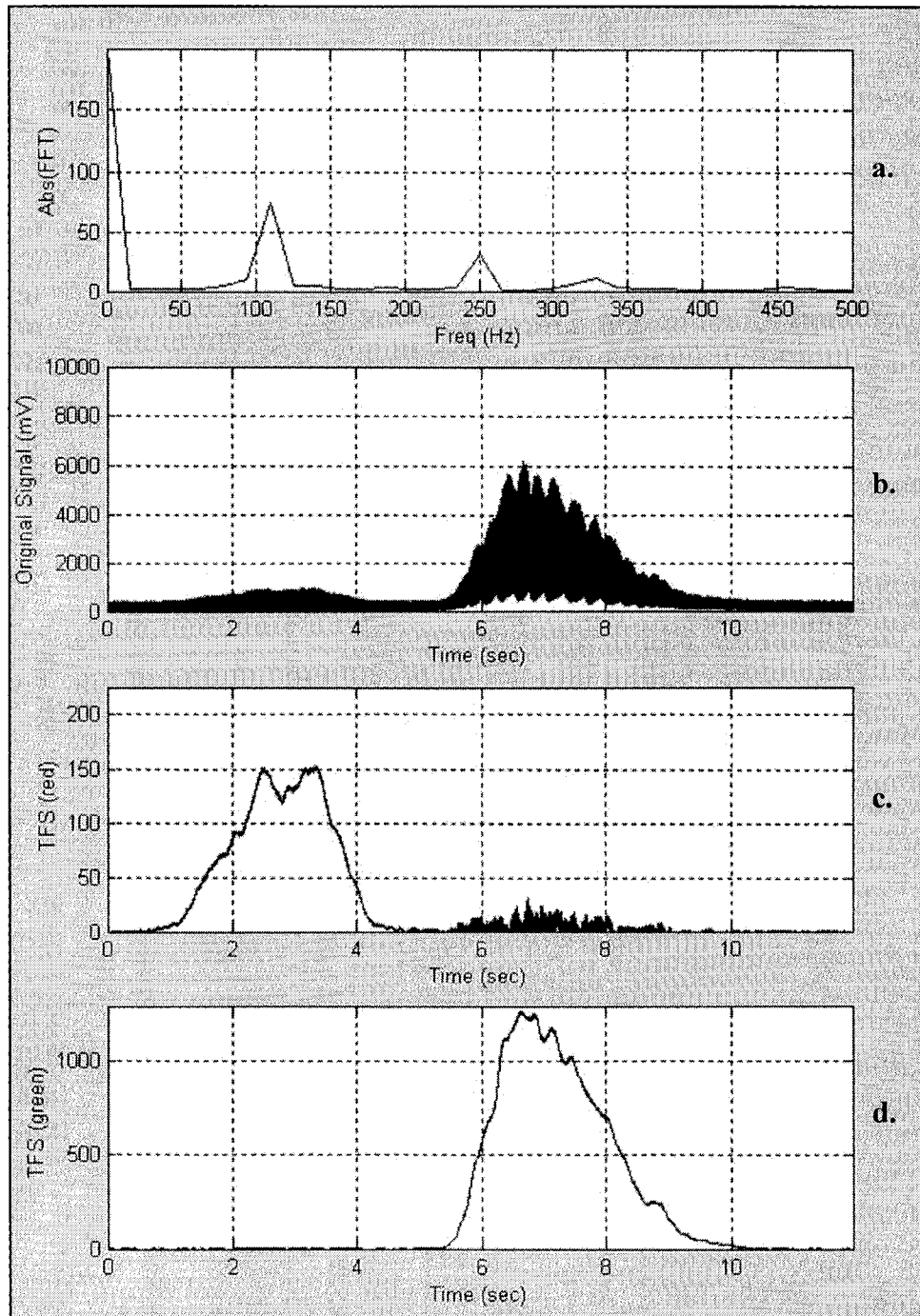
Figure 4.10 Pressure driven flow experiment in liquid core waveguide integrated biochip, 1 scarlet then 1 orange particle pass the detection point in 10 seconds
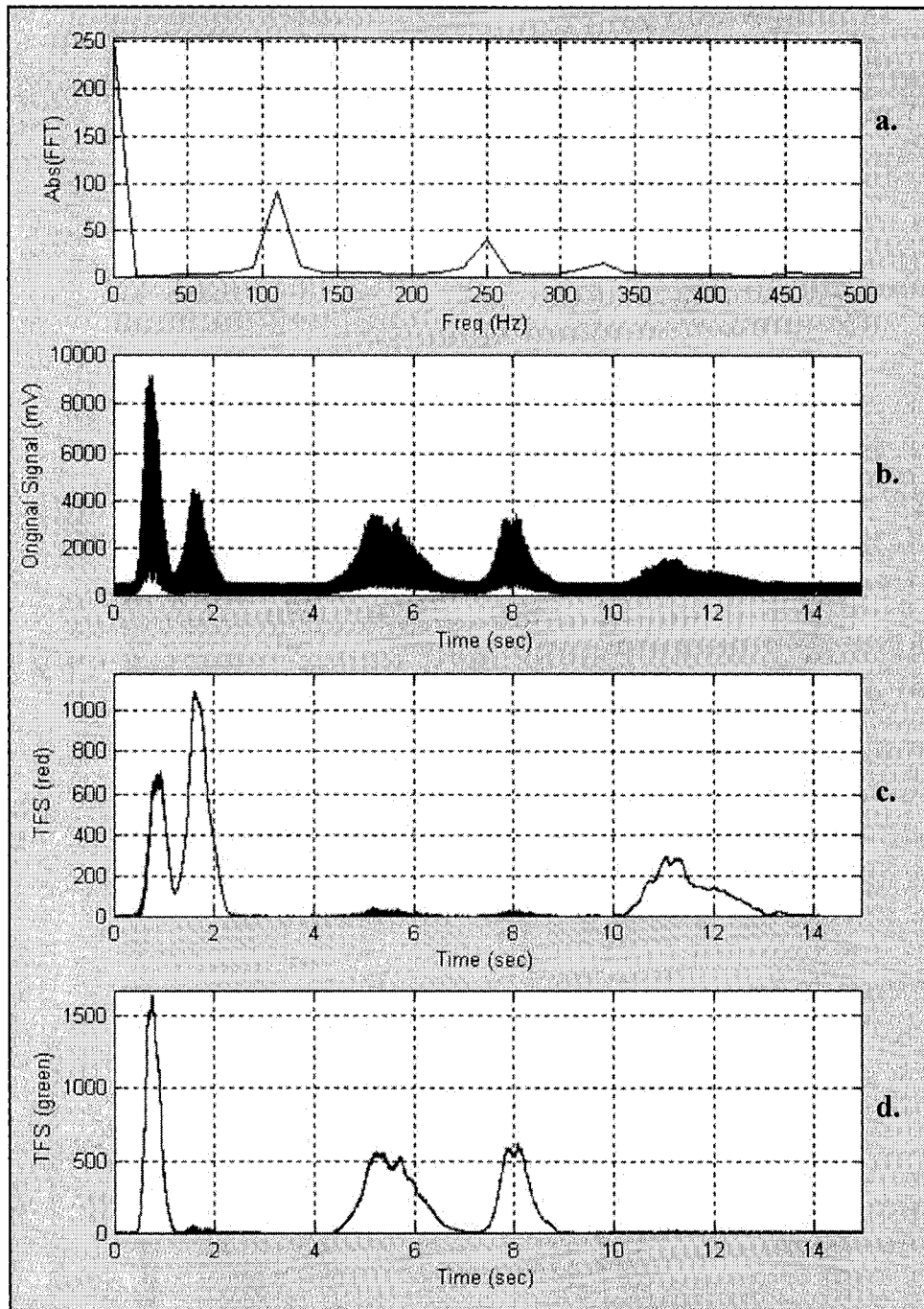
Figure 4.11 Pressure driven flow experiment in liquid core waveguide integrated biochip, first peak: 3 orange and 2 scarlet superimposed

b.The detection point:
Signal is picked up when the bead is between the
two horizontal lines.

c. The original signal picked up when the bead passes the
detection point. (The bright emission form the fluorescent
particle resulted in saturation)
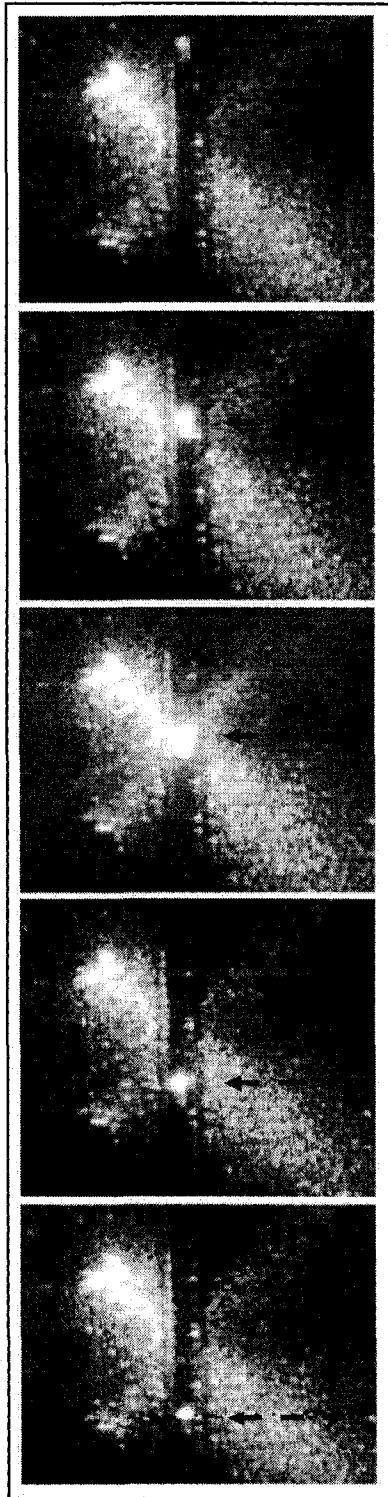
a. 5 frames of the sampling video

Figure 4.12 The pictures/picked up signal of an orange bead passing the detection point

The original signal picked up by the middle LCW is illustrated in Figure 4.12.c. The length of the signal peak is approximately 0.3 seconds which is shorter than the length of the time measured on the video file. The time on the diagram is the duration of time that the bead emitted and the middle LCW collected the light. The fluorescent bead only shines in the region that is adsorbing laser light which is smaller than the distance measured on the video. Considering the differences in times measured in the collected signal and the video, a relation between the measured times is obtained and the velocity measurement system based on the processed signals is created.

4.3. Experimental results: SCW biochips

Experimental results of electroosmotic flow in SCW biochip were also analyzed in the Matlab program. The same setup and parameters used for LCW biochips were employed to capture the video and sample data of EOF driven scarlet and orange bead motion in the biochip. The results are illustrated in Figure 4.13. The original sample file (Figure 4.13.a) shows three peaks in the diagram. In the 19 seconds long sample, two scarlet beads passed the detection point at 4 and 8.5 seconds and an orange bead passed the detection point at 17.5 seconds. The speed of the particle movements changed as the EO voltage changed from 350V to 400V at 12 seconds. This resulted in a narrow distribution of sample points along x axis, time. The speed of the first peak was calculated 0.2 mm/sec.
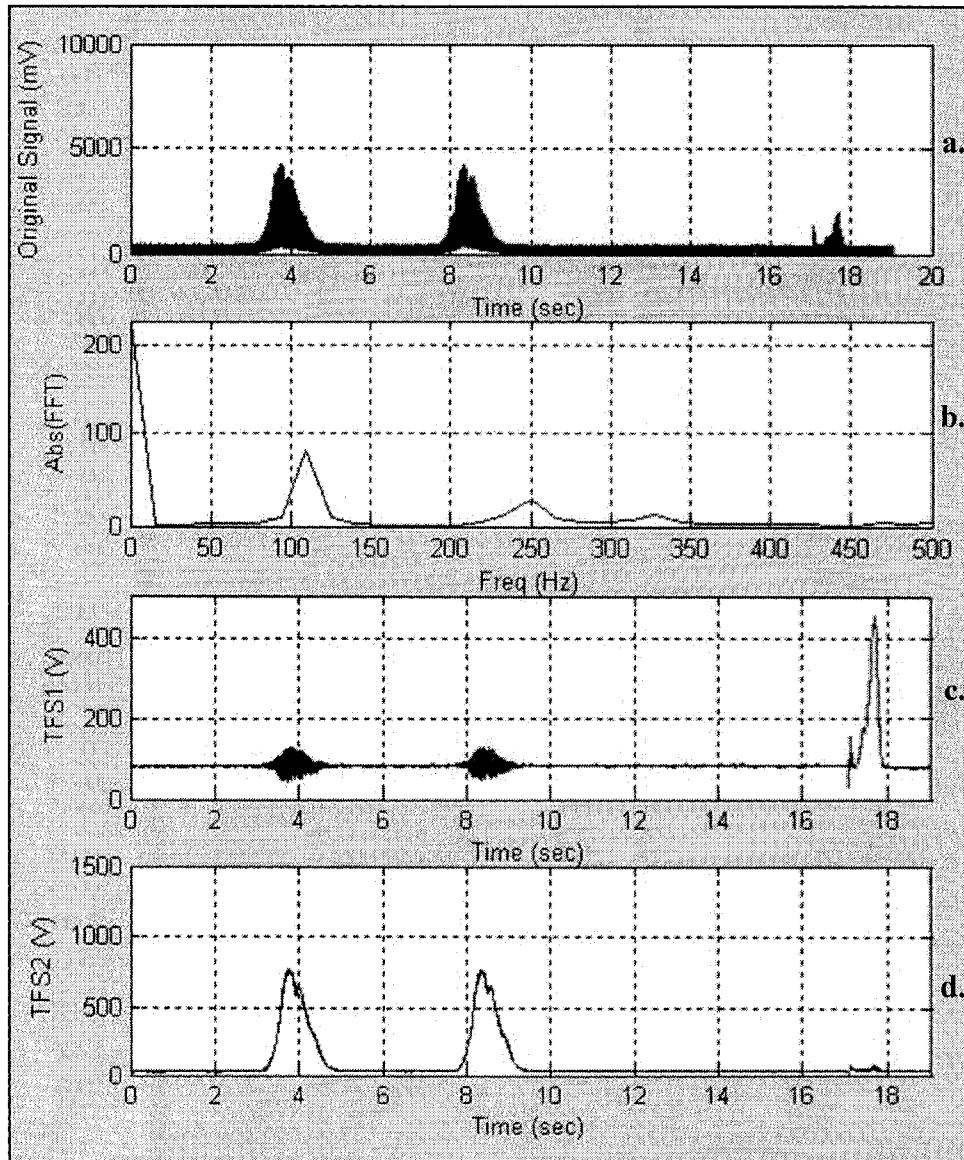
Figure 4.13 Electroosmotic flow experiment in solid core waveguide integrated biochip, 0-12sec V= 350v, 12-19sec V= 400v

CHAPTER 5

CONCLUSIONS

5.1. Summary of Work

This thesis presents a series of projects that resulted in the improvement of multilayer biochips and optics integration into the optofluidic structure. Design and fabrication of four generations of the biochips progressively advanced the prototypes structure by enhancing the material selection, reducing the fabrication costs and process times and improving the functionality of the optical system.

In Chapter 2, multilayer biochips with hollow v-groove waveguides for light delivery and pick up are detailed. First generation of multilayer biochips made in silicon-glass is a re-fabrication of the work by D. Spicer [71] in order to identify the issues with the original design and improve the biochip with minor changes. Second, third and fourth generations of biochips were all resulted from the efforts to replace the expensive material, e.g. silicon, and time-consuming fabrication procedures, e.g. glass HF etch, with better alternatives.

Second generation biochips presented in chapter 2 was semi-polymeric multi-layer biochip with PDMS microfluidic layer. It was also in the second generation that the structural layers' orientation was changed to bring the fluidics and the optics closer together by adding a 50μm-thick PMMA intermediate layer, the fluidic layer was flipped to place the micorchannel on top of thin PMMA.

Third and fourth generation biochips are all-polymeric biochips. Third generation biochips are consisted of a PDMS fluidics layer and a heat or UV cured PMMA optical layer which are bonded with a thin PMMA intermediate layer in between. Fourth generation optofluidic biochips were fabricated using UV-curable PEA optical layer and fluidics in PDMS or UV-curable PSiA.

Chapter 3 presented the gradual improvements in the design fabrication of the fluidic layer used for the fourth generation biochips. The final prototype was designed such that it can be used as a standalone single-layer optofluidic biochip with liquid filled or UV-polymer cured waveguides integrated into this layer.

The details of the experimental testing of the single-layer biochips were described in chapter 4. The results showed excellent optical detection of the fluorescent microparticles in the LCW and SCW integrated biochips. Based on these limited test results, the objectives of the thesis, to make high quality inexpensive biochips, were met.

Fabrication of a polymeric multilayer optofluidic biochip with in-plane and out-of-plane optics is a novel work and was never reported before. In the following page Figure 5.1 illustrates a summary of the fabrication processes, materials and the steps in the production of the optofluidic biochips discussed in this thesis.

Figure 5.1 Four generations of optofluidic biochips: materials, fabrication processes and key characteristics

5.2. Future Work

Resulting from the present work many topics for future work can are possible. Two main subjects can be described as enhancement of microfabrication in polymeric material and more advanced biochip designs. Moreover, improvements to the bonding methods for the the fourth generation biochip layers can assist the production of a commercializable biochip.

5.2.1. Polymeric Material

In order to find alternative material for fabrication of biochips mentioned a project was conducted parallel to the present work. A few PUA mixtures were developed and tested for fabrication of the microfluidics parts. Moreover, one of the mixtures was used to replicate v-groove features from Si master which illustrated good results. In addition, a mixture of acrylated perfluoropolyether, APFPE, was tested for micro-replication. Although many promising results were recorded, it was decided that the feasibility study of fabrication of biochips using such material should be a separate project for future. Figure 5.2.a depicts negative replica of a v-groove in the sample fabricated using PUA and figure 5.2.b ullistrates the reservoir wall in PUA.
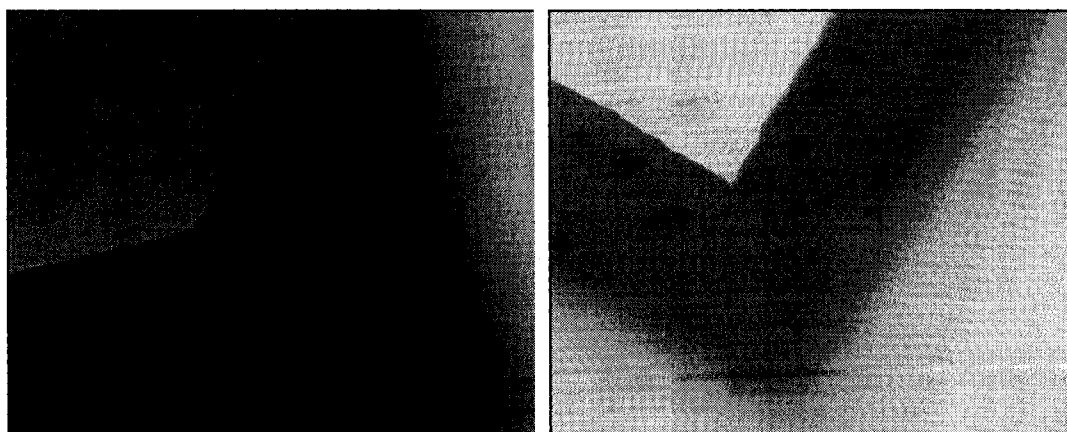
| a. PUA negative replica of a 100μm wide v-groove end facet | b. PUA replica of a reservoir edge etched in glass |

84

5.2.2. Biochip Design and Structure

A future product that can be resulted from this thesis is a multichannel biochip with the capability of parallel optical detection in several microchannels. An idea was recently developed at the microoptical system laboratory by Prof. J.N. McMullin and the author for using a single v-groove waveguide with serial taps to deliver light to six parallel fluidic microchannels. The idea, depicted in the schematic in figure 5.3, was briefly reported in [114]. The multi-tasking micro-features on this design are a set of six parallel microchannels with neighboring LCWs and a matching bottom layer which contains v-grooves and side taps. The biochip has a novel design so that all six fluidic channels are illuminated at a specific point via a single v-groove with serial side taps. Each microchannel is neighboring a LCW that performs the optical pickup.

1. First tap/fluidic channel
2. Second tap/fluidic channel
3. Third tap (end facet)/fluidic channel

I,II,III Liquid Core Waveguides
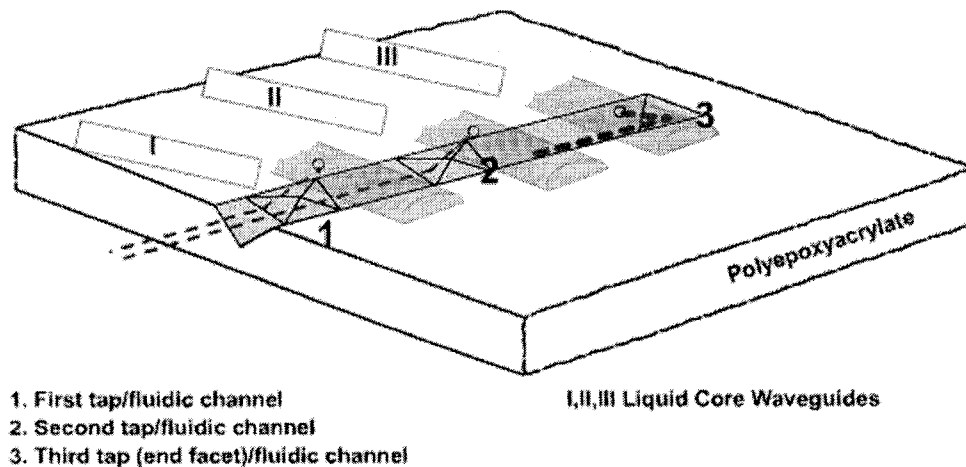
Figure 5.3 Laser beam distribution using side taps in a v-groove

85

In order to test the feasibility and fabricate an alpha prototype, as a side project, fluidics layers were fabricated in elastomeric materials PDMS and PSiA using a DRIE fabricated negative master. (Figure 5.4)

The process of design, fabrication and experimental testing of the beta prototype of this multilayer and multichannel polymeric biochip is another area of work for the future.
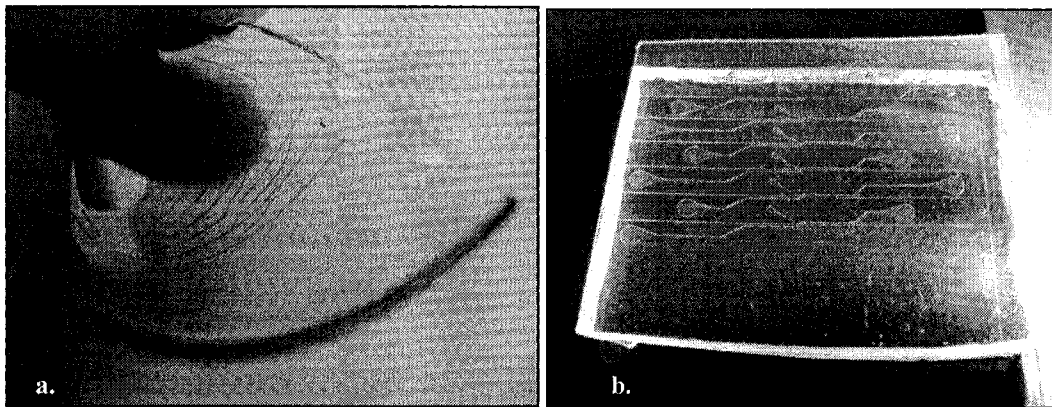
Figure 5.4 Multi-channel biochips a. Elastomeric Multichannel PSiA biochip b. PDMS-capped Multichannel PDMS biochip

REFERENCES

[1]   *CMC Microsystems Annual report,* CMC Microsystems Inc, 2006.

[2]   *The Worldwide Biochips & Equipments Market,* Fuji-Keizai Inc, USA, 2005.

[3]   J. W. Cooper, Y. Wang, and C. S. Lee, "Recent advances in capillary separations for proteomics," *Electrophoresis,* vol. 25, no. 23-24, pp. 3913-3926, 2004.

[4]   P. J. Obeid, T. K. Christopoulos, H. J. Crabtree *et al.,* "Microfabricated Device for DNA and RNA Amplification by Continuous-Flow Polymerase Chain Reaction and Reverse Transcription-Polymerase Chain Reaction with Cycle Number Selection," *Analytical Chemistry,* vol. 75, no. 2, pp. 288-295, 2003.

[5]   G. H. W. Sanders, and A. Manz, "Chip-based microsystems for genomic and proteomic analysis," *Trends in Analytical Chemistry,* vol. 19, pp. 364-378, 2000.

[6]   I. R. Lauks, "Microfabricated Biosensors and Microanalytical Systems for Blood Analysis," *Accounts of Chemical Research,* vol. 31, no. 5, pp. 317-324, 1998.

[7]   A. Daridon, V. Fascio, J. Lichtenberg *et al.,* "Multi-layer microfluidic glass chips for microanalytical applications," *Fresenius' Journal of Analytical Chemistry,* vol. 371, no. 2, pp. 261-269, 2001.

[8]   J. Voldman, M. L. Gray, and M. A. Schmidt, "Microfabrication in Biology and Medicine," *Annual Review of Biomedical Engineering,* vol. 1, no. 1, pp. 401-425, 1999.

[9]   S. C. Terry, J. H. Jerman, and J. B. Angell, "A gas chromatographic air analyzer fabricated on a silicon wafer," *IEEE Transactions on Electron Devices,* vol. 26, no. 12, pp. 1880-1886, 1979.

[10]   H. M. Widmer, "Trends in industrial analytical chemistry," *TrAC Trends in Analytical Chemistry,* vol. 2, no. 1, pp. VIII-X, 1983.

[11]   A. Manz, N. Graber, and H. M. Widmer, "Miniaturized total chemical analysis systems: A novel concept for chemical sensing," *Sensors and Actuators B: Chemical,* vol. 1, no. 1-6, pp. 244-248, 1990.

[12]   M. Toner, and D. Irimia, "BLOOD-ON-A-CHIP," *Annual Review of Biomedical Engineering,* vol. 7, no. 1, pp. 77-103, 2005.

[13]   E. Verpoorte, "Chip vision-optics for microchips," *Lab on a Chip,* vol. 3, no. 3, pp. 42N-52N, 2003.

[14]   P. Datta, J. Hammacher, M. Pease *et al.,* "Development of an Integrated Polymer Microfluidic Stack," *Journal of Physics: Conference Series,* vol. 34, pp. 853-858, 2006.

[15]   R. Go´mez, R. Bashir, A. Sarikaya *et al.,* "Microfluidic Biochip for Impedance Spectroscopy of Biological Species," *Journal of Biomedical Microdevices,* vol. 3, no. 3, pp. 201-209, 2001.

[16]   S. Attiya, A. B. Jemere, T. Tang *et al.,* "Design of an interface to allow microfluidic electrophoresis chips to drink from the fire hose of the external environment," *Electrophoresis,* vol. 22, no. 2, pp. 318-327, 2001.

[17]   A. Y. Fu, C. Spence, A. Scherer *et al.,* "A microfabricated fluorescence-activated cell sorter," *Nature Biotech,* vol. 17, no. 11, pp. 1109-1111, 1999.

[18] R. S. Jayashree, L. Gancs, E. R. Choban *et al.*, "Air-Breathing Laminar Flow-Based Microfluidic Fuel Cell," *Journal of American Chemical Society,* vol. 127, no. 48, pp. 16758-16759, 2005.

[19] I. W. Kaye, and W. R. Discipio, *Method and system for controlling fluid delivery in a fuel cell,* USA Patent no. 7205060, ULTRACELL CORP, U. S. Patent, 2007.

[20] F.-C. Huang, C.-S. Liao, and G.-B. Lee, "An integrated microfluidic chip for DNA/RNA amplification, electrophoresis separation and on-line optical detection," *Electrophoresis,* vol. 27, no. 16, pp. 3297-3305, 2006.

[21] B. Kuswandi, Nuriman, J. Huskens *et al.*, "Optical sensing systems for microfluidic devices: A review," *Analytica Chimica Acta,* vol. 601, no. 2, pp. 141-155, 2007.

[22] K. B. Mogensen, J. El-Ali, A. Wolff *et al.*, "Integration of Polymer Waveguides for Optical Detection in Microfabricated Chemical Analysis Systems," *Applied Optics,* vol. 42, no. 19, pp. 4072-4079, 2003.

[23] H. Qiao, S. Goel, A. Grundmann *et al.*, "Fabrication of micro-optical/microfluidic biochips", Proceedings of SPIE, Applications of Photonic Technology V, vol. 4833, pp. 54-59, 2002.

[24] A. T. Woolley, K. Lao, A. N. Glazer *et al.*, "Capillary Electrophoresis Chips with Integrated Electrochemical Detection," *Journal of Analytical Chemistry,* vol. 70, no. 4, pp. 684-688, 1998.

[25] I. M. Lazar, R. S. Ramsey, S. Sundberg *et al.*, "Subattomole-Sensitivity Microchip Nanoelectrospray Source with Time-of-Flight Mass

Spectrometry Detection," *Journal of Analytical Chemistry,* vol. 71, no. 17, pp. 3627-3631, 1999.

[26]   M. Slyadnev, Y. Tanaka, M. Tokeshi *et al.,* "Non-contact temperature measurement inside microchannel," in Micro Total Analysis Systems, 5th µTAS Symposium, Monterey, CA, 2001, pp. 361–362.

[27]   "Investext Company and Industry Research," *Mergent online,* 2006.

[28]   M. L. Chabinyc, D. T. Chiu, J. C. McDonald *et al.,* "An Integrated Fluorescence Detection System in Poly(dimethylsiloxane) for Microfluidic Applications," *Analytical Chemistry,* vol. 73, no. 18, pp. 4491-4498, 2001.

[29]   T. Pan, R. T. Kelly, M. C. Asplund *et al.,* "Fabrication of calcium fluoride capillary electrophoresis microdevices for on-chip infrared detection," *Journal of Chromatography A,* vol. 1027, no. 1-2, pp. 231-235, 2004.

[30]   A. Bromberg, and R. A. Mathies, "Homogeneous Immunoassay for Detection of TNT and Its Analogues on a Microfabricated Capillary Electrophoresis Chip," *Anal. Chem.,* vol. 75, no. 5, pp. 1188-1195, 2003.

[31]   S. D. Mangru, and D. J. Harrison, "Chemiluminescence detection in integrated post-separation reactors for microchip-based capillary electrophoresis and affinity electrophoresis," *ELECTROPHORESIS,* vol. 19, no. 13, pp. 2301-2307, 1998.

[32]   W. Demtroder, *Laser Spectroscopy: Basic Concepts and Instrumentation,* 3rd ed.: Springer Verlag, 1995.

[33]   P. S. Dittrich, and A. Manz, "Single-molecule fluorescence detection in microfluidic channels—the Holy Grail in µTAS?", *Analytical and Bioanalytical Chemistry,* vol. 382, no. 8, pp. 1771-1782, 2005.

[34] L. Cui, T. Zhang, and H. Morgan, "Optical particle detection integrated in a dielectrophoretic lab-on-a-chip," *Journal of Micromechanics and Microengineering,* vol. 12, no. 1, pp. 7-12, 2002.

[35] D. Psaltis, S. R. Quake, and C. Yang, "Developing optofluidic technology through the fusion of microfluidics and optics," *Nature,* vol. 442, no. 7101, pp. 381-386, 2006.

[36] E. Verpoorte, and N. F. De Rooij, "Microfluidics meets MEMS," *Proceedings of the IEEE,* vol. 91, no. 6, pp. 930-953, 2003.

[37] P. Friis, K. Hoppe, O. Leistiko *et al.,* "Monolithic integration of microfluidic channels and optical waveguides in silica on silicon," *Applied Optics,* vol. 40, no. 34, pp. 6246-6251, 2001.

[38] O. Leistiko, and P. F. Jensen, "Integrated bio/chemical microsystems employing optical detection: the clip-on," *Journal of Micromechanics and Microengineering,* vol. 8, pp. 148-150, 1998.

[39] J. N. McMullin, "Laser fabrication of integrated microfluidic/micro-optic systems", Proceedings of SPIE Photonics North, Applications of Photonic Technology VI, pp. 1050-1055, 2000.

[40] J. N. McMullin, H. Qiao, S. Goel *et al.,* "Integrated optical measurement of microfluid velocity," *Journal of Micromechanics and Microengineering,* vol. 15, pp. 1810-1816, 2005.

[41] S. Borreman, S. Musa, A. Kok *et al.,* "Fabrication of Polymeric Waveguides and devices in SU-8 Photoresist using Selective Polymerization", Proceedings Sysmposium IEEULEOS Benelux Chapter, Amsterdam, pp. 83-86, 2002.

[42]   S. Goel, "Opto-biochips for microcytometry ", Ph.D. Thesis, Dept. Electrical and Computer Engineering, University of Alberta, 2006.

[43]   O. J. A. Schueller, X. Zhao, G. M. Whitesides *et al.*, "Fabrication of Liquid-Core Waveguides by Soft Lithography," *Advanced Materials,* vol. 11, no. 1, pp. 37-41, 1999.

[44]   V. Kostal, M. Zeisbergerova, Z. Hrotekova *et al.*, "Miniaturized liquid core waveguide-based fluorimetric detection cell for capillary separation methods: Application in CE of amino acids," *ELECTROPHORESIS,* vol. 27, no. 23, pp. 4658-4665, 2006.

[45]   N. Blow, "Microfluidics: in search of a killer application," *Nat Meth,* vol. 4, no. 8, pp. 665-670, 2007.

[46]   C.-H. Lin, G.-B. Lee, Y.-H. Lin *et al.*, "A fast prototyping process for fabrication of microfluidic systems on soda-lime glass," *Journal of Micromechanics and Microengineering,* vol. 11, no. 6, pp. 726-732, 2001.

[47]   M. Simion, A. Angelescu, I. Kleps *et al.*, "Micro fluidic biochip for bio-medical application", Proceedings of the 16th International Conference on Microelectronics, pp. 80-83, 2004.

[48]   J. C. McDonald, and G. M. Whitesides, "Poly(dimethylsiloxane) as a Material for Fabricating Microfluidic Devices", *Acc. Chem. Res.,* vol. 35, no. 7, pp. 491-499, 2002.

[49]   Y. Xia, and G. M. Whitesides, "Soft Lithography", *Angewandte Chemie International Edition,* vol. 37, no. 5, pp. 550-575, 1998.

[50] B. K. Long, B. K. Keitz, and C. G. Willson, "Materials for step and flash imprint lithography (S-FIL)," *Journal of Materials Chemistry,* vol. 17, no. 34, pp. 3575-3580, 2007.

[51] S.-m. Kim, D. Kim, and S. Kang, "Replication of micro-optical components by ultraviolet-molding process," *Journal of Microlithography, Microfabrication, and Microsystems,* vol. 2, no. 4, pp. 356-359, 2003.

[52] J. Haisma, M. Verheijen, K. van den Heuvel *et al.*, "Mold-assisted nanolithography: A process for reliable pattern replication", *Journal of Vacuum Science & Technology B: Microelectronics and Nanometer Structures*, vol. 14, issue 6, pp. 4124-4128, 1996.

[53] Y. C. Chung, Y. H. Chiu, H. J. Liu *et al.*, "Ultraviolet curing imprint lithography on flexible indium tin oxide substrates," *Journal of Vacuum Science & Technology B: Microelectronics and Nanometer Structures,* vol. 24, no. 3, pp. 1377-1383, 2006.

[54] S. R. Quake, and A. Scherer, "From Micro- to Nanofabrication with Soft Materials," *Science,* vol. 290, no. 5496, pp. 1536-1540, November 24, 2000, 2000.

[55] K. T. Haraldsson, J. B. Hutchison, R. P. Sebra *et al.*, "3D polymeric microfluidic device fabrication via contact liquid photolithographic polymerization (CLiPP)," *Sensors and Actuators B: Chemical,* vol. 113, no. 1, pp. 454-460, 2006.

[56] W. X. Zhou, and M. B. Chan-Park, "Large area UV casting using diverse polyacrylates of microchannels separated by high aspect ratio microwalls," *Lab on a Chip,* vol. 5, no. 5, pp. 512-18, 2005.

[57] H. Schmid, and B. Michel, "Siloxane Polymers for High-Resolution, High-Accuracy Soft Lithography," *Macromolecules,* vol. 33, no. 8, pp. 3042-3049, 2000.

[58] J. P. Rolland, E. C. Hagberg, K. R. Carter *et al.*, "Perfluoropolyethers as novel materials for soft lithography", Proceedings of the SPIE, Emerging Lithographic Technologies IX, pp. 410-414, 2005.

[59] J. P. Rolland, R. M. VanDam, D. A. Schorzman *et al.*, "Solvent-Resistant Photocurable "Liquid Teflon" for Microfluidic Device Fabrication," *J. Am. Chem. Soc.,* vol. 126, no. 8, pp. 2322-2323, 2004.

[60] Y. Huang, P. Castrataro, C.-C. Lee *et al.*, "Solvent resistant microfluidic DNA synthesizer," *Lab on a Chip,* vol. 7, no. 1, pp. 24-26, 2007.

[61] T. T. Truong, R. Lin, S. Jeon *et al.*, "Soft Lithography Using Acryloxy Perfluoropolyether Composite Stamps," *Langmuir,* vol. 23, no. 5, pp. 2898-2905, 2007.

[62] B. Ziaie, A. Baldi, M. Lei *et al.*, "Hard and soft micromachining for BioMEMS: review of techniques and examples of applications in microfluidics and drug delivery," *Advanced Drug Delivery Reviews,* vol. 56, no. 2, pp. 145-172, 2004.

[63] H. Andersson, and A. Berg, "Microfluidic devices for cellomics," in *Lab-on-Chips for Cellomics*, pp. 1-22, 2006.

[64] H. Andersson, and A. van den Berg, "Microfluidic devices for cellomics: a review," *Sensors and Actuators B: Chemical,* vol. 92, no. 3, pp. 315-325, 2003.

[65] D. J. Beebe, G. A. Mensing, and G. M. Walker, "Physics and applications of microfluidics in biology" *Annual Review of Biomedical Engineering,* vol. 4, no. 1, pp. 261-286, 2002.

[66] N. T. Nguyen, and S. T. Wereley, *Fundamentals and Applications of Microfluidics,* second ed.: Artech House, 2006.

[67] Y. Kikutani, A. Hibara, K. Uchiyama *et al.,* "Pile-up glass microreactor," *Lab Chip,* vol. 2, pp. 193-196, 2002.

[68] J.-B. Yoon, C.-H. Han, E. Yoon *et al.,* "Novel monolithic and multilevel integration of high-precision 3-D microfluidic components", Proceedings of SPIE Microfluidic Devices and Systems, pp. 183-191, 1998.

[69] A. Han, M. Graff, O. Wang *et al.,* "An approach to multilayer microfluidic systems with integrated electrical, optical, and mechanical functionality," *Sensors Journal, IEEE,* vol. 5, no. 1, pp. 82-89, 2005.

[70] D. Spicer, J. N. McMullin, and H. Rourke, "A multi-layer biochip with integrated hollow waveguides," *Journal of Micromechanics and Microengineering,* vol. 16, no. 8, pp. 1674-1680, 2006.

[71] D. Spicer, "Multi-layer biochip with integrated hollow waveguides," M.Sc. thesis, Dept. of Electrical and Computer Engineering., University of Alberta, 2005.

[72] P. J. Hesketh, C. Ju, S. Gowda *et al.,* "Surface Free Energy Model of Silicon Anisotropic Etching," *Journal of The Electrochemical Society,* vol. 140, no. 4, pp. 1080-1085, 1993.

[73] J. Frühauf, "Orientation Dependent Etching of Silicon" in *Shape and Functional Elements of the Bulk Silicon Microtechnique*, pp. 17-69: Springer Berlin Heidelberg, 2005.

[74] J. N. McMullin, R. Narendra, and C. R. James, "Hollow metallic waveguides in silicon V-grooves," *Photonics Technology Letters, IEEE,* vol. 5, no. 9, pp. 1080-1082, 1993.

[75] D. J. Sadler, M. J. Garter, C. H. Ahn *et al.*, "Optical reflectivity of micromachined {111}-oriented silicon mirrors for optical input - output couplers," *Journal of Micromechanics and Microengineering,* vol. 7, pp. 263-269, 1997.

[76] C. Strandman, L. Rosengren, H. G. A. Elderstig *et al.*, "Fabrication of 45° mirrors together with well-defined v-grooves using wet anisotropic etching of silicon," *Journal of Microelectromechanical Systems,* vol. 4, no. 4, pp. 213-219, 1995.

[77] R. M. Tiggelaar, T. T. Veenstra, R. G. P. Sanders *et al.*, "A light detection cell to be used in a micro analysis system for ammonia," *Talanta,* vol. 56, pp. 331-339, 2002.

[78] S.-H. Huang, and F.-G. Tseng, "Development of a monolithic total internal reflection-based biochip utilizing a microprism array for fluorescence sensing," *Journal of Micromechanics and Microengineering,* vol. 15, no. 12, pp. 2235-2242, 2005.

[79] M. A. Powers, S. T. Koev, A. Schleunitz *et al.*, "A fabrication platform for electrically mediated optically active biofunctionalized sites in BioMEMS," *Lab on a Chip,* vol. 5, no. 6, pp. 583-586, 2005.

[80] C. L. Bliss, J. N. McMullin, and C. J. Backhouse, "Rapid fabrication of a microfluidic device with integrated optical waveguides for DNA fragment analysis," *Lab on a Chip,* vol. 7, no. 10, pp. 1280-1287, 2007.

[81] C. L. Bliss, J. N. McMullin, and C. J. Backhouse, "Integrated wavelength-selective optical waveguides for microfluidic-based laser-induced fluorescence detection," *Lab on a Chip,* vol. 8, no. 1, pp. 143-151, 2008.

[82] D. Li, *Electrokinetics in Microfluidics,* Academic Press, 2004.

[83] "Norcada Inc.," January 20, 2008; http://www.norcada.com/.

[84] "Norland Optical Adhesives " January, 25, 2008; https://www.norlandprod.com/UVdefault.tpl.

[85] "Goodfellow Corporation," January, 25, 2008; www.goodfellow.com/.

[86] "Zygo surface profilometer, Zygo Inc," January, 25, 2008; www.ZYGO.com.

[87] S. Bhattacharya, A. Datta, J. M. Berg *et al.,* "Studies on surface wettability of poly(dimethyl) siloxane (PDMS) and glass under oxygen-plasma treatment and correlation with bond strength," *Microelectromechanical Systems, Journal of,* vol. 14, no. 3, pp. 590-597, 2005.

[88] J. Kameoka, H. G. Craighead, H. Zhang *et al.,* "A Polymeric Microfluidic Chip for CE/MS Determination of Small Molecules," *Anal. Chem.,* vol. 73, no. 9, pp. 1935-1941, 2001.

[89] C. L. Bliss, C. J. Backhouse, and J. N. McMullin, "Two-colour microparticle detection in PDMS biochips with integrated optics", Proceedings of the SPIE Photonics North, Ottawa, Canada, 2007.

[90]   F. Perennes, B. Marmiroli, M. Matteucci *et al.*, "Sharp beveled tip hollow microneedle arrays fabricated by LIGA and 3D soft lithography with polyvinyl alcohol," *Journal of Micromechanics and Microengineering*, vol. 16, no. 3, pp. 473-479, 2006.

[91]   C. D. Schaper, "Nanofabrication with water-dissolvable polymer masks of polyvinyl alcohol (PVA): MxL." Proceedings of the SPIE conference on Emerging Lithographic Technologies VIII, pp. 325-336, 2004.

[92]   K. Kim, S. Park, J. B. Lee *et al.*, "Rapid replication of polymeric and metallic high aspect ratio microstructures using PDMS and LIGA technology," *Microsystem Technologies*, vol. 9, no. 1, pp. 5-10, 2002.

[93]   K. Nakamatsu, K. Tone, T. Ohtake *et al.*, "Nanoimprint and lift-off process using poly vinyl alcohol", Japanese Journal of Applied Physics vol. 44, no. 11, pp. 8186-8188, 2005.

[94]   J. Jo, K.-Y. Kim, E.-S. Lee *et al.*, "Nanocontact printing of nonplanar substrate by using flexible h-PDMS stamp", Proceedings of SPIE conference on Device and Process Technologies for Microelectronics, MEMS, and Photonics, 2006.

[95]   D. K. Maurya, W. Y. Ng, K. Ansari Mahabadi *et al.*, "Fabrication of lab-on chip platforms by hot embossing and photo patterning", *Biotechnology Journal*, vol. 2, no. 11, pp. 1381-1388, 2007.

[96]   J. B. Orhan, V. K. Parashar, A. Sayah *et al.*, "Fabrication and Characterization of Three-Dimensional Microlens Arrays in Sol-Gel Glass", *Journal of Microelectromechanical Systems*, vol. 15, no. 5, pp. 1159-1164, 2006.

[97]   "Partall® Coverall Film," January, 29, 2007; http://www.rexco-usa.com/part1.htm.

[98]   J. A. Dobrowolski, *Optical properties of films and coatings*, Second edition ed.: McGraw-Hill Professional, 1995.

[99]   L. Gladius, "Properties of acrylic bone cement: State of the art review," *Journal of Biomedical Materials Research*, vol. 38, no. 2, pp. 155-182, 1997.

[100]   H. Morawetz, "Water-soluble Polymers: Synthesis, Solution Properties and Applications " *Journal of Polymers for Advanced Technologies,* vol. 3, no. 2, pp. 95, 1992.

[101]   "Ciba Specialty Chemicals " January, 25, 2008; http://www.ciba.com/.

[102]   "Sartomer Company," January, 25, 2008; http://www.sartomer.com/.

[103]   "Ebecryl 150," January, 20, 2008; http://www.cytec.com/specialty-chemicals/spec_pdfs/IC-R.pdf.

[104]   S. J. Lee, W. Shi, P. Maciel *et al.*, "Top-edge profile control for SU-8 structural photoresist", Proceedings of th 15th Bienial Univesity/Government/Industry Microelectronics Symposium, San Jose, USA, pp. 389-390, 2003.

[105]   "SU-8: Thick Photo-Resist for MEMS," January, 20, 2008; http://memscyclopedia.org/su8.html.

[106]   M. J. Madou, *Fundamentals of Microfabrication: The Science of Miniaturization*, 2nd edition ed.: CRC press, 2002.

[107]   K. Koski, J. Holsa, and P. Juliet, "Deposition of aluminium oxide thin films by reactive magnetron sputtering," *Journal of Surface and Coatings Technology*, vol. 116-119, pp. 716-720, 1999.

[108]   D. Depla, J. Haemers, G. Buyle *et al.*, "Hysteresis behavior during reactive magnetron sputtering of Al_2O_3 using a rotating cylindrical magnetron," *Journal of Vacuum Science & Technology A: Vacuum, Surfaces, and Films*, vol. 24, no. 4, pp. 934-938, 2006.

[109]   W. D. Sproul, D. J. Christie, and D. C. Carter, "The Reactive Sputter Deposition of Aluminum Oxide Coatings Using High Power Pulsed Magnetron Sputtering (HPPMS)," in Society of Vacuum Coaters 47th Annual Technical Conference, Dallas, USA, pp. 96-100, 2004.

[110]   K. Koski, J. Holsa, and P. Juliet, "Voltage controlled reactive sputtering process for aluminium oxide thin films," *Journal of Thin Solid Films*, vol. 326, no. 1-2, pp. 189-193, 1998.

[111]   B. E. A. Saleh, and M. C. Teich, *Fundamentals of Photonics*: John Wiley & Sons, Inc., 1991.

[112]   P. Ponsaud, B. Defoort, and X. Coqueret, "Reactivity and Network Structure of UV- and EB-Cured Bis-Phenol A Ethoxy Diacrylate," Proceedings of RadTech Europe, Barcelona, Spain, 2005.

[113]   January, 15, 2008; http://probes.invitrogen.com/handbook/sections/0605.html.

[114]   H. Hosseinkhannazer, L. Kostiuk, and J. N. McMullin, "Multilayer biochips with integrated optics replicated in PMMA and PDMS.", Proceedings of Photonics North, Ottawa, Canada, 2007.

Appendix A. Polymer Background

This section describes polymers, the classification of polymers and the polymerization processes. Also, the role of polymer mixtures additives and the physical characteristics of the products are discussed here in this part. Addition of this section to the thesis is to provide a summary of polymer science and technology theory and fundamentals. [1-4] were used as main references for this section.

A.1. Polymers

A polymer is a material composed of large and long-chained molecules, usually monomers, repeatedly structured through the medium and joined by covalent chemical bonds. Historically, monomers are molecules with carbon (C) atoms dominating the structure. Consequently, all biological systems are constructed of polymers. Some natural polymeric materials perform mechanical functions (such as wood or bone) and some regulate chemical reactions i.e. veins and cells. Only in the late half of the previous century did humans learn how to make polymers of their own. In the early years, the synthesis of these new polymers did not replace our all time favorite materials, such as natural polymers like rubber and nonpolymeric material such as as metals, but by implementing nature's examples, for instance developing composites, human made plastics have come to dominate the market and have proved to be good replacements for traditional material from metals to glass and from silicon to rubber. These new polymers are able to crystallize, cross-link and orient the chains of molecules to create structures that are comparable to durable metal alloys.

Polymers can be designed or synthesized for new applications or when a new set of characteristics are needed, but sometimes, it is easier to make a new compound by simply adding different volumes of monomer solutions and

engineer a new product. In this project this latter methodology was used to create the desired polymeric compounds from non-standard mixtures containing commercial thin film and plastic coating products or sealing products. This section provides background to the field of polymers and polymerization with an emphasis on the materials and processes used in this thesis.

A.1.1. Polymer Classification and Types

There are different methods for grouping or classifying "engineering" polymers. Classification of polymers, especially the material used by engineers in manufacturing, has always been a confusing process. Identification of the monomers that a polymer contains is the first important step in classification. Following this step comes naming or grouping the polymer with the regards to monomer classification. Polymers comprising only a single species of monomer are called homopolymers and polymers containing a mixture of monomers are called copolymers. In this way we divide the polymers as single-monomers constructed (A-A-A-A) and co-polymers consisting two or more kinds of molecules (A-B-A-B). Co-polymers can be a structure of different combinations of a few kinds of molecules which, depending on how the species are repeated in the bulk body macromolecules, can be:

1. Statistical (random) Copolymers: Random or uneven distribution of molecules

2. Alternating Copolymers: units distributed in a regular alternating fashion

3. Block Copolymers: Blocks of monomers joined together

4. Graft Copolymers: Side blocks or chains are added to the main blocks.

A.1.2. Plastics vs. Polymers

The word polymer can address any of the macromolecules with organic backbone; plastics, DNA or proteins. It is common to refer to a group of bulk, usually in solid form and commonly used commercial polymers as "plastics". In

this work, the words plastic and polymer are used interchangeably and address solid plastics.

A.1.3. Classification of Plastics by Temperature

When creating polymer mixtures to produce new materials, a generic list of plastics are usually in mind. By defining behaviour of plastics in different temperatures, reaction to thermal situations, we can sort the plastics in a different classification method. Basically, this taxonomy is built on the molecule-molecule interactions and the various bonds monomers and molecular chains have in a structured plastic.

Sometimes, glass transition temperature can be a good measure for characterizing a polymer. Glass transition temperature (T_g) is the temperature below which the physical properties of materials resemble those of a solid phase, and above which materials behave like liquids. Looking closely at the medium, glass transition temperature, is the temperature below which molecules have little relative mobility. Not all plastics show this phase change soley as a function of temperature.

Considering molecular bonds and macroscale behaviour of the polymer when reacting to changes in mechanics or temperature, general engineering plastics can be categorized as thermoplastics, thermosets or resins, elastomers or rubbers, and natural polymers.

A.1.3.1. Thermoplastics

Thermoplastic are known for softening upon heating and often described as linear polymers. Linearity, when the polymer molecule is a single straight chain, describes the characteristics of the polymer as the monomer chains are not cross-

103

linked[1]. (This structure is different from branching when either the main chain or one or more side chains branches.

Thermoplastics are the largest class of engineering polymer. Thermoplastic monomers are linear chains that have two active bonds; bifunctional[2]. In such structure, a molecule with only one active bond can act as a chain terminator, but it cannot form a link in a chain.

Being linear, following heat exposure, the thermoplastics soften if the polymer is heated. This change to a softer form is due to the split of the secondary bonds binding the molecules to each other and eventually forming a viscous liquid. The molecules in linear polymers can be of a range of molecular weights. Configuration of molecules in the structure usually referred to as crystallinity or the degree of structural order in a solid part is another chrematistic that differs among thermoplastics. In a crystal, principally, the atoms or molecules are arranged in a regular, periodic manner. Amorphous materials, such as liquids, some plastics and glasses, might only have order in molecule orientation and placement within a specific small region and time. Some thermoplastics, like polystyrene, are amorphous; others, like polyethylene, are partly crystalline. Having a range of molecular weights and packing geometries results in thermoplastic material with no precise melting point. Polyethylene (PE), Polypropylene (PP), Polytetrafluoroethylene (PTFE,Teflon) Polystyrene (PS), Polyvinylchloride (PVC), Polymethylmethacrylate (PMMA, Perspex, plexiglass) are some of the most popular engineering thermoplastics.

The simplest linear-chain polymer is polyethylene. In the ethylene molecule, C_2H_4, by replacing one H atom of the monomer by a side-group or radical, R, the

---

[1] Cross-linking happens when covalent bonds link one polymer chain to another and is a characteristic property of thermosetting polymer materials.

[2] Monomers with three or more active sites, polyfunctional monomers, form networks and can make cross-links. Polyfunctional monomers are the basis of thermosetting polymers, or resins.

vinyl group of polymers is prepared. The vinyl group can be used to produce polyvinyl chloride, polypropylene and polystyrene.

If two of the hydrogens of ethylene are replaced by radicals, the second simplest group of linear polymers is produced, the vinylidene group. Polymethylmethacrylate (PMMA) is from this family: the two radicals in Methylmethacrylate, $C_5H_8O_2$, are —CH3 and —COOCH3.

A.1.3.2. Thermosets or Resins

A good example of a thermoset or resin is epoxy, the popular adhesive, which hardens when two of the components, resin and a hardener, are heated together or even at room temperature. The result is usually a heavily cross-linked plastic. That is why thermosets are sometimes described as network polymers. The cross-links are formed in the first stages of the polymerisation of the liquid resin and hardener, so the structure is almost always amorphous. When being heated again, the additional secondary bonds melt, and the cross-links prevent true melting or viscous flow so the polymer may only turn into a rubber-like material and further heating just causes a decomposition of the material. The network of cross-linked monomers in thermoset material, is like a woven fabric and due to the presence of many cross-links, thermosets are usually harder compared to amorphous thermoplastics. Moreover, they cannot easily be crystallised or oriented, so it is not easily possible to change their properties by processing.

Usually, to produce thermosets, the polymer scientists start with large polyfunctional monomers. These polyfunctional molecules can react with each other or with small, linking molecules in a condensation reaction. Condensation is a process in which one molecule gives an —OH and another provides a —H to produce H2O as a by-product and the two molecules can bond. Since at least one of the two molecules is polyfunctional, a random three-dimensional network is very likely to form. Cross-linked thermosets do not dissolve in solvents, which

particularly, this makes them good candidates for adhesives, coating material, the matrix medium for composites.

A.1.3.3. Elastomers or Rubbers

Elastomers or rubbers are nearly linear polymers with few random and intermittent cross-links in which, at room temperature, the secondary bonds have already melted. The cross-links make the material a shape-memory polymer, so when deformed, it returns to its original shape upon load release. Some of the better known elastomers are polyisoprene or natural rubber and polybutadiene, also known as synthetic rubber that is mainly used for car tires. Elastomers are polymers with glass transition temperatures that are far below room temperature meaning the secondary bonds have melted.

A.1.3.4. Natural polymers

Cellulose, lignin and protein are common species of this group. Always present in most plant and animal life, usually, these polymers are comprised of long molecules with a covalent bond on their backbone consisting carbon atoms. The long monomers are bonded together by weak Van der Waals and hydrogen bonds, and occasionally with extra covalent cross-links.

A.1.4. Polymer chain

As mentioned above, the simplest form of polymer molecule is a straight chain, or polymer composed of a single main chain. The monomer chain structure is the most important characteristic that decides the type of the polymer resulting from monomers interaction. When there is a branch point, by cross-linking, four or more distinctive chains emanate. In the case of very high crosslink concentration, the formation of an infinite network of molecules is very likely and is called polymer gel. Simply, gel is a network of chains with unlimited extent.

Polymer chain size is another decisive factor in polymer bulk characteristics. In polymer science, molecular weight is usually used to emphasize the molecule size. The number of monomer units which comprise the polymer, also known as degree of polymerization, is another factor in polymer classification.

Sometimes, a finite group of monomers makes a block called an oligomer that can react with the other monomers and oligomers in the environment and polymerize as well. Oligomers can be seen as a group or chain-like block that has molecules with functional groups that can react and bond to monomers and other oligomers and shape a polymer.

A.2. Polymerization

Polymerization is a process in which macro molecules or monomers bond to each other and the product is called polymer or polymerized matter. Polymerization can occur in different manners. Identification of polymerization mechanisms, similar to polymer classification, is yet subject to debate. Historically polymer scientist grouped the polymerization mechanisms into two classical types: addition polymerization, some times classified as Chain-Growth and condensation, also confusingly known as Step-Growth, polymerization. Considering that the classification based on polymer structure, differentiates polymers into condensation and addition polymers, whereas the other approach, focusing on polymerization mechanism, divides polymerizations into step and chain growth polymerizations, one can correctly choose the classification method. Much confusion arises when the two classifications are used casually and interchangeably. Given the vast number of polymers available, some cannot be classified with the above mentioned grouping method, here, a more comprehensive method is used. The polymer polymerization mechanisms can be classified as chain-reaction polymerization. ionic and coordination

polymerization, step-growth polymerization, ring-opening polymerization, and supramolecular polymerization.

A.2.1. Chain-reaction Polymerization

In a process when unsaturated molecules are rapidly being added to the ends of a chain, chain-reaction polymerization is taking place. This process is an important industrial method of polymer preparation.

Although radical polymerization theory was established in the1950s, this mechanism is still one of the most studied chemical processes. Approximately half of all manufacturing of synthetic polymers worldwide are carried out using free radical polymerization

Initiation:

$$I \rightarrow I^{\cdot}$$

$$I^{\cdot} + M \rightarrow I\text{-}M^{\cdot}$$

Propagation:

$$I\text{-}M^{\cdot} + n M \rightarrow I\text{-}M_n\text{-}M^{\cdot}$$

Termination:

$$2\ I\text{-}M_n\text{-}M^{\cdot} \rightarrow I\text{-}M_n\text{-}M\text{-}M\text{-}M_n\text{-}I$$

$$2\ I\text{-}M_n\text{-}M^{\cdot} \rightarrow I\text{-}M_n\text{-}M' + I\text{-}M_n\text{-}M''$$
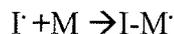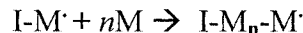
Figure A.1 Free-radical polymerization mechanism

The most common unsaturated compounds that undergo chain-reaction polymerization are olefins. Alkene or olefin is an unsaturated chemical compound containing at least one carbon-to-carbon double bond. The growing polymer in this mechanism is known as free radical. Chain-reaction polymerization starts with the introduction of reagents that can produce free-radicals to the mixture or by adding ionic initiators. There are three usual and major steps known for this

mechanism: initiation, propagation, and termination. Depending on the mixture structure, a fourth step called chain transfer can occur in some polymerizations. Figure A.1 depicts the steps in taking place in a free-radical polymerization. I, the initiator breaks to form the free radical which makes bonds with the monomer, M.

A.2.1.1. Initiation

Initiation starts with a monomer being attracted to free radicals, molecules with atoms containing unpaired electrons. Exposed to heat, light such as ultraviolet (UV), or high-energy irradiation, the active site acquisition would spontaneously start. In practice, for more frequent initiation, and in order to have a more efficient free-radical polymerization small quantities of compounds called initiators are added to monomer or oligomer solutions. Initiators, weak organic molecules, decompose thermally or by irradiation to produce free radicals. Since the initiation of the chain and acceleration of polymerization rate comes after addition of initiators but the molecules are changed chemically in the course of polymerization, initiators are not grouped with catalysts. Usually initiators can be peroxides, azo compounds, and organometallic reagents. Benzoyl peroxide (Figure A.2), azobisisobutyronitrile (AIBN), and di-butylperoxide are the most commonly used free-radical initiators. .
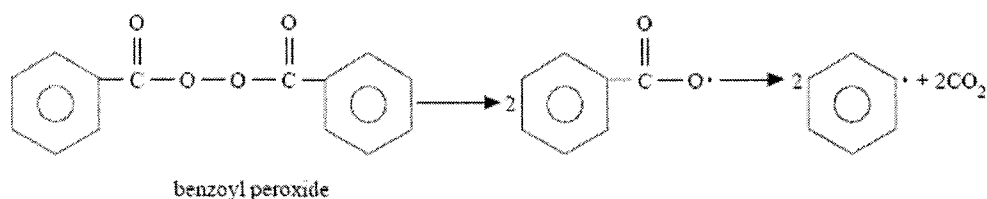
benzoyl peroxide

Figure A.2 Benzoyl peroxide molecule breaking into two free-radicals [5]

Similar to other controlled chemical reactions carried out for industry production, there are important parameters to be considered that will determine the results of free-radical polymerization. For example, the temperature range to be used for the polymerization and the reactivity of the radicals formed will

decide the selection of initiators. There are certain promoters and accelerators, such as amine group derivatives like N,N-dimethyl-p-toluidine, whose presence along with the nature of the monomer affects the rate of decomposition of initiators.

Being robust to the presence of moisture, free radical is very sensitive to the presence of oxygen since free radicals are retarded due to the reaction with oxygen to form peroxides or hydroperoxides. For monomers such as methylmethacrylate that are subject to such inhibition, an oxygen-free environment such as nitrogen purge system[3] is used.

Initiation:

$$I \rightarrow I^{\cdot} \quad a.$$

$$I^{\cdot} + M \rightarrow I\text{-}M^{\cdot} \quad b.$$
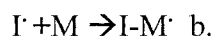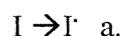
Figure A.3 Initiation step, free-radical polymerization

The initiation of polymerization takes place in two consecutive steps. The first step is the formation of radicals according to the processes which is illustrated in Figure A.3.a. The second step is the addition of the initiator radical to the monomer molecule mixture (Figure A.3.b)

As mentioned above, initiation can have different sources:

Thermal initiation: Thermal decomposition of azo- and peroxy-type molecules causes initiation

Photoinitiation: The molecules are subject to decay upon irradiation with UV or visible light that originates polymerization

---

[3] Appendix B.4

A.2.1.2. Propagation

Propagation is a stage in radical polymerization in which other monomers are added to the initiated monomer described above in a rapid sequence. The process is a succession of the addition of a free radical to the double bond of a monomer along with the regeneration of another radical. Thus, constantly, the active site is relocated at the end of the growing polymer chain and once in the sequence the propagation of the growing chain radical is stopped by chain termination or transfer. (Figure A.4)

Propagation:

$$I\text{-}M^{\cdot} + n M \rightarrow I\text{-}M_n\text{-}M^{\cdot}$$
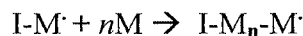
Figure A.4 Propagation step, free-radical polymerization

A.2.1.3. Termination

Once the growth activity of a polymer chain radical is ended due to reaction of the molecule with another free radical in the system, the termination of the chain will result. Sometimes, the reaction of the polymer radical with initiator radicals would cause termination as well which is unproductive and can be easily avoided by designing the system to preserve a low rate for initiation. There are two types of termination reactions that are mostly emphasized in polymer production resources: Combination or coupling and disproportionation. In the first process, combination of two growing polymer chains in a reaction will result in the production of a single molecule and termination of the polymerization (Figure A.5.a). In disproportionation, a hydrogen atom is transferred from one polymer radical to another resulting in two polymers from the two reacting polymer chain radicals (Figure A.5.b). Depending on the nature of the reacting monomer and the temperature, either of the mentioned termination mechanisms would dominate. Having high reaction temperatures, since chemical bonds are harder to break in disproportionation, this kind would be more expected whereas combination of

111

growing polymer radicals would be the main cause of termination at low temperatures.

Termination:

$$2 \text{ I-M}_n\text{-M}^{\cdot} \rightarrow \text{I-M}_n\text{-M-M-M}_n\text{-I} \qquad \text{a.}$$

$$2 \text{ I-M}_n\text{-M}^{\cdot} \rightarrow \text{I-M}_n\text{-M'} + \text{I-M}_n\text{-M''} \qquad \text{b.}$$
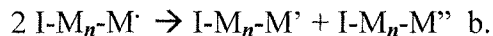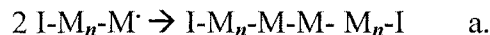
Figure A.5 Termination step, free-radical polymerization

A.2.1.4. Chain Transfer

Chain transfer involves the process of a growing polymer chain being deactivated or terminated by transferring its growth activity to a previously inactive species which could be a monomer, polymer, solvent molecule, or other molecules intentionally or accidentally brought into the reaction blend. The new radical might initiate the growth of another polymer chain if the reactivity this newborn is comparable to that of the propagating chain radical and if not, the overall reaction rate is retarded. Occasionally, the new molecule is unreactive toward the monomer and the reaction could totally be repressed. It is important to express that transfer reactions will not originate any creation or destruction of radicals meaning that at any moment, the number of growing radicals is constant throughout the mixture. Nevertheless, transfer reactions result in the decrease of the average polymer chain length or branching of polymer chain.

A.2.2. Ionic and Coordination Polymerization

The second type of polymerization is ionic polymerization which can be categorized as cationic, anionic, or coordination polymerization depending on the nature of the reactive center. Counterions in ionic polymerization or coordination complex (ion mixture) in coordination polymerization originate the polymer molecule growth. Chain carriers or reactive centers, usually organic ions or charged organic groups, assist the ionic polymerizations. Cationic polymerization

112

involves a growing chain end with a positive charge or carbonium ion whereas anionic polymerization is based on a growing chain with an end that carries a negative charge or carbanions. In coordination polymerization, it is theorized that the formation of a coordination compound between the catalyst, monomer, and growing chain is carrying out the process. Transfer of an ion or an electron to or from the monomer usually initiates the ionic polymerization and the polarity would determine the expansion of polymerization process.

A.2.3. Cationic Polymerization

Cationic catalysts are usually monomers with electron-donating group which form stable positive charges and initiate the polymerization. Boron trifluoride (BF_3) or $AlCl_3$, respectively a Lewis acid and a Friedel–Crafts catalyst, in the presence of a cocatalyst, source of proton like water, can initiate cationic polymerization. Addition of a proton to the monomer and formation of a carbonium ion and its association with the counterion would cause the initiation. Propagation is successive addition of monomer molecules to the carbonium ion at the growing chain end and termination, in this type of polymerization, is a relocation process resulting in the production of a polymer with an unsaturated terminal unit and changing the original complex to a monomer, polymer or solvent molecule. Polymerization rates, with this mechanism, are usually fast at low temperatures. If the intimate association between the cation and the counterion is too strong, propagation by means of monomer insertion will not occur. This would definitely make the solvent selection a delicate task.

A.2.4. Anionic Polymerization

Mixtures of monomers containing electron-withdrawing groups such as styrene, methacrylates and acrylates, can typically favour anionic polymerization. Anionic polymerization initiator can be a compound providing strong nucleophile,

113

compounds. A nucleophile is a reagent that forms a chemical bond to its reaction partner, electrophile, by donating both bonding electrons. In this type of polymerization, initiation starts with the addition of the initiator to the double bond of the monomer. Propagation occurs when monomer molecules are consecutively filled in by anionic attack of the carbanion. Having a low temperature environment would generally guarantee that no chain transfer or branching result. Introduction of oxygen, carbon dioxide, methanol, water, or any other molecule that is capable of reacting with the active chain ends can cause termination. In anionic polymerization as well as free-radical polymerization, the resulting polymer molecule contains the initiator or parts of it as an attachment to the nongrowing chain end. On the other hand, in cationic polymerization the catalyst causes both initiation and propagation, but is regenerated at the termination step.

Again to emphasize, starting with pure reagents and the polymerization reactor purged of all oxygen and traces of water, it is always possible to avoid the termination step. The result is the production of polymer molecules that might be even active, living polymers, after all the monomer molecules are consumed and by adding fresh monomer, polymerization can resume.

A.2.5. Coordination Polymerization

In some mixtures, coordination polymerization occurs as monomers with side groups, unevenly likely to be attracted to form double bonds, produce polymers in which the side groups have a special spatial arrangement in molecule structure. That means that the alliance of initiating ion and counterion causes a favoured placement of asymmetric substituted monomers.

114

A.2.6. Step-Growth Polymerization

Step-growth polymerization is a sequence of reactions in which any two species, monomers or oligomers, can react at any time, leading to a larger molecule and the monomer or oligomer chains always maintain their reactivity and continue to react together to form longer chains during the polymerization. The stepwise reaction occurs between pairs of chemically reactive or functional groups on the reacting molecules. Sometimes, if the molecules in the environment have a functionality number more that two, the molecules can cross-link as well. This mechanism usually involves multifunctional monomer molecules that may cause intermolecular reaction between growing chains, no mater what size, and result in very long chains.

Two main categories of step-growth polymerizations have been proposed: polycondensation and polyaddition. The polymerization mechanism in which a small molecule is eliminated at each step is polycondensation and polyaddition happens is when monomers react without the elimination of a small molecule. The structural unit in step-growth polymers, In contrast to addition polymers, is not equal to the chemical structure of the starting monomer or oligomer.

Step-growth polymerizations generally involve one or more types of monomers with at least two reactive (functional) groups. When only one type of monomer is involved, also known as A-B step-growth polymerization, the functional groups on the monomer is not the same and intramolecular reactions occur between these sites.

A.2.7. Ring-Opening Polymerization

Ring-opening polymerization involves essentially an initial ring-opening of the cyclic monomer followed by polyaddition. Ring-opening polymerization is, to some extent, similar to both condensation and addition polymerization mechanism, but in contrast to condensation polymerization, no small molecule is

115

split off in ring-opening polymerization and unlike olefin addition polymerization, the ring-opening polymerization is not initiated from the loss of unsaturation.

Many polymers have been manufactured using the ring-opening of cyclic organic compounds, including epoxides such as ethylene and propylene oxides, cycloolefins, and siloxane. The resulting polymers are normally linear and their structural units usually have the same composition as the monomer. These polymers are, generally, used in coatings, fibers, elastomers, adhesives, and thermoplastics- and thermoset-based composite systems.

A.2.8. Supramolecular Polymerization

This relatively new class of polymers, supramolecular polymers, are structurally shaped of monomeric repeating units and, unlike conventional macromolecular species, are held together with directional and reversible, noncovalent, secondary interactions. (Fig.6)

(a) (b)
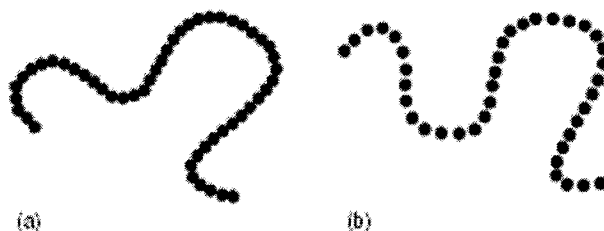
Fig.6

Figure A.6 Schematic representation of (a) a covalent polymer and (b) a supramolecular polymer [6]

Two main factors decide the polymer properties in supramolecular bonding: the directionality and strength of the bonding. The bonding can be hydrogen bonding, metal coordination, and p–p interactions. To form a linear supramolecular polymer structure, the molecules in the environment should have strong and highly directional interactions as a reversible alternative for the covalent bond. Since hydrogen bonds between neutral organic molecules are not strong enough, comparing to noncovalent interactions, the supramolecular bond is

116

either multiple hydrogen bonds or hydrogen bonds supported by additional forces like excluded volume interactions.

A.3. Photopolymerization

Photopolymerization or light-induced polymerization, producing long chain polymers as a result of exposure to light, can be used for efficient and fast curing of polymers. Generally, a free-radical or cationic polymerization mechanism is started after introduction of the photoinitiator (PI) along with mixture exposure to irradiation. Nowadays, there is a complete source of photoinitiators for every polymer which by trimming and optimizing the mixture contents, one can polymerize the monomeric solutions in seconds. Usually, Electron Beam (EB) and Ultraviolet (UV) wavelengths are used as photopolymerization light sources but it is often easier and less expensive to produce photoinitiators and equipment for UV-curing compared to EB technology. (Table.A.1)

Radiation	Wavelength, μm	Frequency, Hz
Infrared	$1\sim 10^2$	$10^{15}\sim 10^{12}$
Ultraviolet	$10^2\sim 1$	$10^{17}\sim 10^{15}$
Microwave	$10^3\sim 10^5$	$10^{12}\sim 10^{10}$
Electron beam	$10^{-7}\sim 10^{-4}$	$10^{21}\sim 10^{18}$

Table A.1 Frequency and Wavelength of Various Types of Electromagnetic Radiation [7]

UV/EB photopolymerization can bring other advantages to processing technology for polymers: Low energy consumption, no emission of solvent, ambient temperature operations, and flexibility in production and having tailor-made properties for polymers produced. Although UV and EB radiation have a great deal in common, UV-curing process is the lower-cost option because the equipment is simpler, smaller and considerably less expensive to purchase and operate.

Commercial UV-curable material, usually coating and varnish products, are commonly designed with the processes that result in increase in chain length and presence of more multifunctional monomers. This will guarantee that the material hardens faster and the reaction chain develops in seconds. This characteristic is due to the chemical bonding between component building that generates a highly crosslinked polymer network and is originated from high intensity UV illumination and free-radical photoinitiators. Since free-radical photoinitiators can produce most of the acrylic and epoxy based materials, almost 80% of the market is dominated by these products. In such products, exposure to UV light casues the photoinitiator to split into two free radicals. This process is called photolysis. The free radicals will attack the monomers and oligomers and join those molecules and initiate free-radical polymerization.

On the other hand, cationic materials can also be used as photoinitiators and in some cases, would attain better some characteristics such as flexibility and adhesion to substrates in the final products. It is obvious that due to a different mechanism in cationic polymerization the curing process and types of cationic photoinitiators are dramatically different from the ones that cause free-radical polymerizations.

Regardless of polymerization mechanism, UV-curing technology allows the engineers to have a precise control of the duration and rate at which the initiating species are produced. The essential ingredients UV-polymerization system can be described as:

1. Reactive base oligomer: Usually this part decides the properties of the final product.

2. Monofunctional monomer(s): A critical part that dilutes the mixture and contributes to the mixture's specific viscosity.

3. Multifunctional monomer(s): Both dilutant and corss-link provider.

Commercial UV-curable material, usually coatings, are mostly to be used on substrates ranging from paper and wood to plastics and glass and majority of them are based on acrylate, having acrylic base: ($CH_2=CHCOO^-$) the ion of acrylic acid, chemistry. The range of oligo-acrylates available in the market is usually close to fifty products in each group of mechanical properties i.e. hardness, clarity, elasticity etc.

As mentioned above, electromagnetic radiation, light, can be used for curing of a variety of processes involving functional monomers, oligomers and polymers. For such applications, the ultraviolet spectral range, extending from 200 to 400 nm (Figure A.7), is regularly used and Xenon lamps that provide significant emissions in the 450 to 550 nm range are the most common of all industrial equipments employed. The irradiation energy increases in higher frequencies, low wavelengths, and the design of any UV-curing systems is such that the irradiation is capable of originating certain chemical reactions in a system and the absorbed energy can generate species that are capable of initiating polymerization or cross-linking reactions; i.e. initiating radicals. Occasionally the system only involves a polymerization process, but for most of the efficient UV-curable materials, both polymerization and cross-linking will occur simultaneously. Moreover, as mentioned earlier, monomers and oligomers with the functionality of two form linear polymers, while multifunctional polymers shape cross-linked networks that expand into three dimensions which in most cases, cross-linked material guarantees solvent and heat resistance as well as increased hardness.

A.3.1. Photopolymerization: Basic Theory

A photochemical reaction can occur when a photon of light is absorbed. This rule, known as the Grotthus-Draper Law, can explain both photopolymerization and photodegradation of plastics due to absorption of light by impurities near UV spectrum.

Chemical class/Group	Formula	Structural	Example
Hydroperoxy	ROOH	
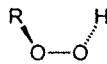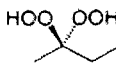
Methyl ethyl ketone peroxide |
| Carbonyl | C=O |
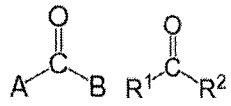
Carbonyl /Ketone |
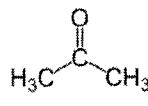
Acetone |
| Aromatic (Aryl) | RC$_6$H$_5$ | |
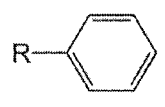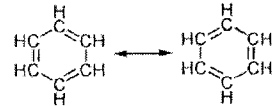
Benzene |

Table A.2 Photosensitive chemical groups

Chemicals containing C = O, ROOH and aromatic groups, containing ring of unsaturated bonds, are known as light (UV) adsorbing material. When a molecule absorbs light, a specific wavelength is transmitted or reflected in another certain wavelength. A chromophore is a part of a molecule where the energy difference between two different molecular orbitals falls within the range of the spectrum. The energy state diagram shown in Figure A.8 is for a ketone, a common chromophore in polymers, exposed to light source. When the molecule is hit by photon, many processes can occur at the molecular scale. Photochemical reactions such as reemission of a photon as fluorescence or phosphorescence, radiationless decay to the ground state and crossing from one excited state to another are some of the expected behaviours of every light-exposed molecular system.
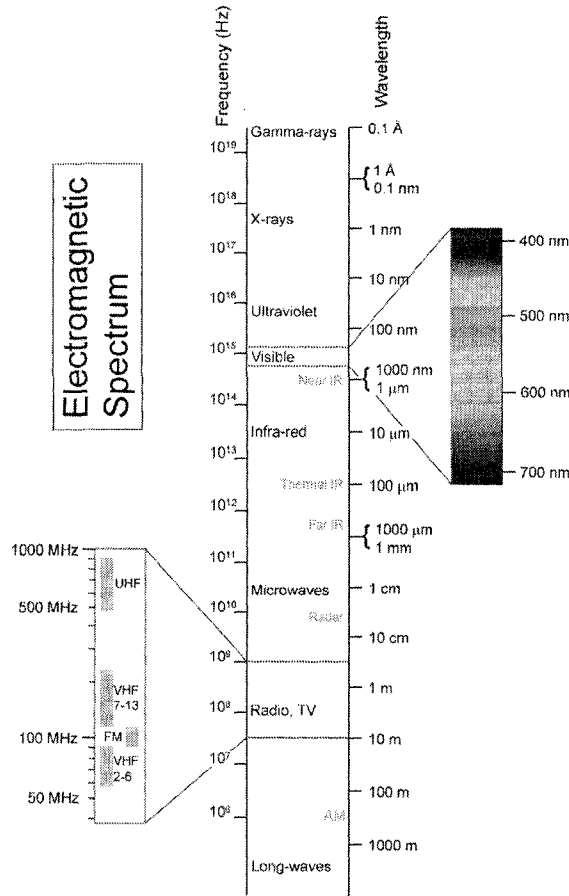
Figure A.7 Courtesy of Louis E. Keiner, Coastal Carolina University
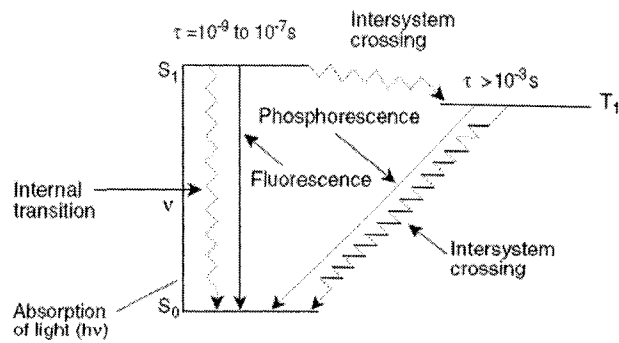
Figure A.8 Process of activation of a UV radical initiator [8]

At the zero state, before light exposure, almost all organic compounds have electron spins in pairs. Following photon absorption, the energy state will change i.e. S0 to a higher energy S1, S2 ... Sn. This will result in production of triplet species (T1, T2 ... Tn) with two unpaired spins. A triplet state is always lower in energy than the corresponding singlet state. The summary of this process is depicted in the diagram below:
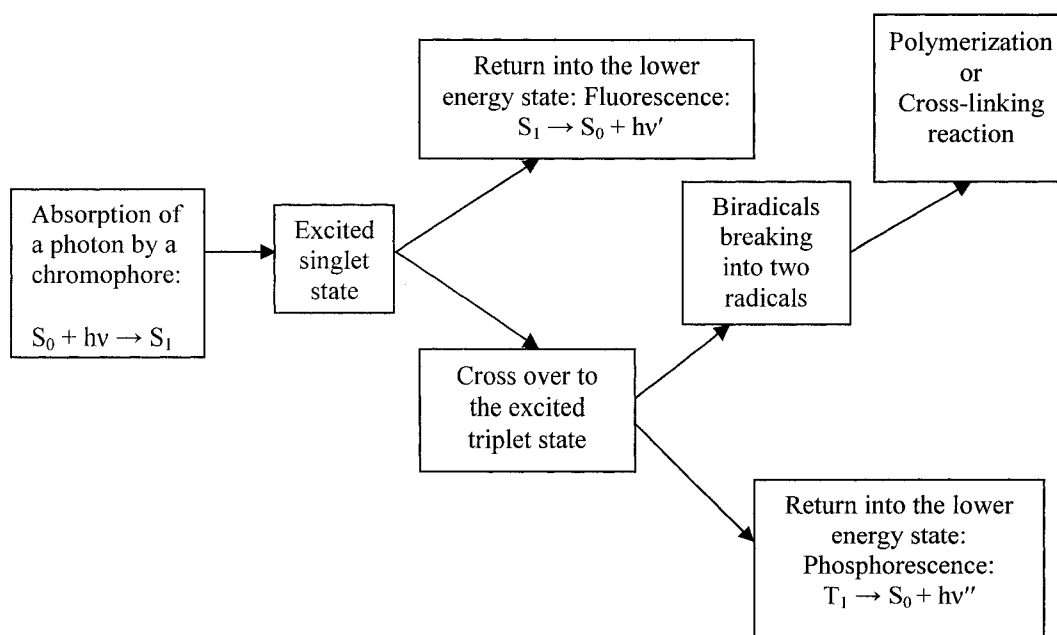
Fig.3

Figure A.9 Photoinitiators' chemical reaction upon light exposure (h: Planck's constant)

Depending on the chemical nature of the material involved the mixture exposed to light source and the wavelength of the light, ultraviolet, visible and laser, polymerization of functional monomers, cross-linking or degradation of the polymers could be the result. Degradation is more likely when oxygen is available in the environment.

A.3.2. Photoinitiators vs. Photosensitizers

Photoinitiators and photosensitizers are both used in the UV curing of polymers. Both of these compounds can absorb light and generate reactive molecules. The difference between these two compounds is that, when exposed to a light source, a photoinitiator will generate initiator species, free radicals or ions that will start polymerization or cross-linking whereas a photosensitizer will energize some molecules that will activate other molecules that produce reactive species such as photoinitiators. Photosensitizers are usually used to extend the range of spectral sensitivity of photopolymerization compounds as these molecules can adsorb light at longer wavelengths and transfers energy to a photoinitiator. It is important to pick specific photoinitiators and photosensitizers for every compound since the molecules' reactions to light is different among monomers and oligomers and the chromophore of every molecule are sensitive to a specific bandwidth. Moreover, in commercial scale, photoinitiators may be added to the polymer or grafted onto the polymer chains.

A.3.3. Free-radical Photoinitiators

Free-radical photopolymerization is the most common among all types of light-induced polymerization. For instance, monomers and oligomers such as acrylate, methacrylate and vinyl ether systems are all polymerized using free radical initiation. As mentioned above, the photoinitiator is excited and forms into the singlet state once it adsorbs a photon and then a radical forms when the molecular system has triplet state. Radicals can form by either Type I or Type II *Norrish[9]* reactions.

The type I photoinitiator reaction can be described in the following steps: First, triplet state decomposes into a couple of radicals by homolytic decomposition. Homolysis or homolytic fission is chemical bond dissociation of a neutral molecule generating two free radicals. Next, the direct formation of

123

radicals that can initiate polmerization, meaning that the absorbed radiation causes bond fissure between a carbonyl group and an neighbouring carbon.
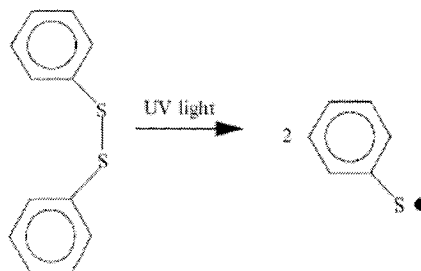
Figure A.10 Free-radical photoinitiator, diphenyldisulfide, undergoing light exposure and breaks into two radicals [10]

Type II reactions on the other hand, start with triplet states of ketones that have a hydogen that reacts with suitable hydrogen-donating compounds by hydrogen abstraction. Then by a homolytic breakage of the R-H bond or via a transitional charge transfer complex followed by proton transfer, the radical couple is produced.

The excited initiator species are usually active for up to 10 seconds. Depending on the amount of energy absorbed and being sensitive enough to the irradiation wavelength, the excited molecules can decompose to the original state again and give away energy by emission of light and heat or produce a reactive intermediary, free radical or ion, and react with another free radicals or monomers to start the polymerization.

A.3.3.1. Type I Photoinitiators

This type of photosensitive material experiences a homolytic cleavage reaction following irradiation and supplies two radicals. Genrally, an aromatic carbonyl is sitting in place of the chromophore in type I photoinitiators. Majority of the Type I products are carrying benzoyl radical as initiating element. Specifically, benzoin ether derivatives, benzil ketals, hydroxylalkylphenones, α-aminoketones and

acylphosphine oxides are the light adsorbent aromatic carbonyl in such substances. (Figures A.10 and A.11)

A.3.3.2. Type II Photoinitiators

Type II initiators, aromatic ketones such as benzophenone, substituted benzophenones, benzils, fluorenone, xanthone and thioxantones, are usually combined with amine synergists. Amines are organic compounds as well as a type of functional group that nitrogen is the key atom in their structure. Life processes depend on amino acids that all contain an amine group. There are essentially two classes of amine synergists; aliphatic and aromatic. (Table A.3)

Aliphatic amines that can be subgrouped into three types of primary, secondary and tertiary amine are transparent to light down to the wavelength of 260 nm so UV light with wavelength above that number would start a much more efficient polymerization process when it is used for benzophenone that contains aliphatic amine. On the other, aromatic amines that have a nitrogen atom connected to an aromatic ring, also known as anilines, adsorb a large amount of the UV light energy around 300 nm so when using thioxanthones, due the strong absorption at wavelengths greater than 340 nm, aromatic amines are the best choice. (Fig A.12)

Primary amine	Secondary amine	Tertiary amine
one of three hydrogen atoms in ammonia(NH3) is replaced by an organic substituent	two organic substituents bound to N together with one H	three hydrogen atoms are replaced by organic substituents
R^1—N($\cdots$H)(H)	R^1—N($\cdots$H)(R^2)	R^1—N($\cdots$$R^3$)($R^2$)

Table A.3 Aliphatic amines

125

R1= H3CS,

R2= CH3,CH2Ph,C2H5

R3= N(CH3)3

Aminoalkylphenones

R1= H or alkyl

R2= H or substituted alkyl

Benzoin ethers

R1 = H, iso-C3H7, HOCH2CH2O

R2= CH3, OCH3, OC2H5

R3= H, Ph, OH

Acetophenones

R = C6H5 OCH3

Acylphosphines
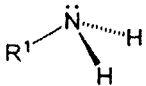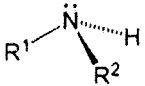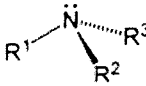
Benzoyloximes
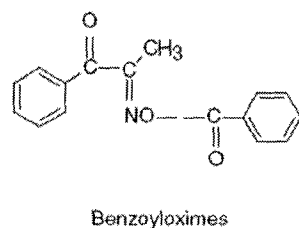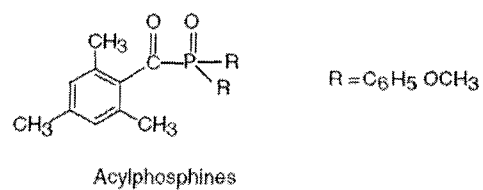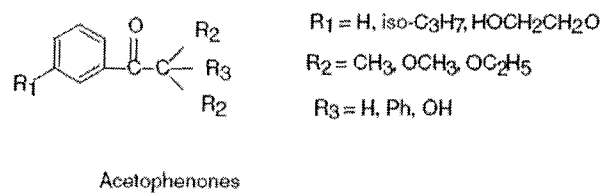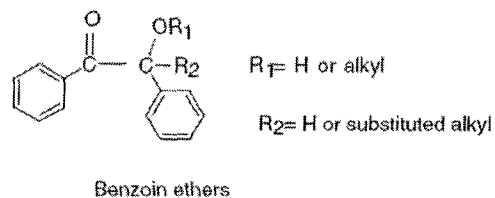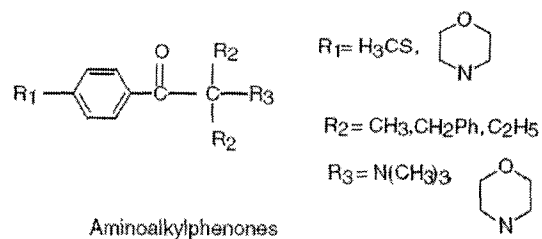
Figure A.11 Type I free-radical photoinitiators

126
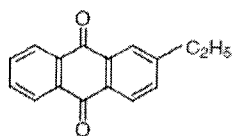
Anthrachinones
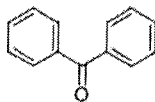
Benzophenone
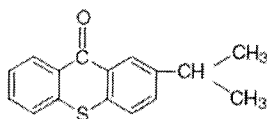
2-Isopropyl thioxanthone(ITX)

Figure A.12 Type II free-radical photoinitiators

A.3.4. Cationic and Anionic Photoinitiators

When exposed to UV or visible radiation, cationic photoinitiators release an acidic catalyst that influences the environment and originates the polymerization process. (Figures A.13 and A.14)

Anionic photoinitiators, once containing tertiary amine salts of ketocarboxylic, are now based on peptide chemistry and are usually used in nano and micro lithography.
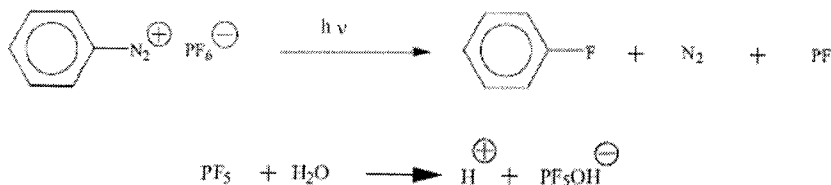
Figure A.13 Cationic Photoinitiator, aryldiazonium, decomposing under light exposure [8]

127

A.3.5. Oxygen Inhibition

As mentioned in free-radical polymerization section, the presence of oxygen reduces the efficiency of polymerization by extinguishing the triplet states of photoinitiators in addition to scavenging the initiator generated radicals as well as growing macroradicals. Generally using an inert gaseous environment is the solution to avoid such dysfunction in photopolymerization. Commercially a nitrogen blanket purge or a film cover, polyester, is employed as protection. Addition of a tertiary amine into the system is another solution, but in many cases it results in discolouration or photo-yellowing of the cured polymer in long term.

A.3.6. Nitrogen purge

As motioned above, curing of free radical polymer mixtures is prone to inhibition by oxygen and curing under a nitrogen blanket can prevent that effect. Since the running costs of nitrogen, depending on the level of purity and the amount of residual oxygen in the mixture, can be high, it is necessary to first find out if the nitrogen purge is the best solution for the process. As discussed earlier, though the amines might not inhibit the oxygen activity completely, sometimes adding amine group polymers can solve the problem. Second parameter is the scale and the design of the nitrogen purging system. Commercial approaches to this problem suggest nitrogen blanketing is better than nitrogen purging. Normally, it is not necessary to use nitrogen inerting, which adds to operating expenses. The custom designed nitrogen purge used for this project is discussed in the chapter on nanofabrication and in the appendix.
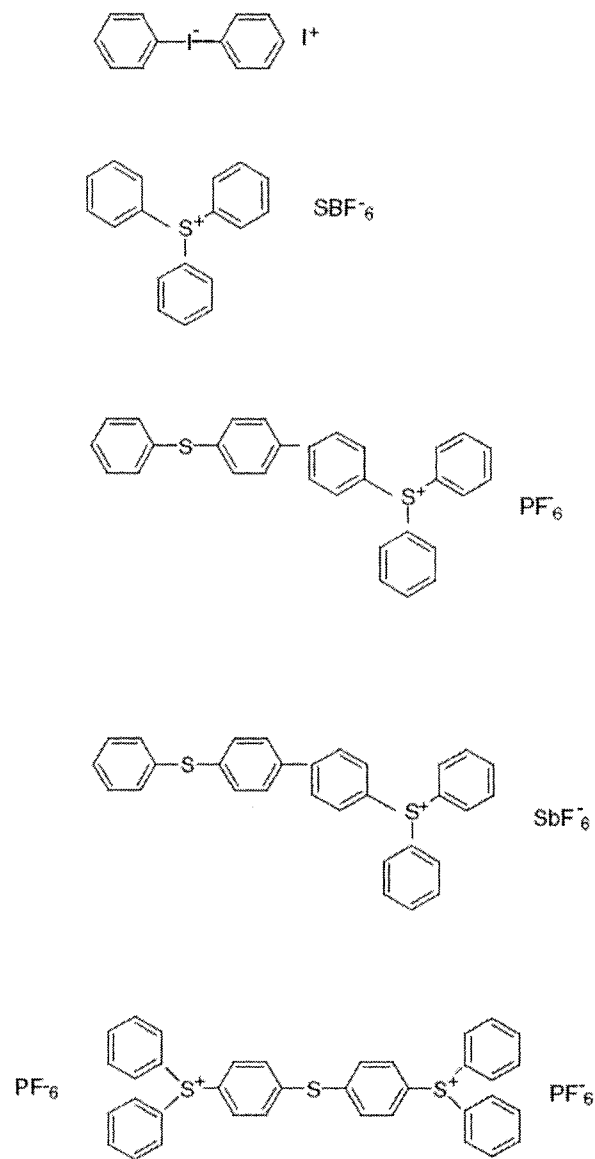
Figure A.14 Cationic photoinitiators [8]

A.3.7. UV Hybrid Polymerization

In some applications there is a need for photoinitiators for originating polymerization by two different mechanisms. One example of such situation, also known as UV hybrid curing, is the photodecomposition of arylsulphonium salts

resulting in both radicals and Bronsted acids[4]. The radicals can initiate the polymerization of acrylates and the acid, cationic initiator, can initiate the polymerization of vinyl ethers. The product has an interpenetrating polymer network containing both the acrylate and vinyl ether components. Hybrid curing systems increase the rate of cure and improve the polymer solvent resistance. In comparison to free radical polymerization, better adhesion to substrates and lower oxygen sensitivity are the advantages of hybrid polymerization methods.

A.3.8. Photocross-linking of Polymers

Ultraviolet or visible light induced cross-linking, also known as photocross-linking, is widely used in printed circuits for electronic equipment, printing inks and coatings for optical fiber. Moreover, most of the photoresists used in micro- and nanolithography technology, such as SU-8, are only useful due to the photocross-linkability of the polymers involved. In industry, photocross-linking is used for any size of molecules; monomers, oligomers and highmolecular-weight polymers.

Depending on chemical structure and molecular weight as well as the ordering of the polymer segments, photocross-linkability can differ from one mixture to another. Photocross-linkable polymers can be synthesized using the following two methods:

1. Addition of photosensitizers that absorb photons and induce formation of free radicals. For example, addition of benzophenone to polymers followed by absorption of ultraviolet radiation results in production of radical capable of cross-linking by combination reactions.

2. Insertion of organic material into the polymer structure and enabling light-initiated cross-linking polymerization. Copolymers of vinyl esters and fluorinated monomers that can be cross-linked by ultraviolet radiation.

---

[4] Hydrogen ion releasing molecule

Association of vinyl ester UV-cross-linkable copolymers parallel to benzophenone, photosensitizer, can produce a well structured cross-linked polymer network.

A.4. Plasticizers

"Plasticizers are the materials which, when added to a polymer, cause an increase in the flexibility and workability, brought about by a decrease in the glass-transition temperature, Tg, of the polymer" [11]. The plasticizing effect can be achieved by either chemical modification of the polymer or monomers, internal plasticizing, by the addition of a plasticizing agent, external plasticizing. Due to the latitude in formulation and lower overall cost, external plasticizers are more common in industry. A more practical approach to the application of plasticizers is described in the PMMA mixtures section.

A.5. Shrinkage of Polymer Material

Shrinkage is a normal result of any polymerization process especially when polymer internetworking and cross-linking are more likely. Simply, shrinkage is due to double bond polymerization which depends on the functionality, density and molecular weight of the monomers involved in the compound. Obviously, shrinkage is a disadvantage and not only because of decreasing the precision in polymer replication, but because of reducing the adhesion of the polymer to the substrate.

The main reason for shrinkage is the substitution of weak long distance intermolecular Van der Waals bonds by strong and short covalent bonds between the carbon atoms of different monomer units.

Shrinkage can be measured using density. A comprehensive method to describe shrinkage is to use the following formula:

Shrinkage (%) = 100 x (dM − dp)/dp - [1]

where, dp is density of the cured polymer and dM is the density of the monomer.

A.6. Polymethylmethacrylate (PMMA)

Polymethylmethacrylate (PMMA) or poly (methyl 2-methylpropanoate) is the polymerized form of methyl methacrylate $(C_5O_2H_8)_n$. Commonly known as a transparent thermoplastic, it is sold under the trademarks such as Plexiglas, Limacryl, R-Cast, Perspex, Plazcryl, Acrylex, Acrylite, Acrylplast, Altuglas, Polycast and Lucite. Developed in 1928 in different laboratories, PMMA was only commercialized in 1932 by Rohm and Haas Company. PMMA has a moderate T_g of 105°C that makes this polymer a good choice for extrusion and other thermal-shaping manufacturing methods. Moreover, because PMMA is a clear, colourless, hard but brittle and fairly rigid material, it can be drilled, carved, machined or sawn. [12]

Due to outstanding optical clarity and resistance to degradation by UV light, it has been marketed and used as a replacement for glass. Also, its total internal reflection characteristics provide room for a wide light beam to be transmitted through PMMA long fibers even when bent. (Index of refraction for commercial PMMA is 1.49 @ 589 nm)

This material has applications in consumer goods packaging, dental cements/resins, hard contact lenses and bone reconstruction. In addition it can be used as a prototyping material instead of metal for experimental mechanical setups. In microfabrication, it is widely used as a photoresist with sensitivity to both UV and electron beam.

There are many ways for preparing the polymerization mixture for acrylic products. Many used a combination of PMMA and other monomers and

132

oligomers and some might be more interested in making pure PMMA structure. Usually, the polymerization is of the free-radical initiated type and peroxides or UV initiators are added to MMA monomer to cure or polymerize the solution. Shrinkage and brittleness are common results of such MMA polymerization procedure.[12, 13]

A.6.1. Polymerization of Methylmethacrylate

PMMA can be polymerized through different polymerization mechanisms. Usually in the industrial applications free radical polymerization of MMA is the first choice which is a chain polymerization across the double bond of the monomer.

Since oxygen terminates free radical polymerizations by reacting with the radicals, the free radical polymerization of MMA can only work well when most of the oxygen in the environment is removed. Radicals can be generated with radiation, heat, or chemical agents usually in conjunction with radiation or heat.

A.6.1.1. Heat Initiated Polymerization of MMA

The heat initiated polymerization of MMA can be achieved by adding peroxides such as benzoyl peroxide or thermally libel molecules of 2,2'-azobisisobutyronitrile (AIBN) (Figure A.15).Free radicals are the result of thermal initiators subjected to heat exposure. Free radicals initiate the chain polymerization and produce high molecular weight PMMA. [3, 12]

benzoyl peroxide

AIBN ("VAZO 64")
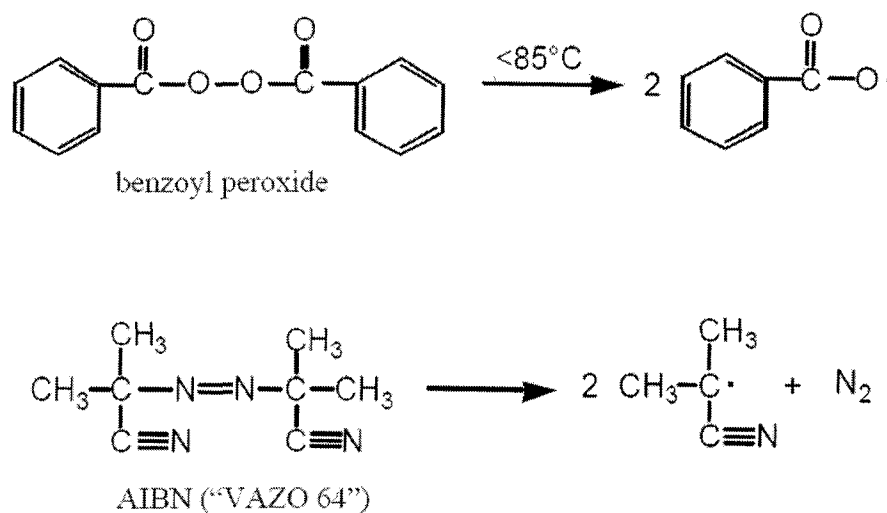
Figure A.15 Benzoyl peroxide and AIBN molecules breaking into free radicals [14]

A.6.1.2. Radiation Initiated Polymerization of MMA

Visible light, UV or δ-radiation can initiate the polymerization of MMA. While photoinitiation of MMA, using UV or visible light, can be achieved without sensitizers and free radical mechanism would make the PMMA structure to come together. Upon exposure to light, a radical is formed or a hydrogen atom is removed from the monomer or solvent and delivers the initiative components to the solution. MMA photoinitiation is usually a good method for bulk polymerization and generally for rapidly producing polymeric materials with well defined characteristics and particularly for cross-linked polymer networks. Since the reactivity of the acrylate double bond plays an important role in polymerization and polymer network structure, acrylic and methacrylic molecules, such as PMMA are mostly used in photo-curable mixtures.

134

A.6.2. Inhibitors

Inhibitors are usually added to the monomeric compounds or monomer solutions to avoid polymerization in the container. It is mostly uses as a safety and inventory technique for shelf storage of chemicals. A critical step in designing a polymeric solution is to find the inhibition system used in the monomer sources and plan for reducing or eliminating this effect before attempting to initiate the polymerization. Inhibitors can stop every radical, and the polymerization completely stops until the inhibitor is consumed. There are other polymerization restraining techniques such as the use of retarders, which are less effective, and only stop a portion of the radicals. [3, 12, 13]

Oxygen is powerful inhibitor that reacts with radicals to from relatively unreactive peroxy radicals, which reacts with itself or other propagating radicals and forms inactive products. Hence, usually, the polymerization of acrylates and methacrylates happens nitrogen gas purge (repeated several times. Other inhibitors can be removed prior to polymerization by careful distillation over a nitrogen atmosphere. Figure A.16 illustrates the different inhibitors and their mechanisms.

<u>Phenols</u>: (Inhibitor/Retarder)
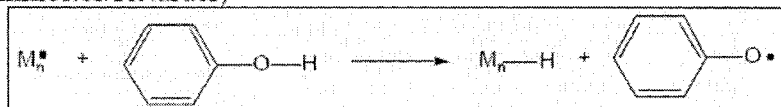
•Electron donating groups at the ortho positions can make this a better inhibitor.

•Phenol can be synergistic with oxygen as an inhibitor.
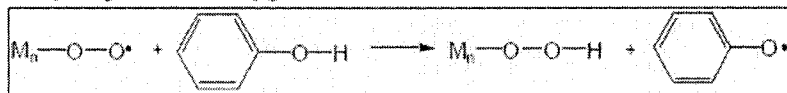
•Oxidants such as $FeCl_3$ and $CuCl_2$ are strong inhibitors.
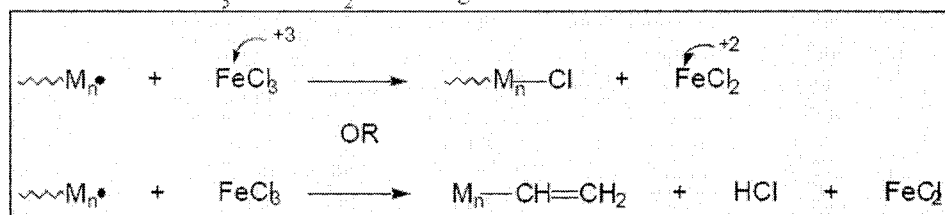
Figure A.16 Different inhibitors and their mechanisms [14]

Appendix B. Mechanical parts

The appendix B.1 describes the micro-replication clamps used for the replication of microfluidic and microoptical features. The next section, B.2, introduces the design and characteristics of the polymer punches for fabrication of the fluidic reservoir opening. The design, material selection and parts for experimental setup stand and the nitrogen purge system are introduced in sections B.3 and B.4 respectively.

B.1. Polymer replication clamps

Replication clamps are mechanical parts that can hold a master, i.e., Si wafer with micro and nano scale features, inside an area called a replication reservoir. In a three step process, pouring polymer compound into the replication reservoir, covering the surface of the master wafer and curing the polymer in a vacuum oven (PDMS) or UV light (PSiA), features are negatively replicated on the surface of the cured polymer.
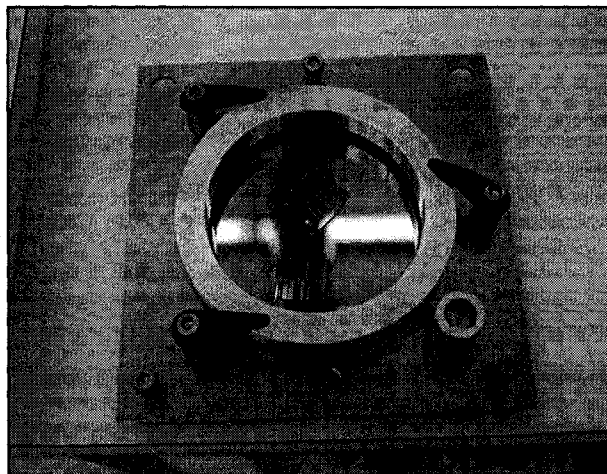
Figure B.1 Nanofab PDMS curingclamp

Although University of Alberta Nanofab has a clamp for PDMS curing, Figure B.1, due to its simple design, it cannot be used for replication of features fabricated on the edged of the wafer. Moreover, the sealing system only works for very viscous fluids like PDMS pre-polymer. In order to solve the problems with this clamp and add more useful features, two clamps were designed and manufactured for this project. The first prototype was constructed from aluminum and then later the system was refined and constructed from stainless steel.

B.1.1. Aluminum Clamp

This clamp was designed to be used for PVA and PDMS replication processes. Due to chemical compatibility with most of the polymer compounds, aluminum was chosen as the body material. The clamp's major parts are two machined aluminum parts that are connected via 8 screws (size 4) with a silicone rubber O-ring, dash number 250, sandwiched in between.

The bottom part contains a circular stage for holding the master wafer and a groove around this stage that is filled with polymer. When the polymer is cured, the part that is replicated from the groove around the wafer stage acts as walls around the negative replicas of the features. This walled, bowl-like, replica can be easily filled with another polymer compound and manufacture the positive replica, clone, of the wafer features. Figures B.2 and B.3 show the schematic design and dimensions of the aluminum clamp parts and Figures B.4 and B.5 illustrate the clamp with Si wafer on the wafer stage.
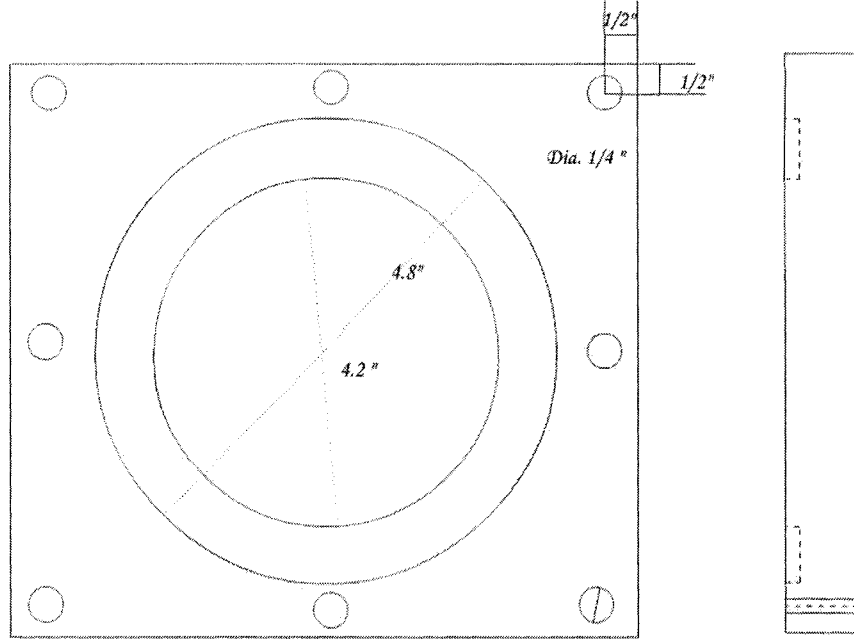
Figure B.2 Aluminum clamp bottom part
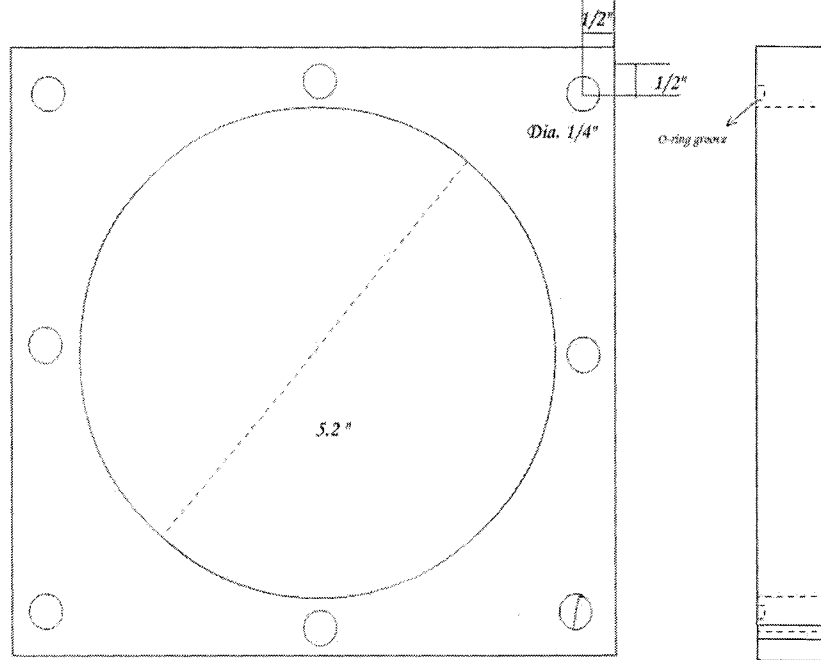
Figure B.3 Aluminum clamp top part
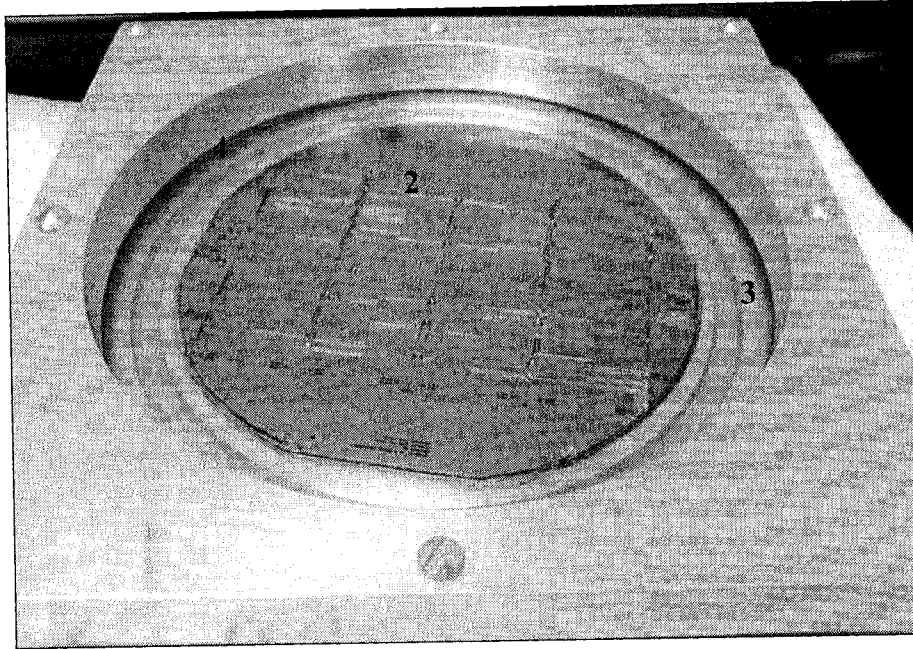
Legend: 1-Top (clamping) part, 2-Si wafer with V-grooves etched on the surface
3-Bottom layer with groove, 4-O-ring sealed edge

Figure B.4 Aluminum clamp with Si wafer on the wafer stage
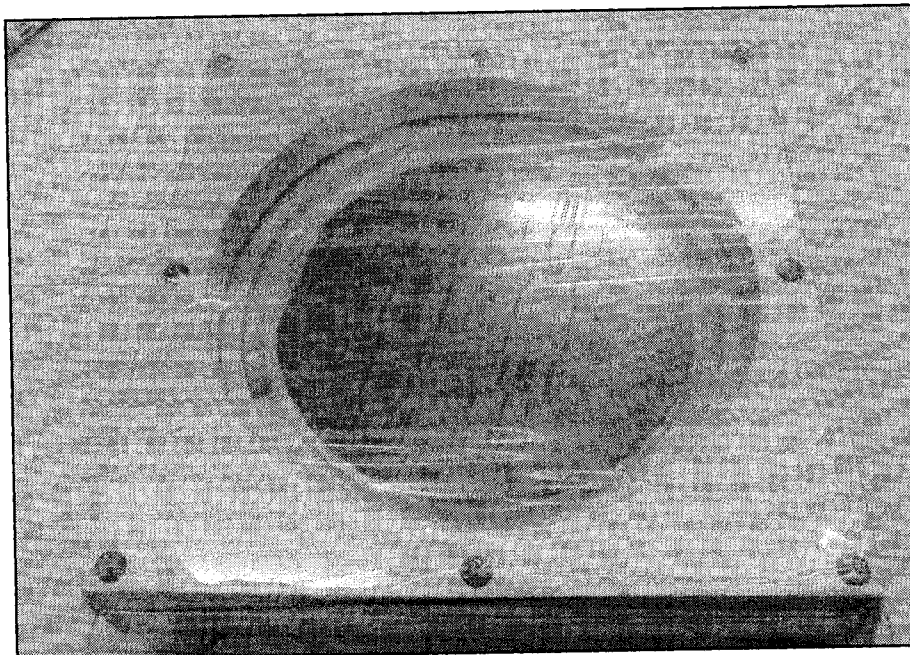
**Figure B.5 Post-silanization blue tape covering of the aluminum clamp with Si
wafer on the wafer stage**

B.1.2. Stainless Steel Clamp:

Stainless steel clamp was designed and manufactured, with a few improvement compared the aluminum clamp, to serve as replication apparatus for PSiA, PDMS, PUA and PVA replicas. Since the aluminum clamp was not chemically compatible to the UV-curing agents used to cure some of the PUAs, stainless steel was chosen for the major body parts of this instrument. In addition, the replication are, reservoir, consists of a stage to hold the master wafer 5 mm above the flat bottom of the clamp and is sealed using perfluoroelastomer O-rind, dash # 437. Making the reservoir area wider results in thicker wall for the replicated polymeric bowl and eases the peel-off of this repluca from the clamp. Figure B.6 depicts a schematic design of the clamp and Figures B.7 and B.8 show the assembly of the parts drawn in Autocad® software.

1-O-ring   4-Si wafer
2-Clamping screw   5-Bottom layer
3-top(clamping) layer   6-Wafer stage
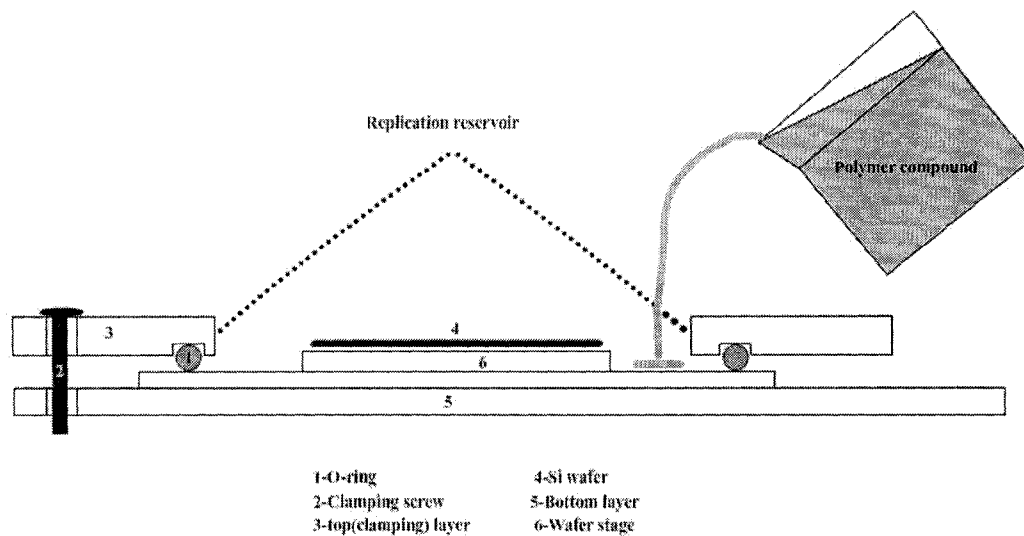
Figure B.6

Six Unbrako Stainless steel screws, UNF 28 - 1/4 x 7/8, connect and clamp the two parts of this clamp.
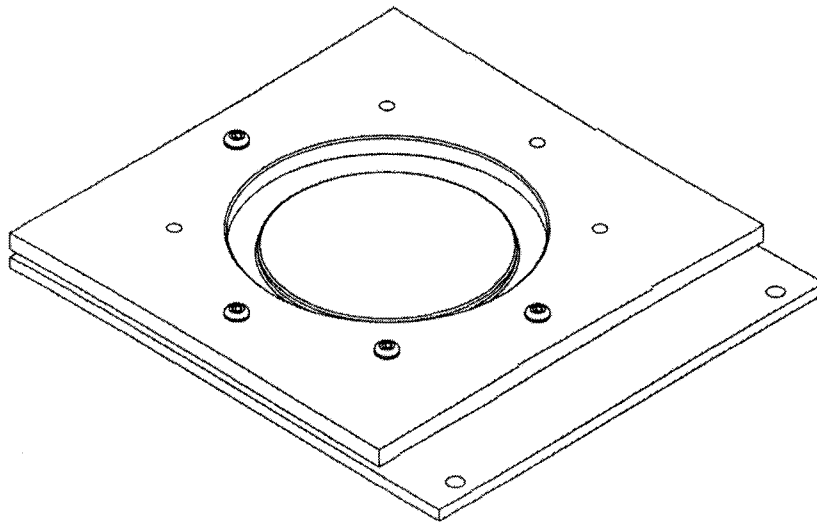
Figure B.7 3D view: Stainless steel clamp
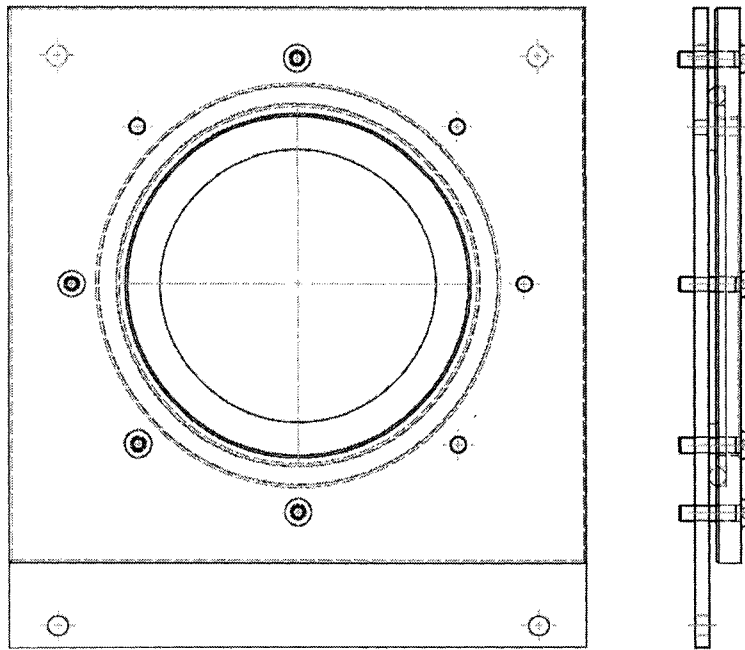
Figure B.8 Top and side view of the stainless steel clamp parts in Autocad®

142
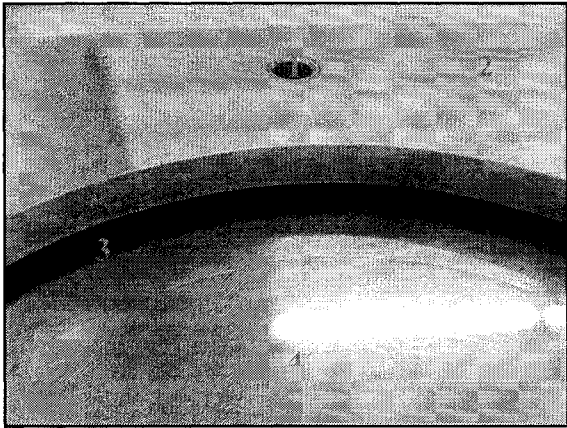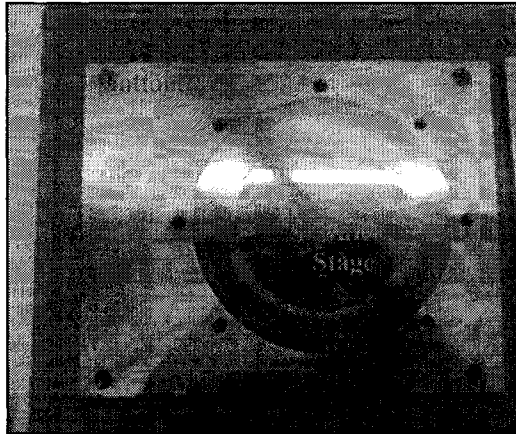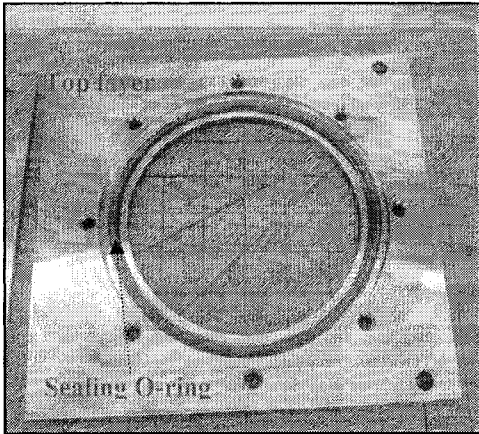
Legend:
1-Clamping screw hole
2-Top(clamping) part
3- Replication reservoir bottom
4-Wafer stage

Figure B.9 Stainless steel clamp parts
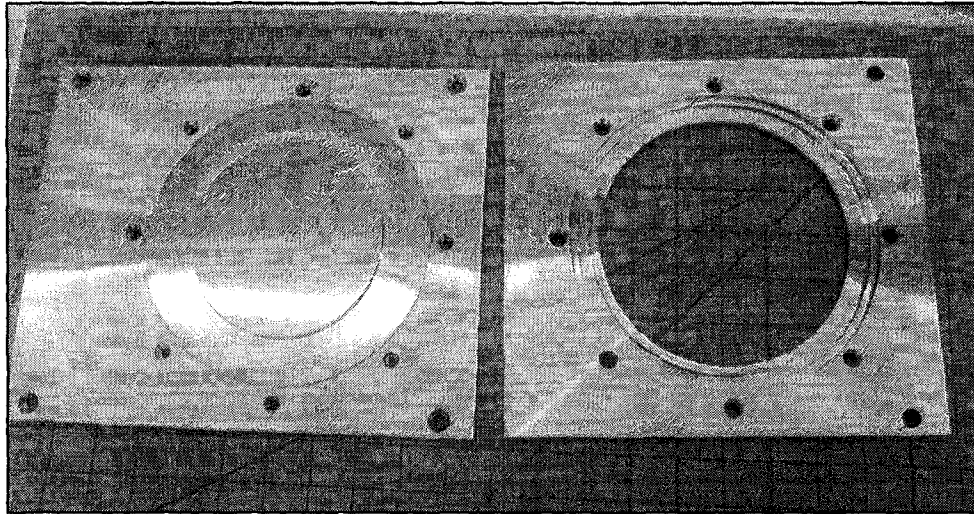
Figure B.10 Stainless steel clamp, Left: bottom part containing wafer stage Right: top part
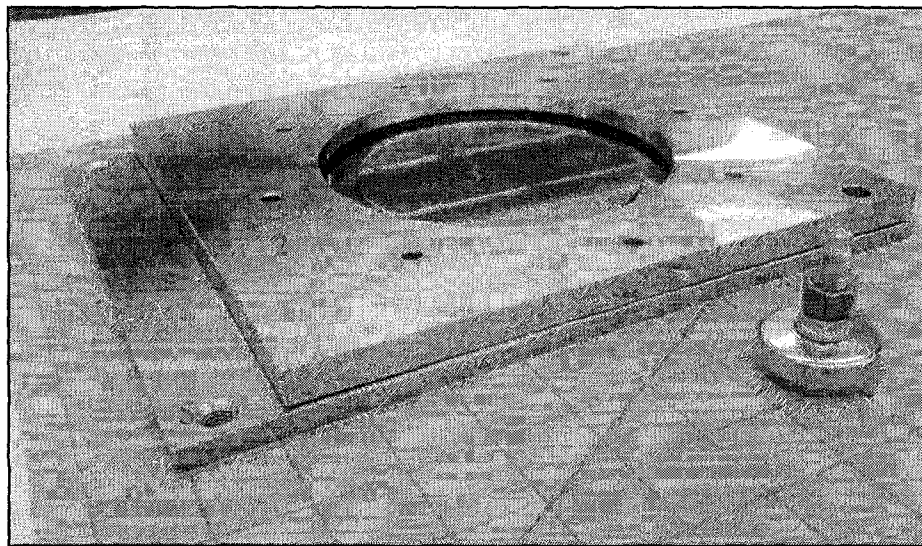
Legend:
1-Bottom part: replication reservoir, wafer stage
2-Top (clamping) layer
3-Wafer stage
4-Clamp adjustable leg
5- Threaded hole for the clamp leg

Figure B.11 Assembled stainless steel clamp

B.2. Polymer Punches

Biochips made of PDMS, PSiA, soft PUA and APFPE can be trimmed and punched easily using a metallic tool. The punches were used to make holes in the polymer layers in order to open the fluidic reservoir opening or tube couplings. Two of the punches were designed for other projects at the Micro-Optical Systems Laboratory. (Figure B.12, C and D)

In the design of all of the four punches, some parameters are similar. All of the punches are made of stainless steel with a punching tip at the end of a hollow small shaft. The hollow shaft will collect and gradually disposes the punched pieces of polymer from the top. The punching tip in the first two designs was of a conical shape and caused insufficient penetration of metal into polymer and left the sample with non-straight cuts.

The cutting/punching edge of the two punches designed for this project, Figure 1, A and B, are straight cylinders with this walls and sharp bottom attached to the conical main part of the punch. The straight part is at lease 4mm which guarantees a punch of such depth in elastomers.

Since the punch tips are very thin-walled, an aluminum punch holder was machined to hold the collection of the punches to prevent damage. (Figure B.13)
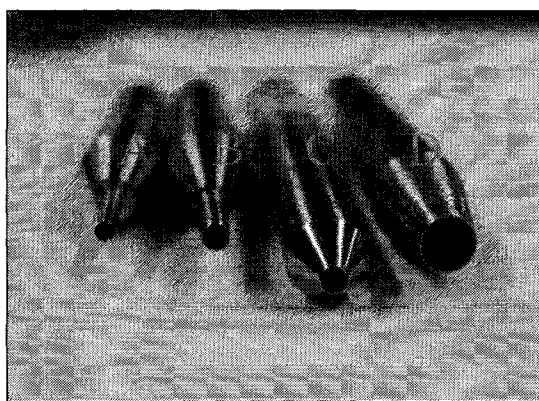
Figure B.12 Polymer punches
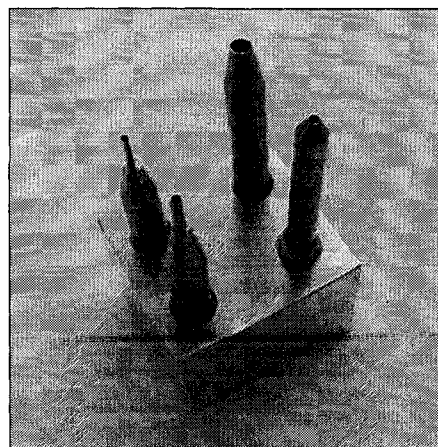
Figure B.13 Punches in the holder

B.3. Experimental Stand

During the experimental phase, all of the biochips were tested by mounting them on a platform that used suction from under the chip to secure their position. In order to hold a variety of sizes of biochips while either shining lasers toward the waveguides or loading the biochip with fluidic samples the biochips required a custom experimental stand that would not interfering with any of these connections. The basic construction of this experimental stand is shown in Figure B.14. The upper layer, where the chips were placed, was made of a 1.5 mm thick sheet of standard grade stainless steel (Figure B.14, A). Small holes were drilled in this stainless steel sheet to provide the suction. The holes in the metallic sheet were connected to various plenums beneath the stainless steel sheet (Figure B.14, B). The plenums were constructed from a 25 mm thick piece of acrylic but only milled to a depth of 18 mm. These two parts were sealed with silicone sheet of 2mm thickness acting as gaskets and six bolts were used to compress this composite assembly together.

The experimental stand was designed to fit different sizes of the rigid biochips; 1.5x2 cm: small Figure B.14, 2), 2x3 cm: medium (Figure B.14, 3), and 2x5 cm: large (Figure B.14, 1), as well as a place to hold flexible polymeric biochips such as PDMS (Figure B.14, 4). Holes of 2mm and 0.75 mm diameter were drilled to into the metal sheet for the rigid and flexible chips, respectively.

These four plenums were connected to the side of the acrylic layer through holes that were drilled and threaded to allow standard tube fitting to be attached. The tube connectors were of barbed fitting design and made of polyethylene or polycarbonate. When fitted into the acrylic threads and the tubes have no leak. Depending on the chip being tested a vacuum pump was connected to the appropriate plenum. Figures Figure B.15 and Figure B.15 are photographs of the experimental stand.
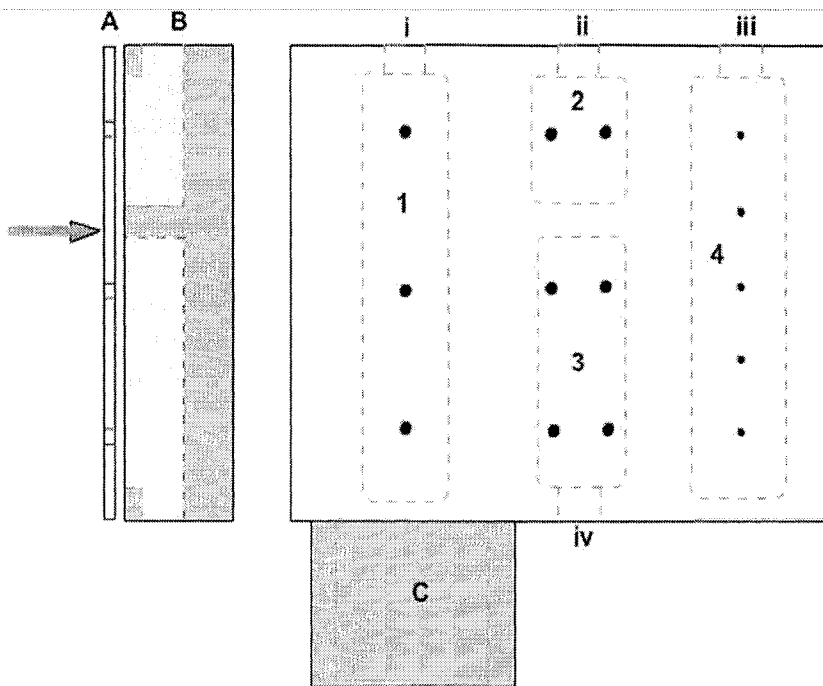
Legend:
i, ii, iii, iv: Vacuum line ports: threaded for tube fitting
1: Stage for long glass biochips
2: Stage for small biochips
3: Stage for medium biochips

4: Stage for long polymeric (flexible) biochips
A: Stainles steel sheet: top part
B: 1" Acrylic bulk with machined vacuum reservoirs
C: 1" Acrylic Stage

Figure B.14 Experimental stand schematic
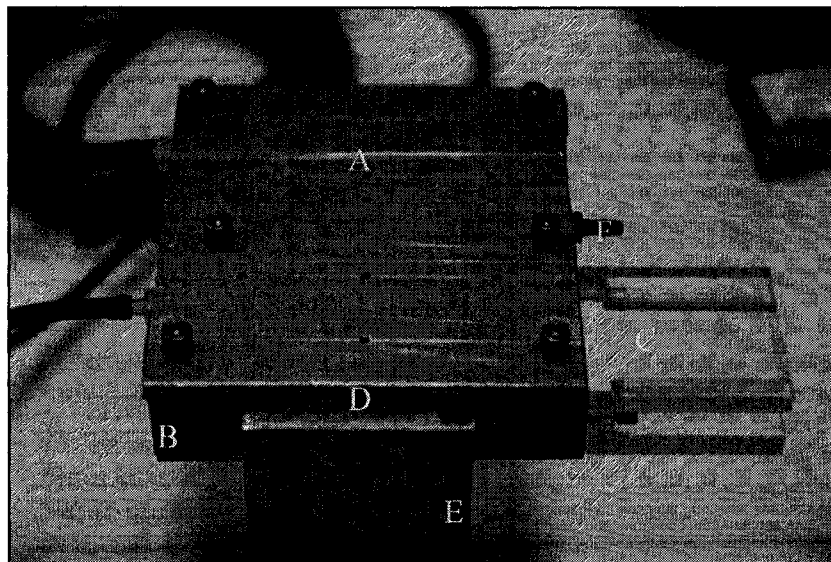
Legend:
A: Stainles steel sheet: top part
B: 1" Acrylic bulk with machined vacuum reservoirs
C: 1" Acrylic Stage

D: Sealing washer sheet
E: Aluminum Stand
F: Barbed Tube Fitting

Figure B.15 Experimental Stand: top

147

Legend:	
A: Stainles steel sheet: top part	E: Aluminum Stand
B: 1" Acrylic bulk with machined vacuum reservoirs	F: Barbed Tube Fitting
D: Sealing washer sheet	G: Vacuum line from pump
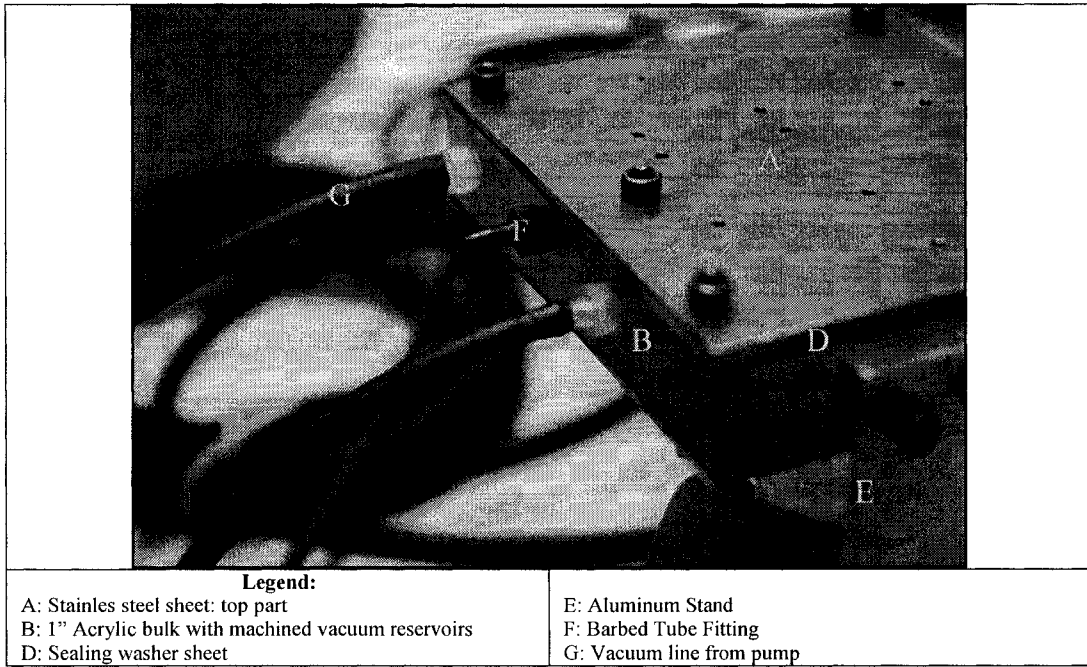
Figure B.16 Experimental Stand: side

B.4. Nitrogen Purge Chamber for Polymer UV-replication

For many UV-curing processes, oxygen prohibition is a must. Usually, a closed environment with nitrogen or argon dominating the gaseous media around the photo-curable solutions is used. A nitrogen purge system is a chamber that can vacuum out all of the air or oxygen carrying gas mixtures and pumps in nitrogen around the samples. In this project, for the purpose of curing PSiA and APFPE samples, a nitrogen purge was designed and manufactured.

The bottom part of this apparatus is stainless steel and the top part is a 3/16" thick quartz discus that is 99% transparent in UV wavelengths. An o-ring is used to seal the top and bottom part and a set of eight stainless steel screws hold these parts together.

Figure B.17 is a schematic view of the purge and tubing to and from the nitrogen purge system. This system is designed to keep a 4 inch round Si wafer on the bottom of the purge chamber. Using a vacuum line, the Si wafer is held down from the bottom and then the UV-curable polymeric solution is poured on top of the wafer. The O-ring and then the quartz disk are adjusted on top of the stainless steel bulk part and all of these parts are bound together using screws. The stainless steel bottom part contains eight threaded holes for the binding screws, one central hole for vacuum wafer holder (connected to the line from 8 to 5 in Figure B.17) in the bottom and three radial holes that are attached to pneumatic tubing from the bottom. The set of three radial holes are respectively attached to a vacuum line for purging (line from 4 to 7), a gauge line for chamber pressure control (point 1) and a composite line that can carry either condensed/filtered air or nitrogen (lines: 9→2→3 / 10→6→3). By opening the valve to vacuum the chamber (point 7) and consequently adding nitrogen (point 9) to the environment, the user can make sure that the chamber is free of oxygen and expose the polymer compound to UV.

A helpful feature designed in the nitrogen purge system, is the adaptor platform for the University of Alberta Nanofab UV mask aligners. The nitrogen purge, which is a stainless steel disk, can be easily put into an aluminum platform that matches the bindings on the mask aligners stage. The adaptor enables the nitrogen purge system sitting in the aluminum platform to be exposed to UV at the same distance that any other mask lithography process is performed. (Figures B.24-27 and B.32)
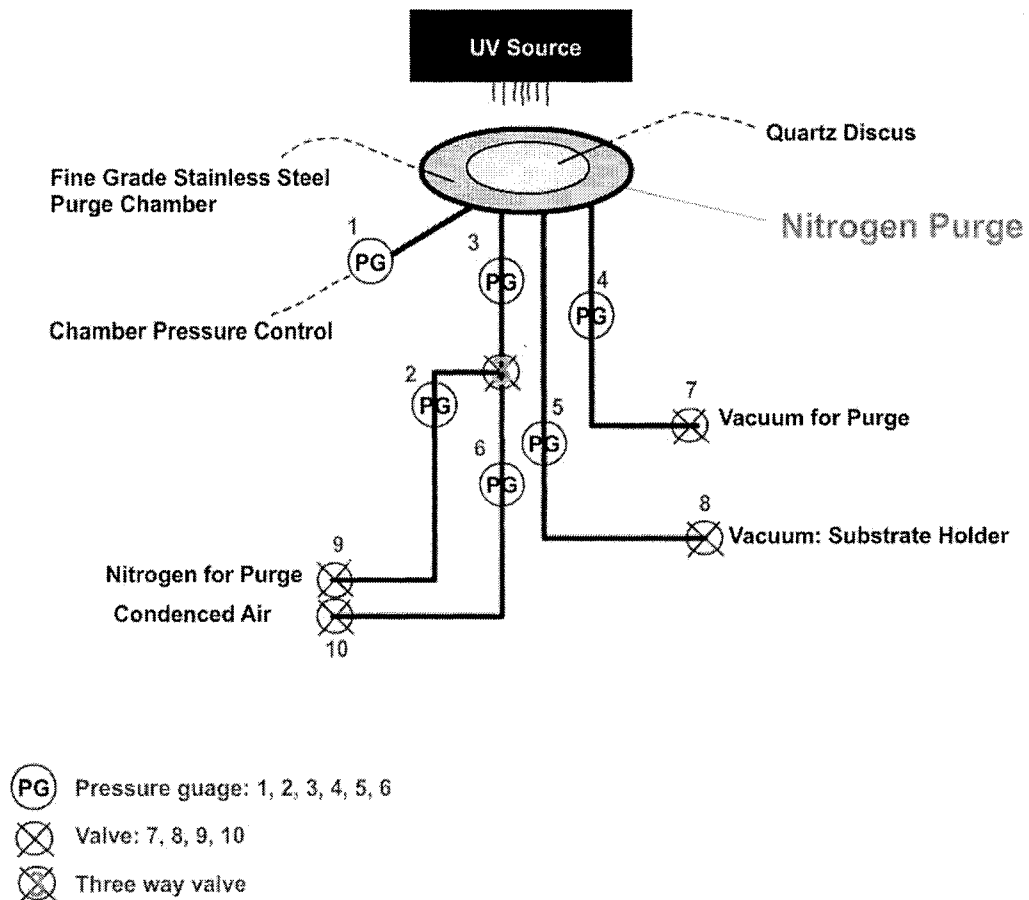
Figure B.17 Nitrogen purge and tubing schematic

Please see Figure B.19 for more information on the system connections

Nitrogen Purge Parts and Materials List list:	Part #	Quantity
Swagelok Valve for Vaccum 1/4"	B-4P4T	4
Pressure Gauge Panel (3 Dials)	PGP-25B-30V/30	1
Pressure Guage Single Dial	PGP-20B-30V/30	1
Quartz Disc 3/16" Ground and Plished Finish, 7" Dia	PQ-2188D-03	1
Male Tube connector, Acetal, 1/4", 1/4" NTP	A4MC4-MG	5
Male Tube connector, Brass, 1/4", 1/4" NTP	W68ML-4-4	4
Polypropylene ball valve Female Elbow, 1/4", 1/4" NTP	PP4VFE4-MG	2
Male Elbow Swivel 90 degrees, 1/4", 10-32 Thrd	W369ML-4-0	4

Table B.1 Nitrogen purge system parts list

In order to achieve good results, it is very important to have a fast an easy to setup system with mimimum leakage in the tubes and connections. Parker 369ML-4-0, push to connect tube fittings Figure B.18), can take a ¼" tube from one end of the elbow and are threaded to 10-32 standard to be attached to the bottom of the purge. Due to the elaborate internal design and the o-ring sitting at the threaded end, these parts can nearly guarantee a good seal in the system and setting up a system with four of these parts barely takes 5 minutes. (Figures B.20, B.28-32)
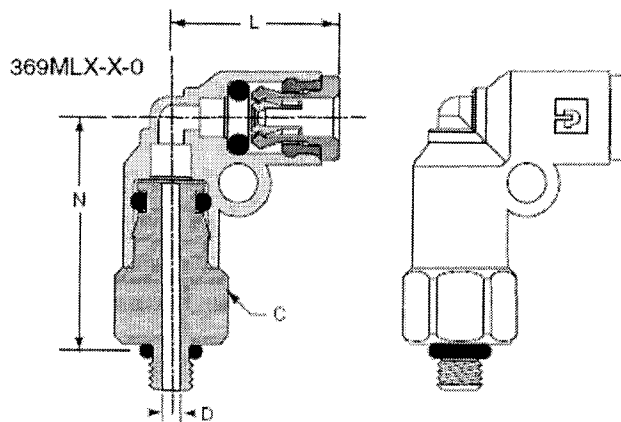
Figure B.18 Schematic: Parker 369ML-4-0
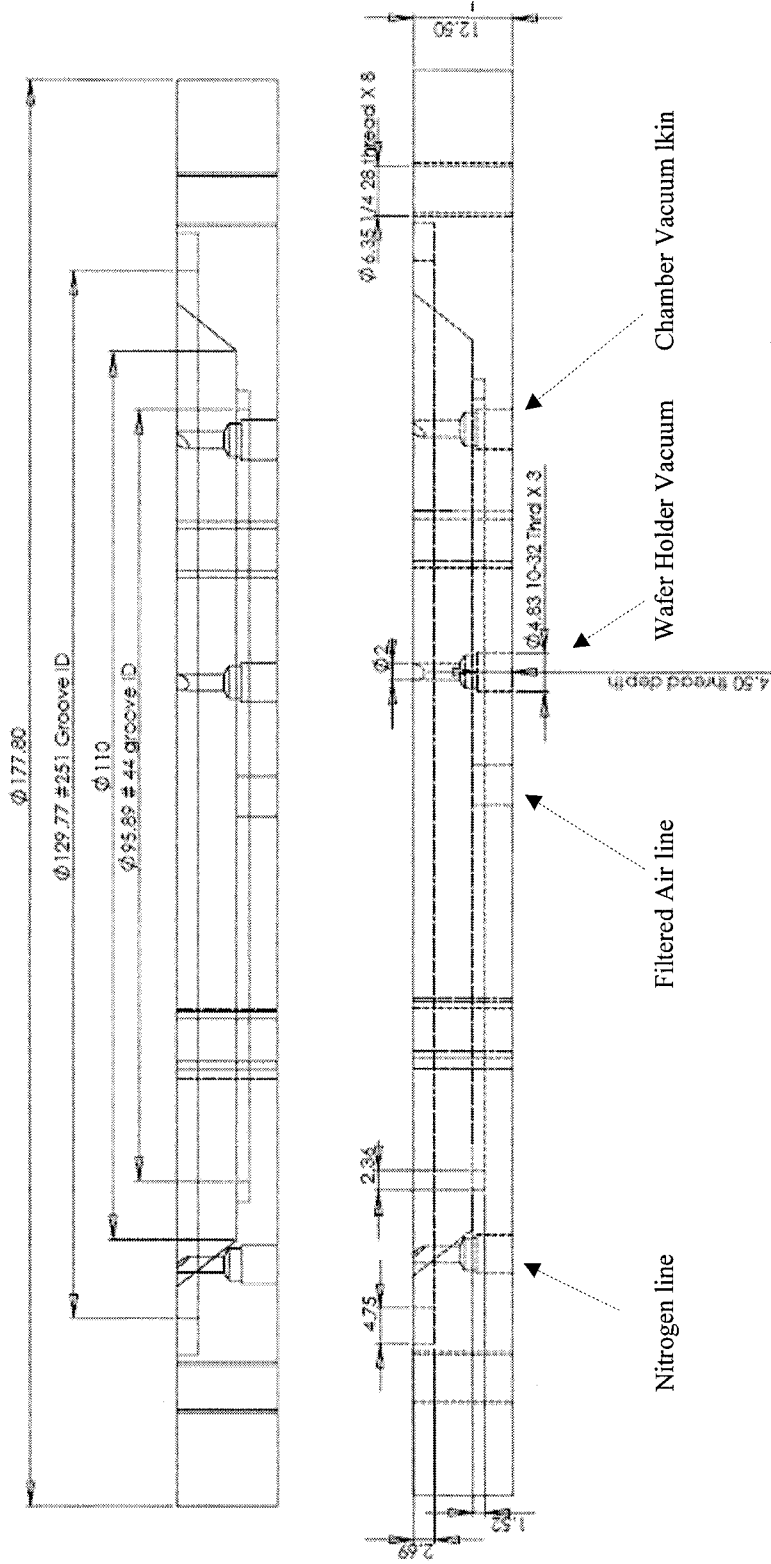
Figure B.19 Nitrogen purge side view (cross section)

152
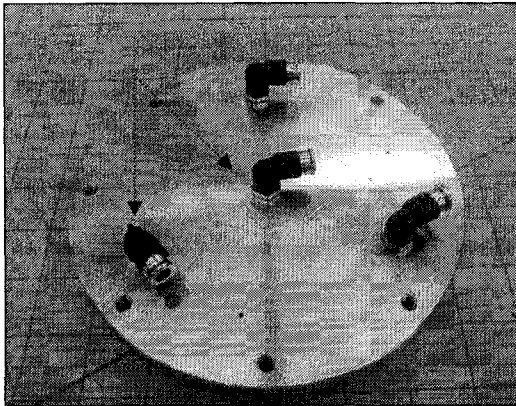
Figure B.20 Bottom of the purge with swivel connectors
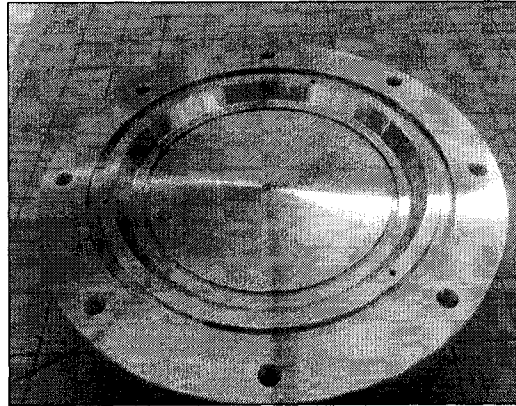
Figure B.21 Top of the purge
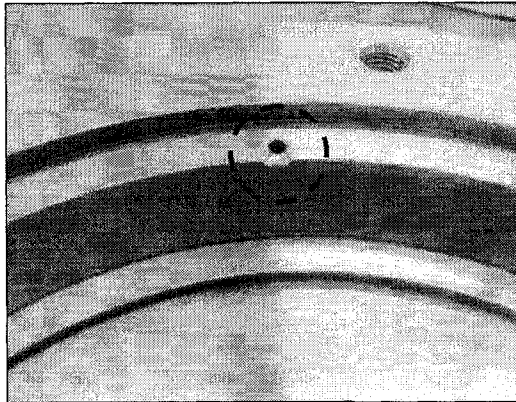
Figure B.22 The radial hole for purge or vacuum
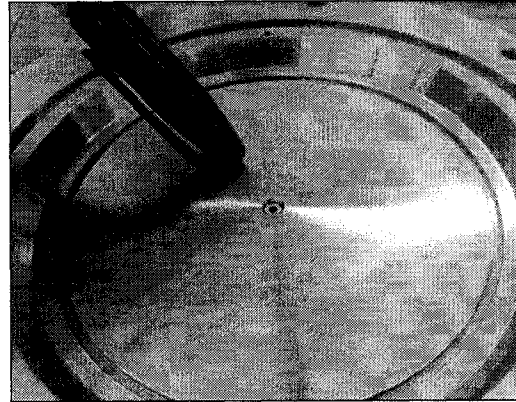
Figure B.23 Substrate holder stage
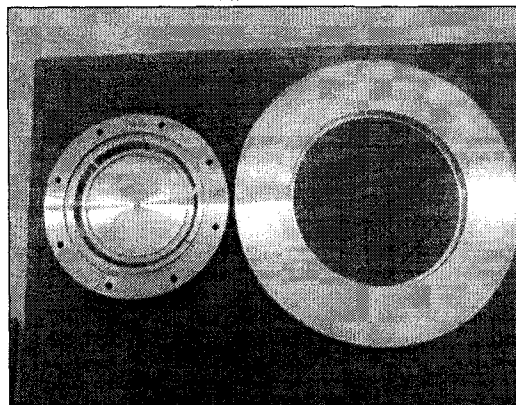
Figure B.24 Left: purge bottom, Right: adaptor platform
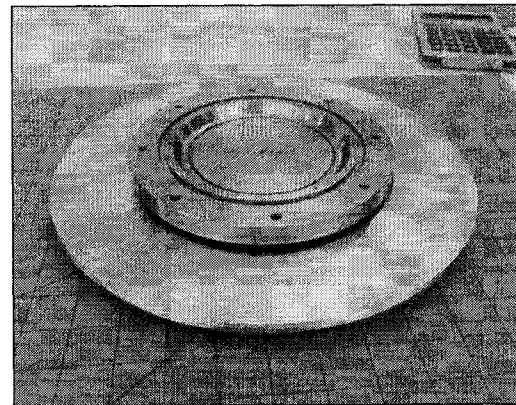
Figure B.25 Step I: put the purge in the middle of the platform

153
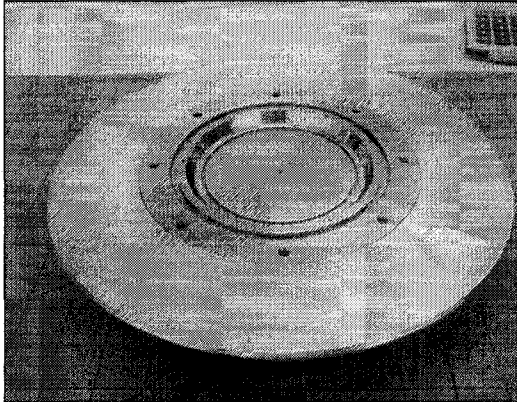
Figure B.26 Step II: slide the platform up-ward

Figure B.27 Step III: put the platform on the UV-laigner stage
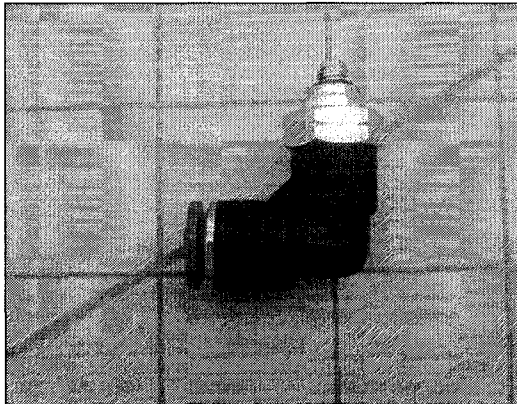
Figure B.28 Parker 369ML-4-0
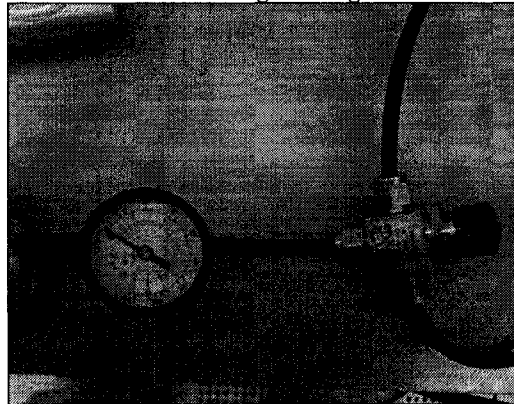
Figure B.29 3-way T-valve for Nitrogen/Air
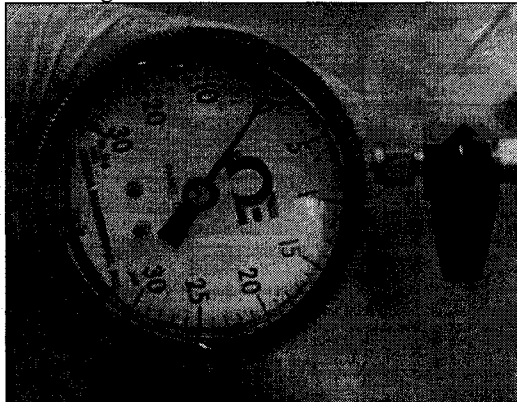
Figure B.30 Purge Vacuum line valve and gauge
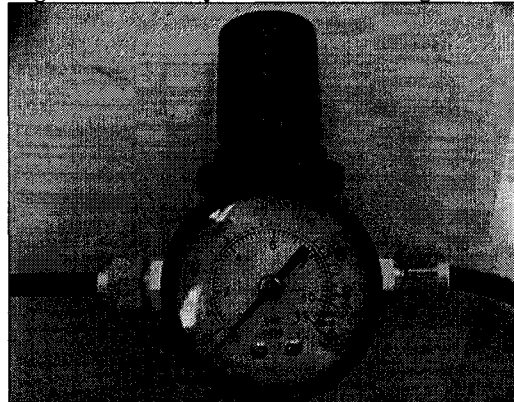
Figure B.31 Nitrogen line initial valve and pressure gauge
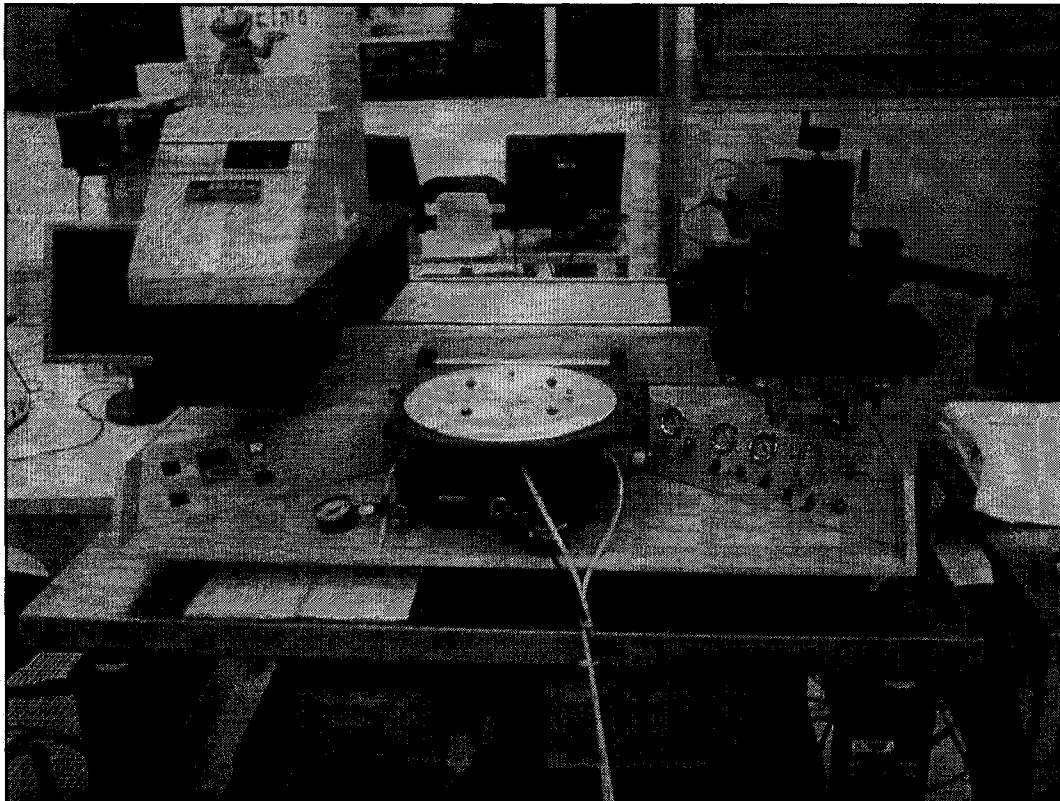
Figure B.32 Nitrogen Purge on the UV-aligner machine before exposure
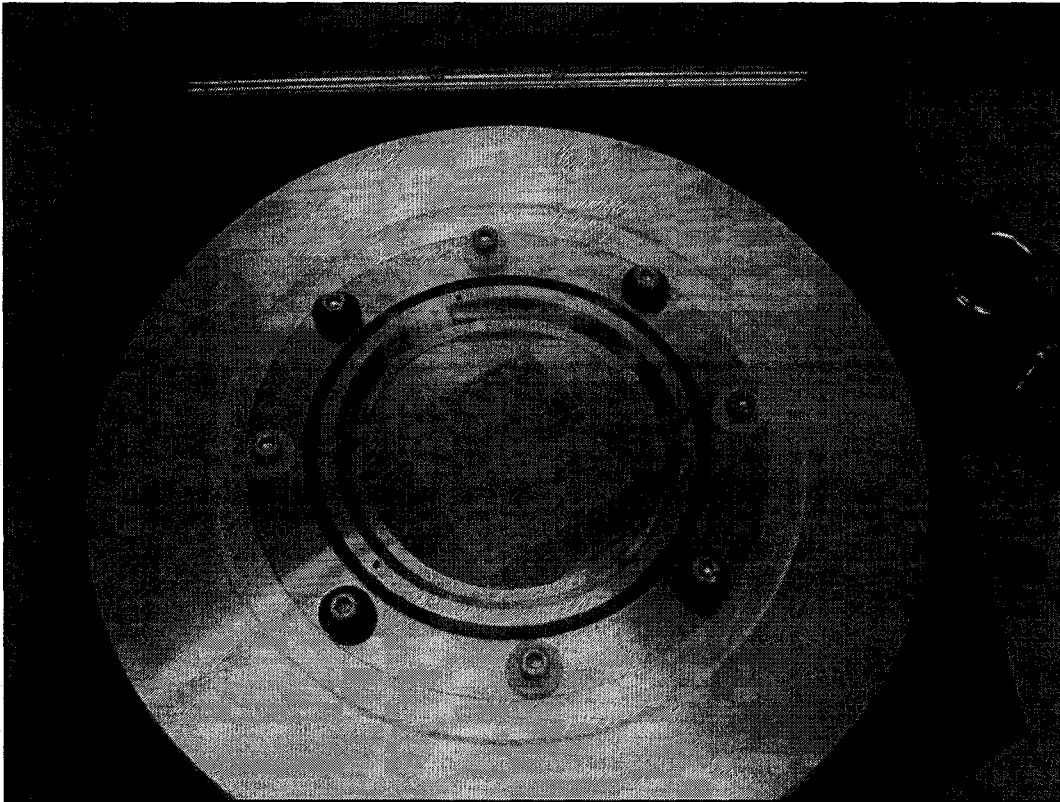
Figure B.33 DRIE fabricated Si master sealed in the nitrogen purge on the UV-aligner

Appendix C. Fabrication Processes

Appendix C.1 is a brief description of silicon crystal identification process as a background to the processes discussed in the main body of the thesis. A summary of DRIE process basics and the advantages two popular procedures are described in C.2

C.1. Silicon crystal planes identification

In order to determine the crystal planes in silicon wafers with an etch barrier mask such as silicon oxide or silicon nitride, by designing a wagon wheel pattern (Figure C.1) on the sides of the lithography mask and opening the shape of this design in the etch barrier. The silicon wafer is then anisotropically etched for 30 minute in a 30% KOH aqueous bath at $80^{\circ}C$ and the Si crystal planes can be identified by finding the groove from the pattern which resulted in the smoothest edges indicating the best alignment with the crystal planes.
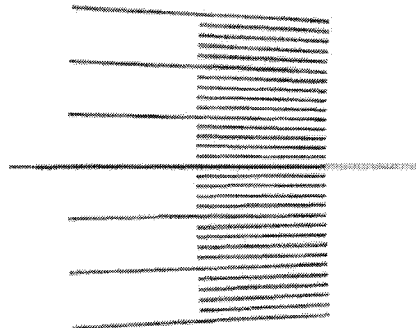
Figure C.1 Wagon wheel pattern for Si crystal identification [15]

The alignment of the mask, straight lines, to the silicon crystal plane is very important to in order to produce features, v-grooves, with no dislocations along the sidewalls. Since dislocations are the source of extra loss in the hollow waveguides. The flat, polished, faces of {100} silicon wafers are machined aligned to {110} plane with +/-0.5 degrees tolerance which in any micron scale

distance can cause roughness of the etched walls. By employing a 10-15 minute pre-etch step using a partial wagon wheel pattern (Figure C.1), written on the sides of the wafer using lithography, and with short spokes every 0.2 degrees and longer spokes every 1 degree the crystal plane orientation can be determined. Having looked at the pre-etch results, one can see one or two (neighbouring) spokes along the crystal plane with no jagged etched walls (Figure C.2).
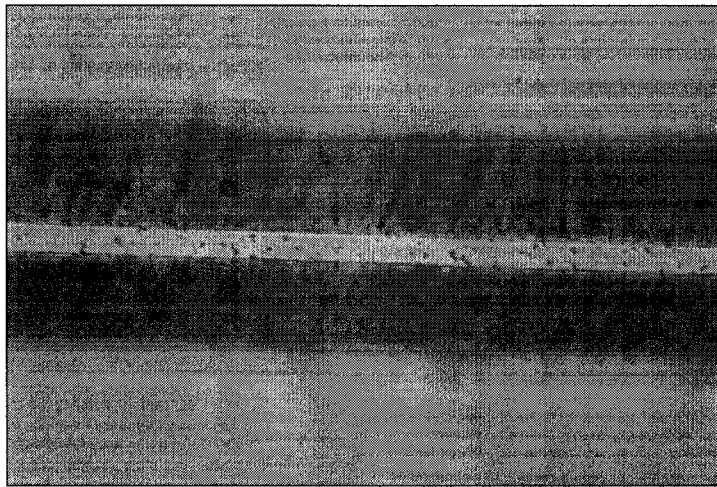
a.
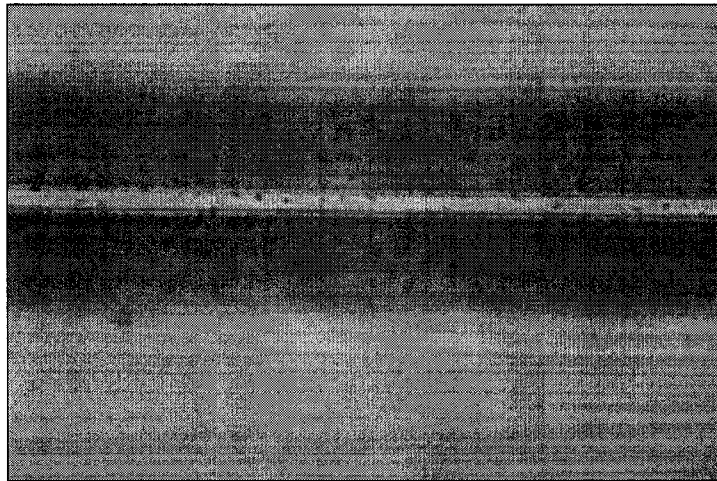
b.

Figure C.2 Crystal plane identification stripes, a. Jagged walls, off the crystal plane, b. On the Crystal plane

C.2. DRIE Fabrication Processes Fundamentals

DRIE is a form of plasma etching which is the generation of chemically reactive ions and radicals. Following the collision of molecules in a reacting gas such as SF6 with electrons excited by an RF field, the ions and radicals are born and form a cloud of electrons, ions and radicals also known as plasma. This cloud of chemically reacting parts is directed to a substrate using an electric field and causes the etching action. Whether it is plasma etching, chemical reaction, or reactive ion etching (RIE), ion bombardment, it has a directional cut which is also referred to as anisotropic etch. If the plasma is produced in higher density, employing inductively coupled coils (ICP-RIE), the etch rate would be significantly higher.[16] (Figure C.3)
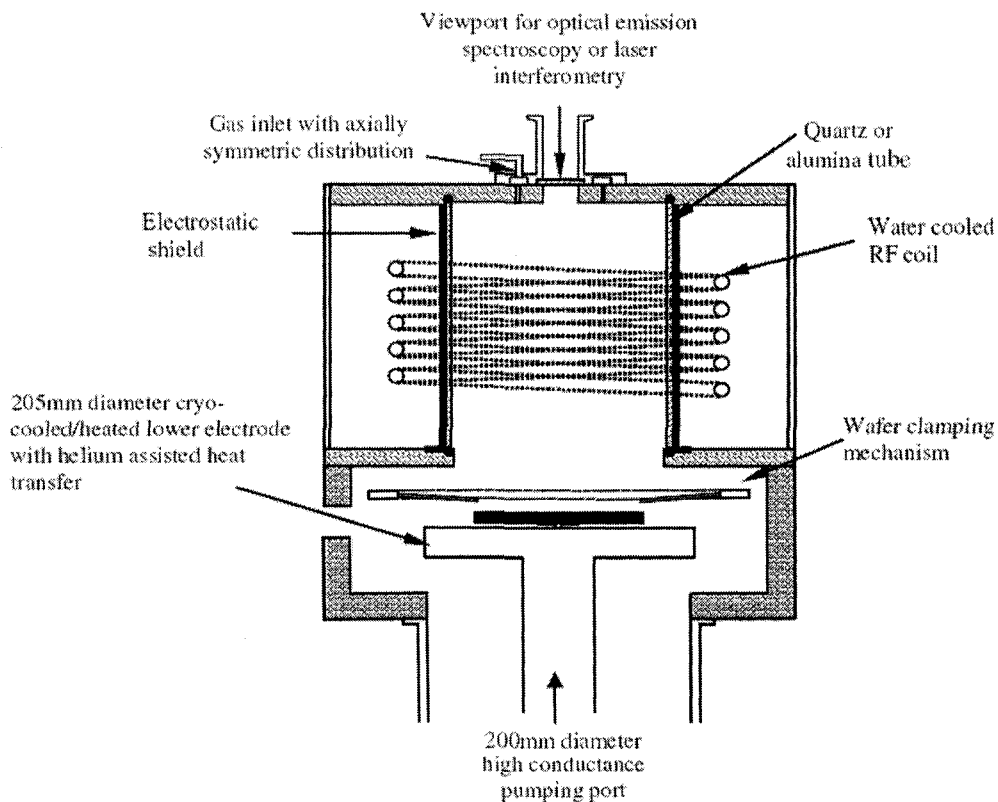
Figure C.3 Schematic of System 100 ICP Etching Tool [16]

A process called passivation, Figure C.4, is used along the sidewalls which perform etching only in the bottom of the deep feature and deposition of protecting material on the walls. There are currently two different DRIE techniques that are capable of the high aspect silicon micromachining: Bosch process, named after its inventor, Robert Bosch and cryogenic temperature DRIE.

C.2.1. Bosch Process

Bosch process usually uses chemicals with flourine backbone to etch the silicon, and a flourocarbon polymer to carry out the passivation. The etch and the passivation cycles are produced using a time scheduling mechanism separately, in which, $SF6$ for etching and $C4F8$ for passivation are commonly used. Etch step consists of a reaction in which $SF6$ molecule breaks up in the plasma and releases flourine radicals that etch the silicon. The 'isotropically' etched silicon, in the unstable form of $SiF4$, is pumped away from the reaction site. This step is usually 12 seconds. In the consequent step, slightly shorter that etch step, passivation occurs: $C4F8$ molecules split in the plasma to form $CF2$ and longer chain radicals and forms a uniform film on the sample. Next etch step involves the ion bombardment which selectively removes the polymer at the bottom of the feature and the anisotropy is accomplished. The flourine radicals will preferentially only etch in the bottom of the trench with etch rates of 1-5μm/min [17]. On the down side though, the alternating etching and passivation steps lead to ripples appearance on the sidewalls. As well, the uniformity of the etched features, depending on many conditions, can be of the order of 2-10%.

C.2.2. Cryo Process

Alternate to Bosch is the cryogenic technique, which is based on cooling the substrate to cryogenic temperatures (−110 °C) using liquid nitrogen. Cryo process, similar to the Bosch technique, uses $SF6$ to supply fluorine radicals for etching silicon but it differs in sidewall passivation technique with Bosch.. In

Bosch, the fluorocarbon polymer is deposited in a separate passivation step whereas in the cryo process a blocking layer of oxide/fluoride (SiO_xF_y) on the sidewalls combined with cryogenic temperatures is employed to reduce the probability of the fluorine radicals etching the walls. The protective material is attained by adding O2 to the SF6 gas in the plasma chamber. Following the deposition of the protecting layer, cryogenic temperature will guarantee the stability of the blocking layer. The etch rate of Cryo process is usually reported as 1-5μm/min with one plasma. [17]

In addition, the cryo process is more preferred for wafer through-hole applications. Also, using the cryo process, there are less problems with silicon grass production. Black silicon, micro grass or silicon grass is a layer of material that is observed at the bottom of high aspect ratio (deep etched) features. With a close look under microscope, it appears as spikes growing as a result of dirty substrate surfaces or oxide contamination form Al mask or the chamber walls. While pre-cleaning step before the process can easily solve the issue, sometimes the grass formation is due to temperature variations caused by poor contact between the wafer and the cathode that should be seriously inspected before the process.[18]

The etching of the features in DRIE process is always performed by deposition of a masking layer and removal of some parts of this film using photolithography and etching processes. The mask layer can be a photoresist, nitride, oxide or a metal. Usually due to instability, lower temperatures can cause some problems with photoresists such as stress cracks, silicon nitride or metal and metal oxide are preferred to be used as mask.
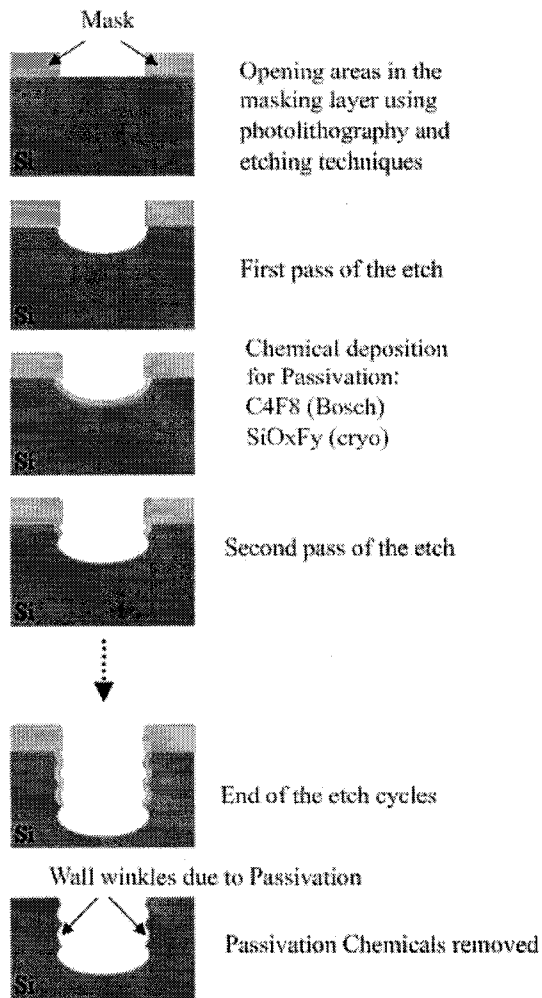
Figure C.4 DRIE process

Appendix References

[1]   C. Hall, *Polymer materials*: McMillan, 1981.

[2]   S. K. R. M. Chanda, *Plastics Technology Handbook*, 4th edition ed.: Taylor & Francis Group, 2006.

[3]   G. Odian, *Principles of polymerization*, 4th Edition ed.: John Wiley and Sons, 2004.

[4]   M. F. Ashby, and D. R. H. Jones, *Engineering materials 2: an introduction to microstructures, processing, and design*, 2nd Edition ed.: Oxford, 1998.

[5]   R. O. Ebewele, *Handbook of Polymer Science and Technology*: CRC Press, 2000.

[6]   L. Brunsveld, B. J. B. Folmer, E. W. Meijer *et al.*, "Supramolecular Polymers," *Chem. Rev.,* vol. 101, no. 12, pp. 4071-4098, 2001.

[7]   N. P. Cheremisinoff, *Advanced Polymer Processing Operations* William Andrew Publishing/Noyes, 1998.

[8]   J. G. Drobny, *Radiation Technology for Polymers*: CRC Press, 2002.

[9]   A. P. Thomas Laue, *Named Organic Reactions*, 2nd Edition ed.: John Wiley and Sons, 2005.

[10]   A. Ravve, *Light-Associated Reactions of Synthetic Polymers*: Springer Inc., 2006.

[11]   "Technical Information on Plasticisers," Jan 31, 2008; http://www.plasticisers.org/index.asp?page=4.

[12]   T. R. M.Stickler, *Polymethacrylates*, 5th Edition ed., p.^pp. 473: Wiley-VCH, 1992.

[13]   R. W. N. B.B. Kine, *Acrylic and Methacrylic Ester Polymers*, 2nd Edition ed.: John Wiley ans Sons, 1985.

[14]   G. L. W. J. E. McGrath, T. Ward, , *ACS Polymer Short Course Notes*, 2001.

[15]   D. Spicer, "Multi-layer biochip with integrated hollow waveguides," M.Sc. thesis, Dept. of Electrical and Computer Engineering., University of Alberta, 2005.

[16]   C. C. Welch, A. L. Goodyear, G. Ditmer *et al.*, "Choice of Silicon Etch Processes for Opto- and Microelectronic Device Fabrication Using Inductively Coupled Plasmas." pp. 13-16.

[17]   K. R. Williams, K. Gupta, and M. Wasilik, "Etch rates for micromachining processing-Part II," *Microelectromechanical Systems, Journal of,* vol. 12, no. 6, pp. 761-778, 2003.

[18]   M. J. Madou, *Fundamentals of Microfabrication: The Science of Miniaturization*, 2nd edition ed.: CRC press, 2002.